# GEO-CHEMO-MECHANICAL STUDIES FOR PERMANENT $CO_2$ STORAGE IN GEOLOGIC RESERVOIRS

Final Report

Reporting Period: 12/1/2009 – 9/30/2013

Principal authors: PI: Peter Kelemen; Co-PI's Ah-hyung Alissa Park and Jürg Matter; graduate students Greeshma Gadikota and Harrison Lisabeth; and Harrison Lisabeth's advisor Wenlu Zhu

March 2014

DOE Award Number: DE-FE0002386

Peter Kelemen, Arthur D. Storke Professor and Vice Chair, Dept. of Earth & Environmental Sciences, Columbia University in the City of New York, Lamont Doherty Earth Observatory, 211 Comer Laboratory, 61 Route 9W - PO Box 1000, Palisades, NY 10964

Tel: 1-845-365-8728, Fax: 1-845-365-8155, E-mail: peterk@ldeo.columbia.edu

Ah-hyung Alissa Park, Tenured Associate Professor, Dept. of Earth & Environmental Engineering, Fung School of Engineering and Applied Science, Columbia University in the City of New York, 918 S. W. Mudd Hall, Mail Code: 4711, 500 West 120th Street, New York, NY 10027

Jürg Matter, Adjunct Senior Research Scientist, Lamont Doherty Earth Observatory, Columbia University in the City of New York, 61 Route 9W - PO Box 1000, Palisades, NY 10964-8000 (also: Reader, Department of Ocean and Earth Science, National Oceanography Centre Southampton, University of Southampton Waterfront Campus, European Way, Southampton SO14 3ZH, United Kingdom)

Harrison Lisabeth & Tenured Associate Professor Wenlu Zhu, Department of Geology, University of Maryland, College Park, Maryland 20742

**DISCLAIMER*--**

“This report was prepared as an account of work sponsored by an agency of the United States Government. Neither the United States Government nor any agency thereof, nor any of their employees, makes any warranty, express or implied, or assumes any legal liability or responsibility for the accuracy, completeness, or usefulness of any information, apparatus, product, or process disclosed, or represents that its use would not infringe privately owned rights. Reference herein to any specific commercial product, process, or service by trade name, trademark, manufacturer, or otherwise does not necessarily constitute or imply its endorsement, recommendation, or favoring by the United States Government or any agency thereof. The views and opinions of authors expressed herein do not necessarily state or reflect those of the United States Government or any agency thereof.”

**ABSTRACT**

This two-pronged study investigated the rates and mechanisms of formation of Ca and Mg carbonate minerals via reaction of aqueous fluids with silicate minerals and rocks, and the geomechanical effects of such reactions. The kinetic studies focused on the separation of variables, following from previous studies demonstrating rapid formation of carbonates via reaction of the mineral olivine with aqueous fluids rich in $NaHCO_3$ (plus $KHCO_3$ and $RbHCO_3$) and NaCl at a high partial pressure of $CO_2$. We wished to separate and quantify the effects of $NaHCO_3$ and NaCl, and to investigate whether bicarbonate-rich, aqueous fluids would also cause rapid formation of carbonates via reaction with other minerals and rocks. Further, we wished to improve upon previous work by adding precise characterization of grain size distributions and surface area, and their changes as a result of reaction.

We confirmed previous reports of very rapid olivine carbonation. We found that at a given temperature and $CO_2$ partial pressure the previously observed rate enhancement in olivine carbonation is due mainly to $NaHCO_3$, and not to dissolved NaCl. Further, though reaction of the mineral plagioclase, and two rock compositions, were all faster in the presence of $NaHCO_3$-rich fluids, compared with saline and de-ionized water, they were all much slower than reaction of olivine.

In the experiments showing the fastest reaction rate, average grain size tended to increase during experiments, presumably due to dissolution of small reactant grains plus growth of product phases on reactant surfaces. Porosity/surface area of grains tended to change with reaction progress, due to the formation of dissolution pits and irregular growth of product phases on reactant grain surfaces. Development of a passivating phase (e.g., a layer of silica) due to incongruent dissolution of solid reactants and/or precipitation of solid products was detected, but was relatively minor and did not have a discernable effect on reaction progress.

Geomechanical experiments did not identify pressure-temperature-composition conditions under which porous olivine aggregates undergo reaction driven cracking. Little carbonate formed in these experiments. Though we fulfilled the milestones for this project, a variety of reasons for this remain to be investigated in the future. Reaction of porous olivine aggregates with brines rich in $NaHCO_3$ caused substantial weakening of samples in compression, due to formation of dissolution pits along olivine-olivine grain boundaries, reducing the solid-solid surface area.

A preliminary modeling study funded in part by this grant emphasized potential rate enhancements due to reaction-driven cracking. In related research, not funded by this grant, several additional experimental and modeling studies of reaction-driven cracking are underway.

# TABLE OF CONTENTS

## EXECUTIVE SUMMARY

This two-pronged study investigated the rates and mechanisms of formation of Ca and Mg carbonate minerals via reaction of aqueous fluids with silicate minerals and rocks, and the geomechanical effects of such reactions. The kinetic studies focused on the separation of variables, following from previous studies demonstrating rapid formation of carbonates via reaction of the mineral olivine with aqueous fluids rich in $NaHCO_3$ (plus $KHCO_3$ and $RbHCO_3$) and NaCl at a high partial pressure of $CO_2$. We wished to separate and quantify the effects of $NaHCO_3$ and NaCl, and to investigate whether bicarbonate-rich, aqueous fluids would also cause rapid formation of carbonates via reaction with other minerals and rocks. Further, we wished to improve upon previous work by adding precise characterization of grain size distributions and surface area, and their changes as a result of reaction.

We confirmed previous reports of very rapid olivine carbonation in the presence of aqueous fluid with > 0.5M dissolved $NaHCO_3$, with consumption of several tens of percent of initial olivine, with an average grain size ~ 30 microns, in an hour, producing magnesium carbonate, magnesite, at an optimal temperature of 185°C and a partial pressure of $CO_2$ > 70 bars. Corresponding rates in a natural system, with fracture spacing ~ 1 meter, would be tens of percent in a year. These results correspond closely to the rate expression previously fit by Kelemen and Matter, 2008, to the data of O'Connor et al., 2004. Combining our new data with that of O'Connor et al. yields

$$mass\ fraction\ of\ olivine\ consumed\ per\ second = 1.03\ \times 10^{-5}\sqrt{P_{CO2}} \times e^{-0.00033\times(T-185)^2}$$

If cumulative olivine consumption is considered, this expression does not vary significantly during experimental runs extending for up to 5 hours, with almost 100% olivine carbonation, yielding a constant rate of about 57% per hour. This observation of a nearly constant rate is striking given past emphasis on progressive passivation of unreacted olivine via formation of an amorphous silica layer via incongruent dissolution of $Mg^{2+}$.

We found that at a given temperature and $CO_2$ partial pressure the previously observed rate enhancement in olivine carbonation is due mainly to $NaHCO_3$, and not to dissolved NaCl. We speculate that the rate enhancement observed in the presence of NaHCO3 is the result of pH buffering, to values between ~ 6 and 6.5, during the experiments. This intermediate pH is low enough for relatively rapid olivine dissolution, but high enough to stabilize solid magnesite ($MgCO_3$) in equilibrium with fluid at a low total Mg concentration. Magnesite precipitation maintains low Mg concentration, which in turn drives continued undersaturation and rapid dissolution of olivine. In a system at lower water/rock ratio, pH would be naturally maintained at pH 6 or higher, so that engineered mineral carbonation processes may or may not require addition of $NaHCO_3$ to reach near optimal rates.

Carbonation of the mineral plagioclase (specifically, the plagioclase variety *labradorite*), and carbonation of two rock compositions, were all faster in the presence of $NaHCO_3$-rich fluids, compared with carbonation in the presence of both saline and de-ionized water. However, carbonation of all of these other materials was ~ 10 times slower than reaction of olivine in terms of weight fraction carbon in the solid products, and in terms of the weight fraction of available cations that were extracted from silicate minerals to form solid carbonates. These results indicate that, while mineral carbonation of the most abundant rock type in the crust, basaltic lava, is possible, olivine-rich lithologies such as peridotite are strongly preferable where available.

In the experiments showing the fastest reaction rate, average grain size tended to increase during experiments, presumably due to dissolution of small reactant grains plus growth of product phases on reactant surfaces. Porosity/surface area of grains tended to increase with reaction progress, due to the formation of dissolution pits and irregular growth of product phases on initially smooth reactant grain surfaces.

Geomechanical experiments did not identify pressure-temperature-composition conditions under which porous olivine aggregates undergo reaction driven cracking. Little carbonate formed in these experiments.

Reaction of porous olivine aggregates with brines rich in $NaHCO_3$ caused substantial weakening of samples in compression, probably due to formation of dissolution pits along olivine-olivine grain boundaries, reducing the solid-solid surface area.

A preliminary modeling study funded in part by this grant emphasized potential rate enhancements due to reaction-driven cracking. In related research, not funded by this grant, several additional experimental and modeling studies of reaction-driven cracking are underway.

## OVERVIEW

Rising concentrations of $CO_2$ in the atmosphere are attributed to increasing human emissions. In turn, high concentrations of $CO_2$ are likely to lead to undesirable changes in global climate, spurring a search for practical ways to reduce emissions via capture of $CO_2$–"at the smokestack" or from the environment – and to store captured $CO_2$ in permanent reservoirs. One of the most stable, permanent, and thermodynamically stable options for storing $CO_2$ is to convert calcium- and magnesium-bearing, rock-forming silicates into solid calcium and magnesium carbonate minerals. This can be achieved by directly injecting $CO_2$ into formations rich in calcium and magnesium silicates, known as *in situ* carbon mineralization or mineral carbonation. Alternatively, Ca and Mg silicates can be mined, crushed and reacted with $CO_2$ in highly engineered processes, known as *ex situ* carbon mineralization. However, the kinetics and mechanisms of silicate mineral-$CO_2$-aqueous fluid interactions are not very well understood. Prior to this study, the fastest reaction rates were documented only in a series of relatively unconventional experiments involving brines rich in bicarbonate conducted on a single mineral (olivine), without evaluation of the effects of individual reagents, without characterization of grain size distributions and surface areas, and without experiments using the same fluid composition and physical conditions to investigate carbonation of other minerals.

Thus, the ultimate goal of this project was to experimentally quantify mineral carbonation rates during the reaction of bicarbonate-rich fluids with commonly occurring, Mg-rich rocks such as basaltic lava and tectonically exposed mantle peridotite.

Proposed methods for *in situ* mineral carbonation are based on observed, natural mineral carbonation systems. In these natural systems, there is a pervasive network of microfractures, with crack spacings of 10's to 100's of microns, that are the sites of carbonate vein formation. Diffusion around these cracks also leads to replacement of the rock matrix between fractures with carbonate minerals. Such crack networks are also observed in rocks that have undergone extensive hydration, but are rare in rocks that have not undergone hydrous and or carbonate alteration. For this and other reasons, it is hypothesized that volume changes during mineral hydration and carbonation lead to stresses that drive rock fracture, maintaining or enhancing both permeability and reactive surface area in a positive feedback mechanism. However, the conditions that initiate and sustain such positive feedback processes are poorly known.

Thus, a second goal was to delineate the conditions under which rapid mineral carbonation in peridotite might lead to a positive feedback via "reactive cracking", in which cracks caused by large volume changes enhance porosity, permeability and reactive surface area.

The major participants in the project were three faculty members and their graduate and undergraduate students at Columbia University. Lead PI, Prof. Peter Kelemen is a member of Columbia's Dept. of Earth & Environmental Sciences, based at the Lamont-Doherty Earth Observatory (LDEO). Co-PI Prof. Alissa Park is a member of Columbia's Dept. of Earth &

Environmental Engineering, in the Fu Foundation School of Engineering and Applied Science. Co-PI Dr. Jürg Matter was a Research Professor at LDEO, and is now a Lecturer in the Dept. of Ocean & Earth Science at University of Southampton (UK). The project included collaboration with Prof. Brian Evans in the Earth, Atmospheric & Planetary Sciences Department at MIT, and Prof. Wenlu Zhu in the Dept. of Geology at the University of Maryland, College Park. Three graduate students, Melodie French, Greeshma Gadikota and Harry Lisabeth, were trained as a part of this project. French left MIT in year 1 to become a PhD candidate at Texas A&M University, focusing on a different project. Gadikota defended her PhD on December 20th, 2013 and will receive her degree in February 2014. Lisabeth is currently a PhD candidate working with Zhu at the University of Maryland. The students benefited from the interdepartmental collaboration and have been well-trained to pursue careers in the field of Carbon Capture Utilization and Storage (CCUS). The research findings from this study were presented at numerous conferences such as the Annual American Institute of Chemical Engineers, the American Geophysical Union Fall Meetings, the Gordon Conference on Rock Deformation, the 5$^{th}$ Biot Conference on Poromechanics in Vienna in 2013, and Annual DOE Project Meetings. In addition, the development of various experimental protocols and the research results were and will be published in various peer-reviewed journals. Publications arising from this study are summarized at the end of this report.

## PROJECT OBJECTIVES

Carbon mineralization ensures safe and permanent storage of $CO_2$. Moreover, when $CO_2$-rich fluid is injected into rocks containing calcium and magnesium bearing minerals such as basalt and peridotite, the process of *in situ* carbon mineralization may be more economical than *ex situ* carbon mineralization where the minerals have to be mined, crushed and combined with fluid at high temperature and pressure in highly engineered reactor vessels. When $CO_2$ is injected into geologic formations, $CO_2$ is expected to be trapped under the caprock (structural trapping), in the pore spaces (residual trapping), dissolve in the formation water (solubility trapping) or form mineral carbonates (mineral trapping). However, the relative rates and mechanisms of carbon mineralization are not very well understood. Moreover, when $CO_2$ is injected into geologic formations, extensive formation of carbonates may exert sufficient crystallization pressure to induce the formation of cracks in a process known as reactive cracking. Reactive cracking increases the surface area and creates more permeable pathways for $CO_2$ migration, as represented in Figure 1. Extensive, reaction-driven cracking could provide a route to rapid, inexpensive *in situ* mineral carbonation. On the other hand, reaction-driven cracking in caprocks could compromise the integrity of reservoirs for storage of $CO_2$-rich fluids in pore space.

In order to improve understanding of mineral carbonation and related fracture formation, the aim of this project is to understand the mechanisms and rates of reaction between $CO_2$-rich fluids and minerals, including the effects of various parameters such as mineralogy, temperature, $CO_2$ partial pressure, chemical additives etc., on the chemical and morphological changes in

various minerals. Chemically induced stresses and strain on the rocks due to mineral dissolution and carbonation are also investigated. Another aim of this project is to train graduate and undergraduate students in the development of technologies related to carbon capture, utilization and storage (CCUS).

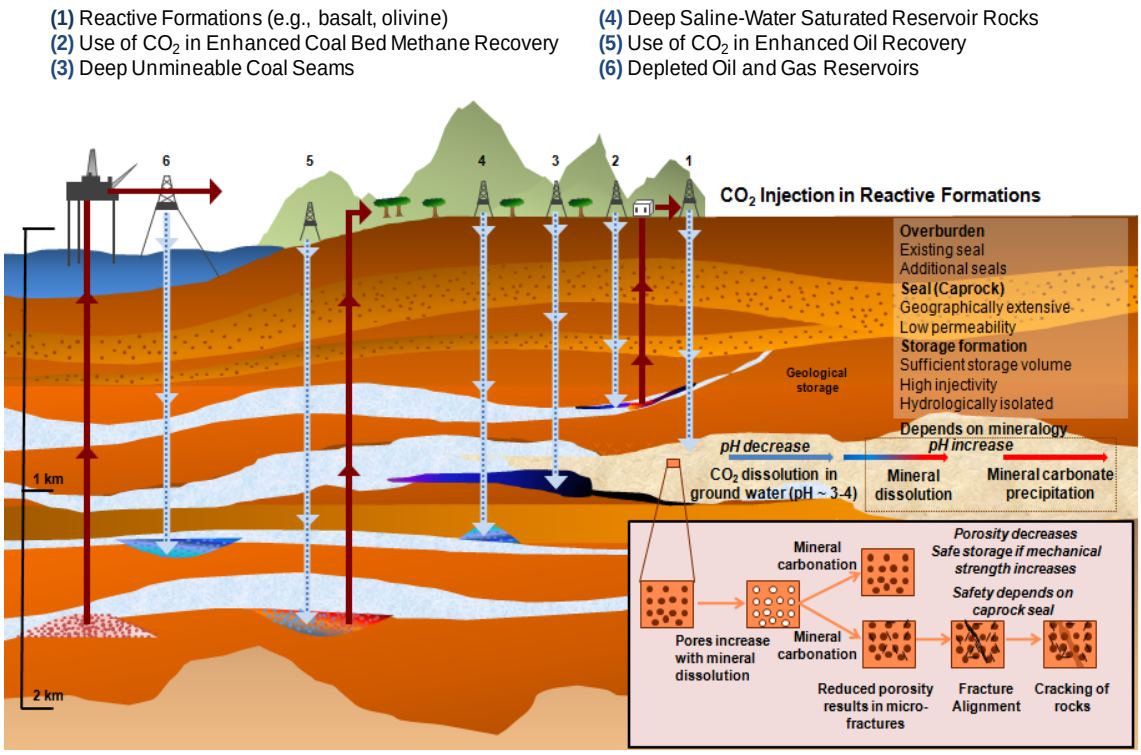


**Figure 1.** Various geologic sites for $CO_2$ storage with the formation of cracks due to reactive cracking represented in the inset.

## SPECIFIC QUESTIONS

The fate of $CO_2$ post capture and compression from power plants has been debated. One of the most economical options is to directly inject $CO_2$-rich fluids into geologic formations (Metz et al., IPCC, 2005). Unlike injection into inert formations such as saline aquifers, when $CO_2$ is injected into reactive formations, it can be converted into insoluble, solid calcium and magnesium carbonate minerals. Formation of solid carbonates reduces the need for monitoring mobile $CO_2$ over time. However, there is considerable uncertainty surrounding the kinetics and mechanisms of the carbon mineralization process, which are essential for predicting the fate of $CO_2$ injected into reactive formations.

The process of carbon mineralization is a multi-step process that involves $CO_2$ hydration, mineral dissolution, and formation of carbonates. This process is complicated by the pH that enhances the different steps. While mineral dissolution rates are enhanced at low pH, formation

of carbonates occurs faster at high pH. Simultaneous chemical and morphological changes also affect the reactivity of minerals.

PI Peter Kelemen and co-PI Juerg Matter study the natural formation of carbonates particularly in Oman where nearly 15,000 $km^3$ of peridotite is available for carbonation. Peridotite naturally reacts with $CO_2$ to form magnesite ($MgCO_3$), dolomite ($CaMgCO_3$) and calcite. In Oman, this is occurring in a near surface weathering horizon at a rate of 10,000 to 100,000 tons of $CO_2$ per year (~ 1000 tons/$km^3$ rock/yr~ 1 gm/$m^3$/yr) (Kelemen & Matter, 2008; Matter & Kelemen, 2009; Paukert et al., 2012; Kelemen et al., 2011; Mervine et al., 2013; Streit et al., 2012). Kelemen and co-workers also specialize in the study of deformation related to volume changes due to fluid-rock reaction, with a focus on mineral hydration and carbonation (Kelemen et al., 2013; Kelemen & Hirth, 2012; Rudge et al., 2010). Co-PI Alissa Park specializes in accelerating mineral reaction kinetics via *ex situ* processes (Park et al., 2003; Park & Fan, 2004). *In situ* conditions can be achieved in a laboratory setting using high temperature and high pressure batch reactors. While *in situ* carbon mineralization is expected to occur over the course of years, in the laboratory processes can be accelerated by grinding to increase the surface area. Combining the understanding of natural and engineered carbon mineralization processes is useful in determining the mechanisms and the rate limiting steps in these processes.

Prior to this project, the PI's compiled the results of various studies to determine the conditions that lead to rapid mineral carbonation. These include coupled mineral dissolution and carbonation experiments performed at Albany Research Center (ARC) and Arizona State University (Chizmeshya et al., 2007; Gerdemann et al., 2007; O'Connor et al., 2004). Some aspects of coupled mineral dissolution and carbonation were not very well documented in these previous studies. The effects of individual fluid species were not separated in experiments involving bicarbonate-rich brines. A substantial acceleration of olivine carbonation using these brines, compared to previous work with de-ionized water and saline solutions was demonstrated, but the potential for similar acceleration in other mineral systems was not investigated. Initial and final grain size distributions, and grain morphology, were not well documented. Therefore, based on a preliminary understanding $CO_2$-reaction fluid-mineral interactions and cross-disciplinary specialization in the project team, we addressed the following research questions:

- What is the effect of mineralogy (e.g, olivine, labradorite, anorthosite and basalt) on carbon mineralization involving bicarbonate-rich fluid reactants?
- What is the effect of reaction time, temperature, and partial pressure of $CO_2$ on carbon mineralization?
- What are the separate effects of chemical additives such as $NaHCO_3$ and NaCl, and their varying concentrations on coupled mineral dissolution and carbonation behavior?
- What are the effects of pore volume, surface area, and particle size on mineral carbonation?
- How does carbon mineralization affect rock rheology? What conditions lead to reaction-driven cracking?

## 1. Sample Preparation and Mineral Cleaning Protocol

Surface area is one of the most important factors determining the rate and extent of reactions for a given mineral volume and reaction time. Thus, in order to achieve a measurable extent of carbonation within a laboratory time scale, significantly less than the geologic time scale, most studies of mineral carbonation are performed with ground mineral samples. It is important to accurately characterize the particle size and surface area for the accurate estimation of the surface reaction rate of mineral dissolution, which can then be extrapolated to natural rock systems with much smaller surface area/volume ratios.

Grinding was also important because some reactants used in this study were chemically heterogeneous. Thus, relatively large samples were ground and well mixed in order to ensure that the small aliquot used for analysis was representative. Ground mineral samples were first dry-sieved to exclude particles greater than 175 μm using a Model RX W.S. Tyler Portable Sieve Shaker. While smaller grain size is desired for the kinetic studies of mineral dissolution, extensive grinding may disrupt the crystal structure of minerals, lowering the activation energy for the reaction (Gerdemann et al., 2007; O'Connor et al., 2004). Very fine particles (< 5 μm) with a higher surface area to volume ratio might include a large fraction of "damaged", highly disordered surfaces. Damaged surfaces heal over time, and as a result they are rare in natural rocks. Therefore, in order to determine the surface reaction rate of mineral dissolution, we chose to eliminate exceptionally fine particles. To achieve this, a systematic protocol was developed (Figure 2). The process of removing particles smaller than 5 μm was called "cleaning" and the samples from which fines were removed were designated as "cleaned". Samples containing fines were called "raw" or "uncleaned".

For a study of the effect of cleaning on olivine carbonation rate described on pages 8-11, 25 grams of the ground solid reactant were cleaned in each batch. This material was first added to the 10 μm sieve along with deionized (D.I.) water. The sieve was then placed in an ultrasonic bath filled with D.I. water and shaken for five minutes. After five minutes, the particle size distribution of the cleaned material was measured. If particles with diameters <5 μm were present, then the cleaning process outlined above was repeated until all fine particles <5 μm were removed. After the cleaning cycles were completed, the samples were dried at 70 $^{o}$C for 24 hours in a vacuum oven, to eliminate reaction between cleaned minerals and air (e.g., with $O_2$ and $CO_2$). Drying samples at temperatures greater than 70 $^{o}$C may result in a change in chemical composition (e.g., dehydroxylation of hydroxide or calcination of carbonate phases).

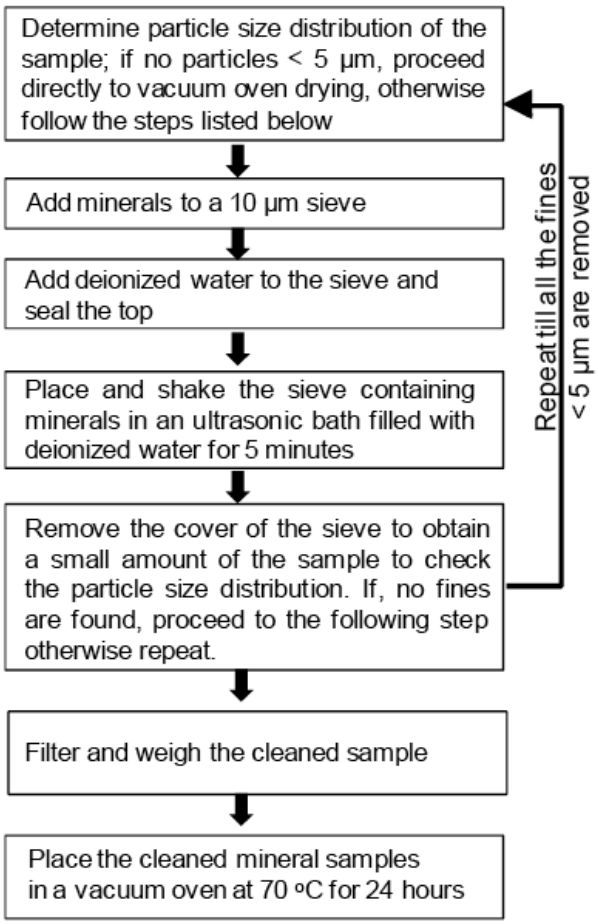


**Figure 2.** Protocol for the removal of fines < 5 µm from minerals.

During our preliminary experiments, another important factor that impacts the reactivity of the minerals was detected. A few previous studies reported that aging of ground reactants such as the mineral diopside ($MgCaSi_2O_6$) resulted in reduced reaction rates (Eggleston et al., 1989). We infer that this is due to reaction with air, perhaps by hydration to form hydrous magnesium silicate phases (e.g., serpentine). In our preliminary experiments, we used the same olivine as that used by O'Connor et al., (2004). About two years prior to the preliminary experiments, this material was ground and cleaned at Columbia using the procedure described above and in Figure 2. The ground material was stored in containers open to the air. At the time of the experiments, XRD and TGA results did not indicate any phases other than olivine in this material. However, reaction rates in our experiments were much lower than in those reported by O'Connor et al. (2004), independent of grain size, as discussed in more detail in the next paragraph.

Our preliminary experiments were intended to reproduce the most widely cited result from the ARC group, in which they reported 68% carbonation of ground, uncleaned olivine after three hours at 185°C at a $CO_2$ partial pressure of 150 atm in an aqueous solution with 1.0 M NaCl + 0.64 M $NaHCO_3$, with 15wt% solid concentration stirred at 1000 rpm (Gerdemann et al.,

2007; O'Connor et al., 2004). In our preliminary experiments, repeated several times, the extents of carbonation of cleaned olivine and a slurry of very fine-grained olivine were only 1.5% and 15.1% respectively, significantly lower than reported by the ARC group, and for similar experiments at Arizona State University (Chizmeshya et al., 2007). Furthermore, on the basis of these results, we concluded that the size of olivine particles was not the major reason for the discrepancy between our results and those in previous studies. Table 1 summarizes findings for five different types of olivine carbonation experiments performed for this study.

**Table 1.** Effect of aging on the carbonation rate of ground olivine. Experiments were performed at 185 $^{o}$C, $P_{CO2}$ = 139 atm in 1.0 M NaCl + 0.64 M $NaHCO_3$ with 15 wt.% solid for a reaction time of 3 hours and a stirring rate of 800 rpm. ***Old*** samples were stored in air for two years after grinding, before use in our experiments. In contrast, ***freshly ground*** olivine was produced by regrinding the old samples immediately (i.e., within a week of grinding) before use in our experiments. The extents of carbonation reported in this table were calculated assuming that both Mg and Fe react to form carbonates. The term "slurry" indicates fluid containing very fine, suspended olivine particles.

| Olivine Sample Type | ***Old***, cleaned olivine sample | Slurry of fine-grained, ***old*** olivine sample | ***Freshly ground***, cleaned olivine sample | Slurry of ***freshly ground***, uncleaned olivine | ***Freshly ground***, uncleaned olivine sample |
|---|---|---|---|---|---|
| Particle Size | 10 – 90 μm | < 20 μm | 10 – 90 μm | < 20 μm | 0.3-92.0 μm |
| Extent of Carbonation | 1.5% | 15.1% | 11.9% | 79.5% | 73.1% |

Thus, we ground and cleaned a new batch of the same olivine, and did experiments immediately afterward. We found that there were significant differences in the reactivity of the freshly ground olivine compared to olivine that had been ground, cleaned, and then stored for two years. The extents of carbonation for freshly ground, cleaned olivine, and for a slurry of freshly ground olivine were 11.9% and 79.5%, respectively. In addition, an experiment was performed using the freshly ground olivine without cleaning. The fraction of fines in uncleaned olivine was 90% (< 37 μm) and 70% (< 20 μm). The extent of carbonation of this olivine sample was 73.1% after three hours, which was close to the previous ARC and Arizona State results.

Comparing the old and freshly ground olivine carbonation data, it seems very likely that a thin layer of passivated material on the olivine grain surfaces inhibited the reactivity of the samples that were ground and cleaned two years before the carbonation experiments.

We performed similar experiments on old (ground two years before the experiment) and freshly ground serpentine (ground less than a week before the experiments) samples. We did not observe passivation of the old serpentine samples. The extents of carbonation of freshly ground

and old serpentine were 15.5% and 14.1%, respectively, at the same experimental conditions as olivine carbonation studies. The particle size distribution of the unreacted antigorite was 2-80 μm.

Aside from the aging effect on the reactivity of ground olivine, our results show that olivine particle size significantly affects mineral dissolution and carbonation rates, qualitatively consistent with previous results from Chizmeshya et al., (2007 Annual Report, Table 3, page 24; 2005 Annual Report, Figures 7 and 8, page 17 and Figure 13, page 22). It seems evident that the extents of carbonation reported for uncleaned powders in previous studies partly reflect the relatively high reactivity of the finer particles. However, Chizmeshya et al. (2007, Figure 13, page 22) found that this grain size effect is largely predictable as a simple function of the increased surface area of the finer particles. If so, then the faster reactivity of fine grained particles is not significantly influenced by energetic effects that might be due to a relatively high proportion of damaged material in the finest grain size fraction.

In fact, Chizmeshya et al. (2007) found that experiments on ground olivine with a broad range of grain sizes had somewhat higher carbonation rates than would be predicted from experiments on narrower ranges of grain size, and proposed that this is due to chemical interaction between adjacent grains with different sizes. In other words, the presence of smaller grains seemed to enhance the reactivity of larger grains (Chizmeshya et al., 2007, Table 3, page 24). In our case, however, it is challenging to quantify the effect of surface area normalized to the volume or weight of the sample since our particle size analyzer cannot measure particles smaller than 0.3 μm.

## 2. Estimation of the Extents of Mineral Carbonation

As shown in Figure 3, there are many different approaches to determine the extent of mineral carbonation ranging from a simple method of the overall weight change to detailed Thermogravimetric Analysis (TGA), Total Carbon Analysis (TCA) and Total Inorganic Carbon Analysis (TIC). The detailed description and the method of deriving the extent of mineral carbonation from the raw data are given in Table 2 for each approach. Untreated antigorite was used to determine the effect of chemical additives such as 1.0 M NaCl + 0.64 M $NaHCO_3$ and 0.1 M Na-oxalate on the extent of carbonation at 185 $^oC$, $P_{CO2}$ = 139 atm for a reaction time of 1 hour with 15 wt% of solid and a stirring rate of 800 rpm. The grain size was in the range of 2-80 μm and the surface area was 10.3 $m^2/g$. The unreacted antigorite sample was composed of 40.5% MgO, 37.1% $SiO_2$, and 7.80% $Fe_2O_3$. Unlike the serpentine samples that were heat-treated at 650 $^oC$ by Albany Research Center, the antigorite samples reported in this study were not heat-treated. The experiments were performed for 1 hour to compare with the results of ARC. The extent of carbonation for our sample was 17.3% which was considerably lower than 50% reported for heat-treated antigorite in the presence of 1.0 M NaCl + 0.64 M $NaHCO_3$, (e.g., O'Connor et al. 2004, Figure 6), very similar to the extent of reaction for antigorite without heat treatment (e.g., O'Connor et al., 2004, Figure 3), and much higher than the extent of reaction for another polymorph of serpentine, lizardite, that was also studied by O'Connor et al.

The differences among TGA, TCA and TIC methods can be illustrated by comparing the results of antigorite carbonation in Figure 3. The TGA analysis of antigorite reacted in 0.1 M Na-oxalate was complicated by the chemical heterogeneity of the carbonated antigorite sample, which contained magnesite, unreacted antigorite, and glushinskite, $Mg(C_2O_4)\cdot 2H_2O$. Reactions 1 and 2 represent the thermal decompositions of glushinskite (Frost et al., 2004), at 148 $^oC$ and 397 $^oC$ with theoretical weight losses of 24.3% and 48.5%, respectively.

$$Mg(C_2O_4).2H_2O_{(s)} \rightarrow MgC_2O_{4(s)} + 2H_2O_{(g)} \quad \text{(Rx. 1)}$$

$$MgC_2O_{4(s)} \rightarrow MgO_{(s)} + CO_{2(s)} + CO_{(g)} \quad \text{(Rx. 2)}$$

**Table 2**. Comparison of various methods of carbon analysis

| Method of Analysis | Characteristics |
|---|---|
| Thermogravimetric Analysis (TGA) | • Change in sample weight is measured as a function of change in temperature over time<br>• Can be used to distinguish between different carbon-bearing minerals based on decomposition temperature<br>• Challenging to estimate the extent of carbonation in materials with low carbon concentration, and in samples containing minerals (carbonates, hydrates, …) with overlapping decomposition curves |
| Total Carbon Analysis (TCA) | • Samples containing carbon are combusted in the presence of $O_2$ at temperatures around 1000 $^oC$ such that all inorganic and organic carbon is converted to $CO_2$<br>• Evolved $CO_2$ in the $O_2$ carrier gas is absorbed in a coulometric titration cell filled with a medium containing ethanolamine and a colorimetric indicator, after which $CO_2$ concentration is determined via optical spectroscopy.<br>• Requires less analysis time compared to TGA or TIC<br>• Essential to have a sample without adsorbed $H_2O$ since carbon concentration calculations includes the weight of the sample<br>• This technique cannot distinguish between organic and inorganic carbon |
| Total Inorganic Carbon Analysis (TIC) | • Samples containing inorganic carbon are titrated with a strong acid and the evolved $CO_2$ is measured. All the samples discussed in this report were heated to 75 to 80 $^oC$ in the acid solution to accelerate the release of $CO_2$<br>• The most reliable method for estimating $CO_2$ present in a material but requires a dry starting material without any moisture as in TCA<br>• Cannot be used to distinguish between different carbonate phases. |

The second thermal decomposition of glushinskite occurrs at 397 $^{o}$C, which coincides with the calcination of magnesite in the range of 300 - 450 $^{o}$C., which is the range of magnesite decomposition for the heating rate (5 $^{o}$C/ min) and gas flow rate (20 ml/min). These conditions were chosen based on methods described in the literature, and our observations based on experiments with pure magnesite and minerals containing magnesite. Given the overlap in decomposition temperatures, it is challenging to estimate the carbon content using TGA in carbonated antigorite samples containing glushinskite.

Use of the weight change during heating (TGA) is the least accurate way of determining the extent of mineral carbonation in most materials. TGA cannot always distinguish weight changes due to thermal decomposition of carbonates (magnesite, dolomite, calcite), hydrates (serpentine, brucite), and phases formed during experiments by combined hydration and carbonation (e.g., nesquehonite, hydromagnesite). However, TGA was the most widely used method in earlier studies (Gerdemann et al., 2007; O'Connor et al., 2004).

The accuracy of TIC analysis depends on the complete digestion of carbonate minerals (e.g., magnesite), which often occurs slowly. Therefore, all the carbonated mineral samples reported in this study were digested at 75-80 $^{o}$C in the presence of perchloric acid to accelerate the inorganic carbon analysis. Furthermore, TIC does not measure the concentration of organic carbon compounds, such as graphite and amorphous carbon as well as hydrocarbons and such exotic species as glushkinite.

TCA in this study, with combustion at 1000°C, results in rapid, complete decomposition of all inorganic and organic carbon compounds. Thus, TCA provides faster analysis compared to the TIC method. However, TCA cannot distinguish inorganic and organic carbon species.

As shown in Figure 3, the estimated extents of carbonation of antigorite reacted in 0.1 M Na-oxalate were 9.22%, 8.73% and 17.62% for TGA, TIC analysis and TCA, respectively. The difference between the TCA and TIC analyses showed that a significant proportion of minerals with organic carbon formed during the reaction. In the presence of 1.0 M NaCl + 0.64 M $NaHCO_3$, the extents of antigorite carbonation were estimated to be 14.9%, 14.4% and 17.1% using TGA, TIC analysis and TCA, respectively. In both cases, TGA and TIC analysis produced similar estimates of the extent of antigorite carbonation, while TCA produced a higher value. As expected, the difference between TGA and TIC results versus TCA result was greatest (~ almost double) for the oxalate case due to the formation of glushinskite. The error associated with TCA results was slightly higher compared to the TGA and TIC data for both samples.

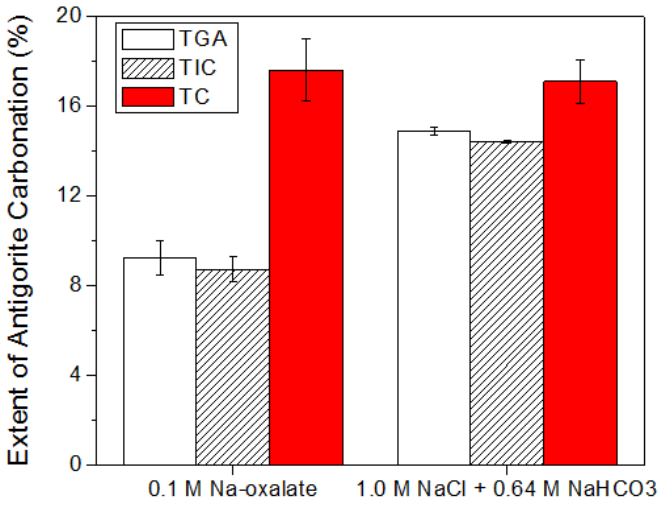


**Figure 3**. Comparison of the extents of antigorite carbonation using Thermogravimetric Analysis (TGA), Total Inorganic Carbon (TIC) and Total Carbon (TC) methods. Experiments were performed at 185 $^{o}$C, $P_{CO2}$ = 139 atm for a reaction time of 1 hour with 15 wt% of solid and a stirring rate of 800 rpm. The grain size was in the range of 2-80 μm.

In addition to the complications of analyzing samples containing a variety of carbon-containing phases, there is uncertainty regarding the appropriate method for estimating the carbon storage potential of minerals and rocks. For example, the determination of the extent of antigorite carbonation required an understanding of all the species that could react with $CO_2$ to form insoluble carbonates. The first step towards this calculation required the determination of the $CO_2$ storage capacity.

$$M^{n+}_{(aq)} + \frac{n}{2} CO^{2-}_{3\,(aq)} \rightarrow M(CO_3)_{\frac{n}{2}\,(s)} \qquad \text{(Rx. 3)}$$

where $M$ refers to all the metal oxide in the minerals and rocks that can react with $CO_2$ to form metal carbonates. Then, the carbon storage potential of the mineral (on a weight basis) can be estimated via the following equation.

$$\frac{W_{CO_2}}{W_{mineral}} = \frac{1}{R_{CO_2}} = \sum \left( \frac{n}{2} . \frac{y_m}{MW_m} \right) \times MW_{CO_2} \qquad \text{(Eq.1)}$$

in which $y_m$ refers to the mass fraction of alkaline metal ($m$) in the mineral to form metal carbonate phases. $W_{CO2}$ and $W_{mineral}$ are weights of $CO_2$ stored in the solid reaction products and the mineral before its carbonation, respectively, $MW_{CO2}$ is the molecular weight of $CO_2$, and $\frac{n}{2}$ refers to the stoichiometric coefficient of $CO_2$ as represented in Reaction 3.11. The mass of $CO_2$ that can be trapped in a unit mass of the unreacted mineral, $\frac{1}{R_{CO_2}}$,is also often used as a measure of $CO_2$ storage capacity of the mineral. Conversely, $R_{CO_2}$ refers to the amount of mineral needed to store a unit mass of $CO_2$ (Gerdemann et al., 2007; O'Connor et al., 2004). The question is

what alkaline metal species would be involved in carbonate formation during the interaction with $CO_2$. There are many metals including Mg, Ca, Fe, Al, Mn, Na and K that form carbonates. However, some of these carbonates might not form in reactor systems due to slow kinetics (e.g., Al) or high solubility in water (e.g., $Na_2CO_3$ and $K_2CO_3$). Since $Na_2CO_3$ and $K_2CO_3$ do not precipitate from solution in experiments at high fluid/rock ratios, their contribution towards $CO_2$ storage in solid carbonates in a natural system with low fluid/rock ratios could be mistakenly ignored in some cases.

In considering carbonation of ultramafic rocks, since Na, K, Mn and Al constitute less than 1 wt% of olivine and antigorite, and are minor components in pyroxene minerals, their contribution to carbon storage can be ignored. Thus, in the actual estimation of carbon storage potential of ultramafic minerals and rocks only Mg, Ca and Fe need to be considered for mineral carbonation. This leads to the reduced form of Eq. 1 given as following:

$$\frac{W_{CO_2}}{W_{mineral}} = \frac{1}{R_{CO_2}} = \left(\frac{y_{Mg}}{MW_{Mg}} + \frac{y_{Ca}}{MW_{Ca}} + \frac{y_{Fe}}{MW_{Fe}}\right) \times MW_{CO_2} \quad \text{(Eq. 2)}$$

Iron (II) oxide is expected to react with $CO_2$ to form siderite ($FeCO_3$). However, experimental formation of siderite may be inhibited by the low solubility of iron oxide, which may precipitate from the solution before siderite is formed. In fact, previous studies have already shown that iron oxide precipitated from the solution during the carbonation of silicate minerals in the absence of chelating agents (Gadikota et al. 2013; Gerdemann et al. 2007; King et al. 2010; O'Connor et al. 2004). As shown here, it is important to understand the chemistry of the mineral in interest to accurately estimate its carbon storage potential and further evaluate its extent of carbonation.

In this study, the extents of antigorite carbonation were calculated assuming that iron carbonate does not form (Eq.3).

$$\frac{W_{CO_2}}{W_{mineral}} = \frac{1}{R_{CO_2}} = \left(\frac{y_{Mg}}{MW_{Mg}} + \frac{y_{Ca}}{MW_{Ca}}\right) \times MW_{CO_2} \quad \text{(Eq. 3)}$$

The yield or extent of carbonation, $Y_{CO_2}$, is defined as the amount of $CO_2$ stored in the mineral as carbonate relative to the $CO_2$ storage capacity of the mineral. As discussed earlier, there are a number of methods of quantifying the amount of $CO_2$ stored in the mineral as carbonates: TGA, TCA and TIC methods. Thus, depending on the analytical method, a different expression of $Y_{CO_2}$ was developed. Using a TGA method, the following expression can be used for $Y_{CO_2}$.

$$Y_{CO_2,TGA} = \left[\frac{Measured\ weight\ ratio\ of\ CO_2\ stored\ in\ mineral}{The\ residual\ CO_2\ storage\ capacity}\right] \times 100\%$$

$$= \frac{\left(\frac{W_{CO_2}}{W_{mineral}}\right)}{\left(\frac{1}{R_{CO_2}}\right)} \times 100\% = R_{CO_2} \times \left(\frac{TGA}{(100 - TGA)}\right) \times 100\% \quad \text{(Eq. 4)}$$

where *TGA* represents the percent weight change of the carbonated solid at its calcination temperature. On the other hand, Eq. 5 can be used if TCA was used for solid analysis.

$$Y_{CO_2,TCA} = R_{CO_2} \times \left(\frac{3.67 \times TCA}{(1 - 3.67 \times TCA)}\right) \times 100\% \quad \text{(Eq. 5)}$$

where *TCA* represents the weight fraction of carbon in the carbonated sample with a unit of $\left[\frac{Weight\ of\ carbon}{Weight\ of\ solid\ sample}\right]$. The coefficient 3.67 is introduced to Eq. 5 to account for the ratio of the molecular weights of $CO_2$ to C. Finally, for the estimation of the yield or extent of carbonation for minerals using TIC analysis, the following equation can be used.

$$Y_{CO_2,TIC} = R_{CO_2} \times \left(\frac{3.67 \times TIC}{(1 - 3.67 \times TIC)}\right) \times 100\% \quad \text{(Eq. 6)}$$

As illustrated here, reaction products with high mineralogical heterogeneity are difficult to study and analyze. Thus, it is important to select the appropriate analytical method and consider the assumptions involved in estimating carbon storage potential and extent of carbonation.

## 3. Investigation of Chemical and Morphological Changes during Mineral Carbonation

Previous studies were mostly focused on the kinetics and the extent of mineral carbonation. Those findings are important for designing engineered mineral carbonation processes and provide valuable insights into natural carbon storage processes in geologic formations. In addition to kinetic and carbonation yield data, additional chemical and morphological analyses of the reacted solid and liquid samples can be performed to shed light on the reaction mechanisms of carbon mineralization (Gadikota et al., 2013, 2014). Significant morphological changes during mineral dissolution and carbonation, in surface area, pore diameter and particle size, have implications for the volume changes, reaction mechanisms and safety of $CO_2$ storage in geologic formations. In experimental results illustrated in Figure 4, there was a significant increase in surface area as antigorite was dissolved in the absence of $CO_2$. For single-step carbonation, the surface area changes are even more complicated since the increase in surface area due to mineral dissolution potentially competes with surface area reduction due to carbonate overgrowths on reactant mineral grains as reported in our previous work (Gadikota et al., 2013, 2014). Either way, the changes in the surface area indicate changes in reactive surface area. This affects estimation of the surface reaction rate, and subsequent modeling of both surface area and reaction rate evolution. Thus, when feasible, it is recommended that future mineral dissolution and carbonation studies be performed in conjunction with in-depth mineralogical and morphological studies.

The formation of various carbonate minerals can be quantitatively and qualitatively assessed using X-Ray Diffraction (XRD) to support the results obtained using TGA, TCA and TIC analysis. Chemical analyses of the reaction fluid before and after the reaction are useful in

determining the overall material balance and the rate-limiting step in a single-step mineral carbonation. Chemical analyses of liquid samples collected throughout the carbonation study, together with the calculation of equilibrium fluid speciation and mineral solubility, can be used to quantify the extent of disequilibrium during experiments. Morphological changes, such as changes in pore volume, particle size and surface area variations during mineral dissolution and carbonation, can be related to mineral dissolution and carbonation mechanisms. Changes in the pore volume and surface area of the mineral are characterized using BET (Brunauer–Emmett–Teller Theory), while changes in the particle diameter and particle size distribution are determined using a Particle Size Analyzer. Morphological and chemical changes are analyzed qualitatively and quantitatively using Scanning Electron Microscopy (SEM), Transmission Electron Microscopy (TEM) coupled with Energy-Dispersive X-Ray Spectroscopy (EDS), and Wavelength Dispersive X-Ray Spectroscopy (WDS). A careful correlation between the kinetic data and the morphological changes is helpful for comprehensive understanding of mineral carbonation processes.

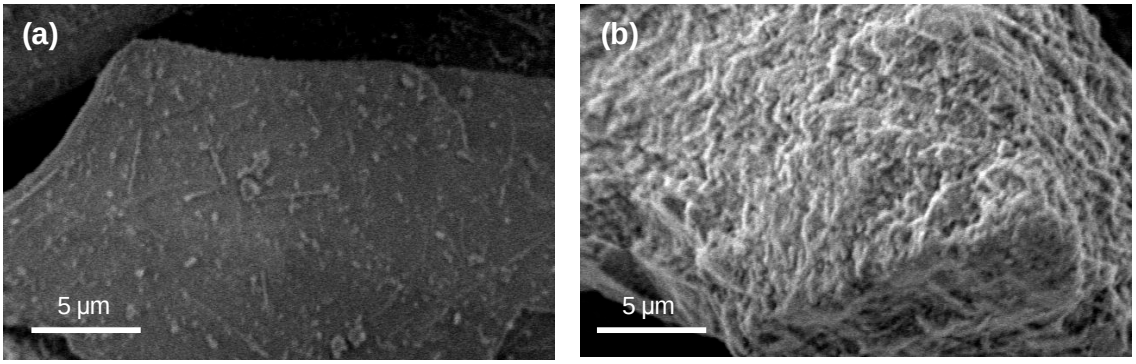


**Figure 4.** Unreacted antigorite (a). Reacted antigorite (b). Dissolution of antigorite in 0.01 M Na-oxalate at pH = 3.5 resulted in significant changes in the surface morphology and formation of etch pits.

## 4. Chemical and Morphological Changes during Olivine Carbonation

*(The contents of this section have published in Gadikota, G., J. Matter, P.B. Kelemen and A.-H. A. Park, Chemical and morphological changes during olivine carbonation for $CO_2$ storage in the presence of NaCl and $NaHCO_3$, Physical Chemistry Chemical Physics 16, 4679-4693, 2014).*

### 4.1 Introduction

The rising concentration of $CO_2$ in the atmosphere has detrimental environmental impacts and can be attributed to the increasing consumption of fossil fuels around the world. Therefore, various technologies and approaches for Carbon Capture, Utilization and Storage (CCUS), have been proposed to ensure more efficient carbon management. Among the carbon storage technologies, one of the safest and most permanent methods is carbon mineralization

(also known as mineral carbonation), which mimics the natural process of mineral weathering. In experiments on abundant, rock forming minerals, other than the comparatively rare mineral, wollastonite, the mineral olivine ($(Mg,Fe)_2SiO_4$) has been found to have the most rapid carbonation rates (Kelemen & Matter, 2008; Kelemen et al., 2011; Matter & Kelemen, 2009). Olivine is very far from equilibrium with the atmosphere and surface waters based on the Gibbs free energy quantified in Kelemen & Hirth (2012). Olivine is also known as the gemstone, peridot, and rocks with more than 40% olivine are called "peridotite". The Earth's upper mantle – from the base of the crust to a depth of ~ 400 km – is composed mainly of peridotite, with Mg/(Mg+Fe) ~0.9. Uplift and erosion exposes mantle peridotite on the surface during plate tectonic collisions. There are large deposits of olivine, including about 15,000 $km^3$ of peridotite in Oman in a block of oceanic crust and upper mantle thrust onto the Arabian continental margin (the SamailOphiolite), that can be used for either *in situ* or *ex situ* carbon mineralization schemes (Kelemen & Hirth, 2012; Kelemen & Matter, 2008; Kelemen et al., 2011; Matter & Kelemen, 2009; Nicolas et al., 2000).

The carbon mineralization process involves the reaction of $CO_2$ with silicate minerals containing Mg and/or Ca (Seifritz, 1990). As $CO_2$ is chemically fixed into the mineral matrix, it forms calcium and/or magnesium carbonates that are insoluble in water, thermally stable and environmentally benign (Lackner, 2002). Carbon mineralization is a multi-step process which involves $CO_2$ hydration as represented by Reactions 4-6 followed by mineral dissolution (Reaction 7) and carbonation (Reaction 8) with the olivine Mg end-member, forsterite ($Mg_2SiO_4$), as the representative mineral. Reaction 9 represents the overall reaction in which forsterite ($Mg_2SiO_4$) directly reacts with $CO_2$ in aqueous phase to form magnesium carbonate minerals (here represented as magnesite, $MgCO_3$) + dissolved $SiO_2$ or solid $SiO_2$ phases (quartz, chalcedony or opal). Depending on reaction conditions such as temperature, $CO_2$ partial pressure, presence of dissolved catalysts, pH, extent of $CO_2$ hydration, the rate of mineral dissolution, and/or the rate of solid carbonate mineral nucleation and growth can have important controls on the rate of carbon mineralization. Many studies have discussed the kinetics of each step of $CO_2$ hydration (Stirling & Pápai, 2010; Wang et al., 2009), forsterite dissolution (Awad et al., 2000; Brady et al., 1999; Chen & Brantley, 2000; Giammar et al., 2005; Hänchen et al., 2006; Oelkers, 2000; Pokrovsky & Schott, 2000; Wogelius & Walther, 1992), and conditions that favor the formation of various Mg-carbonate phases (Hänchen et al., 2008; Saldi et al., 2009, 2012). Understanding the limiting factors when all three steps occur simultaneously requires further investigation since this has implications for *in situ* and *ex situ* carbon mineralization.

$CO_2$ hydration: $2CO_{2\,(g)} \rightarrow 2CO_{2\,(aq)}$ (Rx. 4)

$$2CO_{2\,(aq)} + 2H_2O \leftrightarrow 2H_2CO_{3\,(aq)} \leftrightarrow 2H^+_{(aq)} + 2HCO^-_{3\,(aq)} \quad \text{(Rx. 5)}$$

$$2HCO^-_{3\,(aq)} \leftrightarrow 2CO^{2-}_{3\,(aq)} + 2H^+_{(aq)} \quad \text{(Rx. 6)}$$

Forsterite Dissolution: $Mg_2SiO_{4(s)} + 4H^+_{(aq)} \rightarrow 2Mg^{2+}_{(aq)} + H_4SiO_{4\,(aq)}$ (Rx. 7)

Carbonate Formation: $2Mg^{2+}_{(aq)} + 2CO^-_{3\,(aq)} \rightarrow 2MgCO_{3\,(s)}$ (Rx. 8)

Overall Reaction: $Mg_2SiO_{4(s)} + 2CO_{2(g)} + 2H_2O \rightarrow 2MgCO_{3(s)} + H_4SiO_{4(aq)}$ (Rx. 9)

$CO_2$ can be directly injected into peridotite, or other silicate rocks with abundant Mg and Ca such as basalt (Gislason et al., 2010; Kelemen & Matter, 2008; Matter & Kelemen, 2009; McGrail et al., 2006) to form solid carbonate minerals. This is known as *in situ* carbon storage. Another approach, referred to as *ex situ* carbon mineralization, involves mining and processing of silicate minerals prior to their reaction with $CO_2$ (Chizmeshya et al., 2007; Gerdemann et al., 2007; O'Connor et al., 2004; Park et al., 2003; Park & Fan, 2004; Yegulalp et al., 2001). For both *in situ* and *ex situ* carbon mineralization, a fundamental understanding of mineral dissolution and carbonation kinetics and the reaction mechanisms is important. A number of groups have carried out extensive work in this area (Awad et al., 2000; Chen & Brantley, 2000; Chizmeshya et al., 2007; Gerdemann et al., 2007; Giammar et al., 2005; Gislason et al., 2010; M. Hänchen et al., 2006; Hövelmann et al., 2012; Kelemen & Hirth, 2012; Kelemen & Matter, 2008; Kelemen et al., 2011; Lackner, 2002; Matter & Kelemen, 2009; McGrail et al., 2006; O'Connor et al., 2004; Park et al., 2003; Park & Fan, 2004; Saldi et al., 2009, 2012; Yegulalp et al., 2001).

Much significant work has been carried out to investigate the effects of the reaction temperature and the $CO_2$ partial pressure on carbon mineralization. Mineral dissolution kinetics can be enhanced by increasing reaction temperatures (Awad et al., 2000; Chen & Brantley, 2000; Giammar et al., 2005; Hänchen et al., 2006; Oelkers, 2000), which implies that the geothermal gradient can be utilized to enhance *in situ* carbon mineralization. Carbon mineralization is also found to be affected by the $CO_2$ partial pressure ($P_{CO2}$) and at $P_{CO2}$ greater than 75 atm, the mineral carbonation process can be enhanced due to higher concentrations of carbonate species in the aqueous phase (Gerdemann et al., 2007; O'Connor et al., 2004). Moreover, the reaction temperature and $P_{CO2}$ affect the chemical compositions of the formed magnesium carbonates (Hänchen et al., 2008; Saldi et al., 2009, 2012). At higher temperatures, anhydrous magnesium carbonate is formed (i.e., magnesite, $MgCO_3$), while at lower temperatures hydrated magnesium carbonates such as nesquehonite ($MgCO_3.3H_2O$) and hydromagnesite ($Mg_5(CO_3)_4(OH)_2 \cdot 4H_2O$) are dominant in experimental studies.

In important studies that guided our choices of reagents, O'Connor et al., (2004) at the Department of Energy's Albany Research Center (ARC) and Chizmeshya et al., (2007) at Arizona State University investigated olivine carbonation in $CO_2$ saturated aqueous solutions at varying temperatures and $P_{CO2}$ conditions, with the important addition of dissolved NaCl and bicarbonate compounds (mostly $NaHCO_3$, but also $KHCO_3$ and $RbHCO_3$). These groups found that the presence of these reagents, typically 1.0 M NaCl and 0.64 M $NaHCO_3$, led to a

substantial enhancement in the olivine reaction rate, when compared to studies of olivine dissolution at the same temperature, $P_{CO2}$ and pH. However, "separation of variables" was not completed, so that the independent, potentially catalytic roles of NaCl and $NaHCO_3$ were not well established.

Another important but less studied aspect of the carbon mineralization study is related to the changes in the structural features of the minerals such as the pore volume, surface area and particle size during the dissolution and carbonation processes of silicate minerals. Some studies have suggested that extensive carbonate growth may exert high crystallization pressures sufficient to create microfractures in geologic formations, which would expose additional unreacted mineral surface and increase the $CO_2$ storage capacity (Kelemen & Hirth, 2012; Kelemen & Matter, 2008; Kelemen et al., 2011; Matter & Kelemen, 2009). Others argue that the formation of carbonate crystals in minerals would simply block the pore spaces, reduce the reactive surface area and significantly slow down the *in situ* carbon mineralization process (Hövelmann et al., 2012; King et al., 2010; Xu et al., 2004).

This study investigated a number of these questions regarding reaction kinetics and mechanisms during carbon mineralization. The carbonation of one of the most widely investigated minerals, olivine, was studied to understand the corresponding changes in the chemical compositions and morphological structures during $CO_2$-olivine-water interactions. In addition to determining the morphological changes, there has been a considerable debate and an emerging concern related to appropriate methods for the quantification of $CO_2$(Watson et al., 2005). Therefore, the extents of carbonation were estimated using two separate methods: Thermogravimetric Analysis (TGA) and Total Carbon Analysis (TCA).

## 4.2. Experimental Methods

Ground Twin Sisters olivine procured from Washington State was provided by the group at Albany Research Center (ARC). Table 3 summarizes the composition of olivine. The mean particle size, surface area and cumulative pore volume of the ground unreacted olivine sample were found to be 21.40 µm, 3.77 $m^2$/g and 0.012 ml/g, respectively.

**Table 3.** Composition of Twin Sisters olivine.

| Components | Weight % | Components | Weight % |
|---|---|---|---|
| MgO | 47.30 | MnO | 0.15 |
| CaO | 0.16 | $Na_2O$ | 0.01 |
| $Fe_2O_3$ | 13.90 | $K_2O$ | < 0.01 |
| $SiO_2$ | 39.70 | $TiO_2$ | < 0.01 |
| $Cr_2O_3$ | 0.78 | $P_2O_5$ | < 0.01 |
| $Al_2O_3$ | 0.20 | $V_2O_5$ | < 0.01 |
| | | LOI% | -0.7 |

### 4.2.1. Carbonation of Olivine

The carbonation experiments were performed in a high temperature, high pressure batch reactor (Autoclave Engineers, 100 ml EZE-Seal) and the schematic of the experimental setup is shown in Figure 5. The reactor was connected to a high-pressure syringe pump (Teledyne Isco, 500D, NE), which can deliver up to 200 atm of pressurized $CO_2$ to the reactor. In a typical run, 50 ml of slurry containing 15 wt% of solids in the reaction fluid was charged to the reactor. The reactor was then sealed and the stirring speed was set at 800 rpm throughout the experiment since it was the optimum speed for effective mass and heat transfer within the reactor. Once the reactor temperature set-point was specified, it took about 30 minutes for the reactor temperature to be stabilized. After the desired reaction temperature was reached, the reactor pressure was increased to the desired partial pressure of $CO_2$, which marked the start of the experiment. The interior of the reactor was rinsed in water, and this water was filtered to obtain any solid material that had formed on the vessel walls. The filtered liquid samples were diluted ten times into 2% $HNO_3$ solution to prevent any subsequent precipitation, while the carbonated solid samples were dried at 70 $^oC$ for 12 hours. The amounts of dissolved Mg and other components (i.e., Si), which did not form solid phases, were quantified via elemental analysis of the liquid samples using Inductively Coupled Plasma - Atomic Emission Spectroscopy (ICP-AES, Activa S model, Horiba JobinYvon).

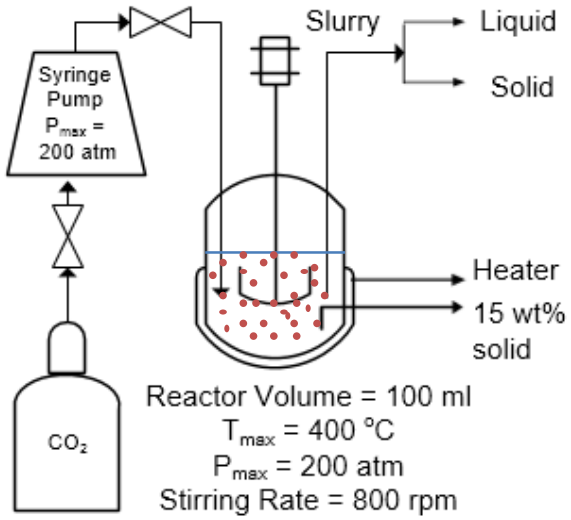


**Figure 5**. Schematic of high pressure, high temperature experimental setup for mineral carbonation.

### 4.2.2 Quantification of Mineralized $CO_2$

Both unreacted mineral and carbonated solid products were dried and analyzed using a battery of experimental techniques. The elemental compositions of the solid samples were determined using Wavelength Dispersion X-Ray Fluorescence (WD-XRF, PananalyticalAxios). The X-Ray diffraction patterns were also obtained (XRD 3000, Inel Inc.) in the range of $20^o$ and $80^o$ and CuKα radiation (λ = 1.5406 Å) to identify the changes in chemical compositions and

crystalline structures during the carbonation reaction. The extent of carbonation was determined using two separate methods: Thermogravimetric Analysis (TGA, Setaram SETSYS) and Total Carbon Analysis (TCA, LECO CS 844).

In a typical TGA run, samples were exposed to a $N_2$ environment (flow rate: 20 $ml \cdot min^{-1}$) as the temperature was ramped from 25 $^oC$ to 650 $^oC$ at a rate of 5 $^oC \cdot min^{-1}$ (Demir et al., 2003). Based on the weight drop related to each dehydroxylation or calcination temperature, the carbonate phase in the solid sample was identified and the extent of carbonation was determined based on the weight drop data (wt% in terms of [g of gas released / g of carbonated solids]. The estimation of the extent of carbonation based on the TGA method provided an insight into the presence of different solid phases (e.g., carbonate and hydrate phases as well as organic carbon with distinct decomposition temperature) and the quantification of each phase in the analyzed sample. On the other hand, the TGA technique can be difficult for samples with overlapping weight drop curves. Thus, the TGA method should be used for samples with clear distinction between weight drop curves, and this was the case for carbonated olivine samples.

In a typical TCA run, samples were placed in a ceramic boat and combusted in the presence of $O_2$ at temperatures as high as 1000 $^oC$. The combustion process converts all carbon – both inorganic and organic - into $CO_2$ and CO. The total carbon reported from the TCA [g of C / g of carbonated solids] was then converted into the extent of carbonation by comparing the TCA data with the theoretical carbon capture capacity of the minerals. The TCA generally provides much faster measurements compared to TGA and is relatively more accurate in measuring the total carbon content in solid samples. However, it cannot distinguish different carbonate or hydrate phases as well as organic carbon in solid samples. Thus, the carbon analysis unit should be used in a Total Inorganic Carbon (TIC) mode using acid digestion, especially when organic additives such as oxalate are present in the reaction fluid. However, the acid digestion method is quite slow compared to the TCA method. Since the reaction fluids used in our study did not contain organic additives, the TCA mode was used in conjunction with the TGA technique to estimate the extents of carbonation for olivine, and the results of both methods were compared to assess consistency.

### 4.2.3. Characterization of Morphological Properties

The changes in the pore structure and the specific surface area were determined using the BET technique (QuantachromeNovaWin BET Analyzer), while particle size and size distributions were determined via a laser diffraction method (Beckman Coulter, Inc., LS 13 320 MW). The surface morphological features and the corresponding elemental concentrations of mineral carbonates were determined using a Scanning Electron Microscopy (SEM, Tescan Vega II) linked to an Energy Dispersive X-ray Spectrometer (EDS, Oxford Instruments, Inca Software).

## 4.3. Results and Discussion

### 4.3.1 Estimation of Extent of Carbonation

The determination of the extent of mineral carbonation can be difficult, particularly if minerals involved are highly heterogeneous. Even for a homogeneous mineral specimen, the preparation of samples (e.g., different grinding methods resulting in distinct particle size distributions) can alter the carbonation results. Thus, the extent of mineral carbonation should be carefully estimated based on the mineralogy of the samples tested. In this study, the extent of carbonation was estimated relative to the theoretical carbon storage capacity of a mineral, $\frac{1}{R_{CO_2}}$ that is defined as the mass of $CO_2$ that can be trapped in a unit mass of the unreacted mineral. Conversely, $R_{CO_2}$ refers to the amount of the mineral needed to store a unit mass of $CO_2$(O'Connor et al., 2004).

The chemical fixation of $CO_2$ in the mineral matrix generally involves the leaching of alkaline metal ions into the aqueous phase and a subsequent carbonation reaction, represented by Reaction 10.

$$M^{n+}{}_{(aq)} + \frac{n}{2} CO_3^{2-}{}_{(aq)} \rightarrow M(CO_3)_{\frac{n}{2}\,(s)} \qquad \text{(Rx. 10)}$$

where M is an alkaline metal such as Ca, Mg and Fe that can react with $CO_2$ to form insoluble and thermodynamically stable mineral carbonates. Therefore, the $CO_2$ storage capacity of minerals, $\frac{1}{R_{CO_2}}$, can be expressed as following.

$$\frac{W_{CO_2}}{W_{mineral}} = \frac{1}{R_{CO_2}} = \sum \left( \frac{n}{2} . \frac{y_m}{MW_m} \right) \times MW_{CO_2} \qquad \text{(Eq. 6)}$$

where$W_{CO2}$ and $W_{mineral}$ are weights of $CO_2$ stored in the solid phase and the mineral before its carbonation, respectively. $y_m$refers to the mass fraction of alkaline metal in the mineral that can react with $CO_2$ to form insoluble metal carbonate. $MW_m$is the molecular weight of alkaline metal species and $\frac{n}{2}$ refers to the stoichiometric coefficient of $CO_2$ as represented in Reaction 10. The divalent alkaline metal species, Mg, Ca and Fe, are the most abundant alkaline metals that form carbonate minerals, with $\frac{n}{2} = 1,$ and thus, Equation 6 can be simplified to Equation 7 below.

$$\frac{W_{CO_2}}{W_{mineral}} = \frac{1}{R_{CO_2}} = \left( \frac{y_{Mg}}{MW_{Mg}} + \frac{y_{Ca}}{MW_{Ca}} + \frac{y_{Fe}}{MW_{Fe}} \right) \times MW_{CO_2} \qquad \text{(Eq. 7)}$$

While iron (II) oxide can react with $CO_2$ to form siderite ($FeCO_3$), it has been reported that the formation of siderite is inhibited by the low solubility of iron oxide, which may precipitate from the solution before siderite is formed(O'Connor et al., 2004). Thus, in this paper the $CO_2$ storage capacity of olivine was calculated using both equations that were developed assuming the formation of iron carbonate (Eq. 7) and the absence of iron carbonate (Eq. 8).

$$\frac{W_{CO_2}}{W_{mineral}} = \frac{1}{R_{CO_2}} = \left(\frac{y_{Mg}}{MW_{Mg}} + \frac{y_{Ca}}{MW_{Ca}}\right) \times MW_{CO_2} \quad \text{(Eq. 8)}$$

The yield or the extent of carbonation, $Y_{CO_2}$, is then defined as the measured amount of $CO_2$ stored in the mineral as solid carbonate relative to the $CO_2$ storage capacity given by Equations 7 or 8. In this study, separate expressions of $Y_{CO2}$ have been developed for the two different carbon analysis techniques, Equations 9 and 10. Where the TGA method was used to analyze the carbonated solids, the following expression was used for Yield or Extent of Carbonation, $Y_{CO_2,TGA}$.

$$Y_{CO_2,TGA} = \left[\frac{Measured\ weight\ ratio\ of\ CO_2\ stored\ in\ mineral}{The\ residual\ CO_2\ storage\ capacity}\right] \times 100\%$$

$$= \frac{\left(\frac{W_{CO_2}}{W_{mineral}}\right)}{\left(\frac{1}{R_{CO_2}}\right)} \times 100\% = R_{CO_2} \times \left(\frac{TGA}{(100 - TGA)}\right) \times 100\% \quad \text{(Eq. 9)}$$

where *TGA* represents the percent weight change of the carbonated solid at its calcination temperature. On the other hand, Equation 10 was used when TCA was used for the solid analysis.

$$Y_{CO_2,TCA} = R_{CO_2} \times \left(\frac{3.67 \times TCA}{(1 - 3.67 \times TCA)}\right) \times 100\% \quad \text{(Eq. 10)}$$

where *TCA* represents the weight fraction of carbon in the carbonated sample with a unit of $\left[\frac{Weight\ of\ carbon}{Weight\ of\ solid\ sample}\right]$. The coefficient 3.67 is introduced to Equation 10 to account for the ratio of the molecular weights of $CO_2$ to carbon. Extents of carbonation using TGA and TCA were compared and reported in the subsequent sections.

### 4.3.2. Effect of Reaction Time

Investigation of the effect of the reaction time on the extent of olivine carbonation provided insight into the kinetics of mineral carbonation. Changes in the morphological structure of olivine as a function of the reaction time were also probed to study reaction mechanisms. Experiments were performed at reaction times of 1, 3, and 5 hours, at 185 $^{o}$C, $P_{CO2}$ of 139 atm ($P_{total}$ = 150 atm) in 1.0 M NaCl + 0.64 M $NaHCO_3$ with 15 wt% solid and a stirring rate of 800 rpm. These were the reaction conditions used in several prior studies, including those of the ARC group (Gerdemann et al., 2007; O'Connor et al., 2004). The extents of olivine carbonation were estimated using both TGA and TCA methods, and their average values are reported in Table 4 and Figure 6(a). These results were compared with the results of similar studies at ARC (Gerdemann et al., 2007; O'Connor et al., 2004). Average values of olivine carbonation range from 49.4-79.1% assuming the formation of Ca, Mg, and Fe carbonates and from 56.6-90.5% assuming Ca, and Mg carbonate formation (Table 4, Figure 6(a)). These results were compared with the results of similar studies at ARC (Gerdemann et al., 2007; O'Connor et al., 2004).

**Table 4.** Summary of mean particle sizes, surface areas and extents of carbonation of olivine reacted at varying reaction times, temperatures, $CO_2$ partial pressures and chemical additives. The slurry concentration was 15 wt% and a stirring speed of 800 rpm was maintained. Extents of carbonation are reported as an average of TGA and TCA estimates.

| | Mean Particle Size (μm) | Surface Area ($m^2/g$) | Extent of Carbonation (%) | |
|---|---|---|---|---|
| | | | (assuming the formation of Ca, Mg and Fe carbonates) | (assuming the formation of Ca and Mg carbonates) |
| ***Effect of Reaction Time*** *(185 $^oC$, $P_{CO2}$ =139 atm, 1.0 M NaCl+0.64 M $NaHCO_3$)* | | | | |
| 1 hour | 23.97 | 1.25 | 49.4 ± 1.3 | 56.6 ± 1.5 |
| 3 hours | 27.34 | 0.96 | 74.6 ± 2.6 | 85.3 ± 3.1 |
| 5 hours | 27.70 | 0.15 | 79.1 ± 4.9 | 90.5 ± 5.6 |
| ***Effect of Partial Pressure of $CO_2$*** *(185 $^oC$, 3 hours, 1.0 M NaCl+0.64 M $NaHCO_3$)* | | | | |
| 64 atm | 20.69 | 3.20 | 34.3 ± 0.8 | 39.3 ± 0.9 |
| 89 atm | 26.19 | 1.73 | 52.3 ± 1.9 | 59.9 ± 2.1 |
| 139 atm | 27.34 | 0.96 | 73.5 ± 2.8 | 85.3 ± 3.1 |
| 164 atm | 27.96 | 0.80 | 73.3 ± 2.5 | 83.9 ± 2.8 |
| ***Effect of Temperature*** *($P_{CO2}$ = 139 atm, 3 hours, 1.0 M NaCl+0.64 M $NaHCO_3$)* | | | | |
| 90 $^oC$ | 15.36 | 2.01 | 2.6 ± 0.3 | 3.0 ± 0.3 |
| 125 $^oC$ | 18.51 | 1.10 | 24.6 ± 0.3 | 28.2 ± 0.4 |
| 150 $^oC$ | 25.40 | 1.07 | 61.6 ± 1.6 | 70.5 ± 1.8 |
| 185 $^oC$ | 27.34 | 0.96 | 73.5 ± 2.8 | 85.3 ± 3.1 |
| ***Effect of [$NaHCO_3$]*** *(185 $^oC$, $P_{CO2}$ = 139 atm, 3 hours)* | | | | |
| Deionized Water | 16.43 | 2.79 | 5.0 ± 0.3 | 5.8 ± 0.3 |
| 0.32 M $NaHCO_3$ | 17.64 | 1.63 | 9.5 ± 0.7 | 10.9 ± 0.8 |
| 0.48 M $NaHCO_3$ | 26.54 | 1.51 | 49.0 ± 0.4 | 56.0 ± 0.5 |
| 0.64 M $NaHCO_3$ | 26.58 | 1.20 | 72.2 ± 3.1 | 82.7 ± 3.6 |
| 1.00 M $NaHCO_3$ | 29.43 | 1.15 | 74.3 ± 1.7 | 85.0 ± 1.9 |
| 2.00 M $NaHCO_3$ | 30.02 | 1.15 | 79.7 ± 5.2 | 91.2 ± 6.0 |
| ***Effect of [NaCl]*** *(185 $^oC$, $P_{CO2}$ = 139 atm, 3 hours)* | | | | |
| Deionized Water | 16.43 | 2.79 | 5.0 ± 0.3 | 5.8 ± 0.3 |
| 0.50 M NaCl | 14.87 | 2.54 | 5.9 ± 0.3 | 6.8 ± 0.3 |
| 0.75 M NaCl | 17.06 | 2.50 | 9.0 ± 0.5 | 10.3 ± 0.6 |
| 1.00 M NaCl | 17.16 | 2.50 | 12.8 ± 0.4 | 14.4 ± 0.9 |

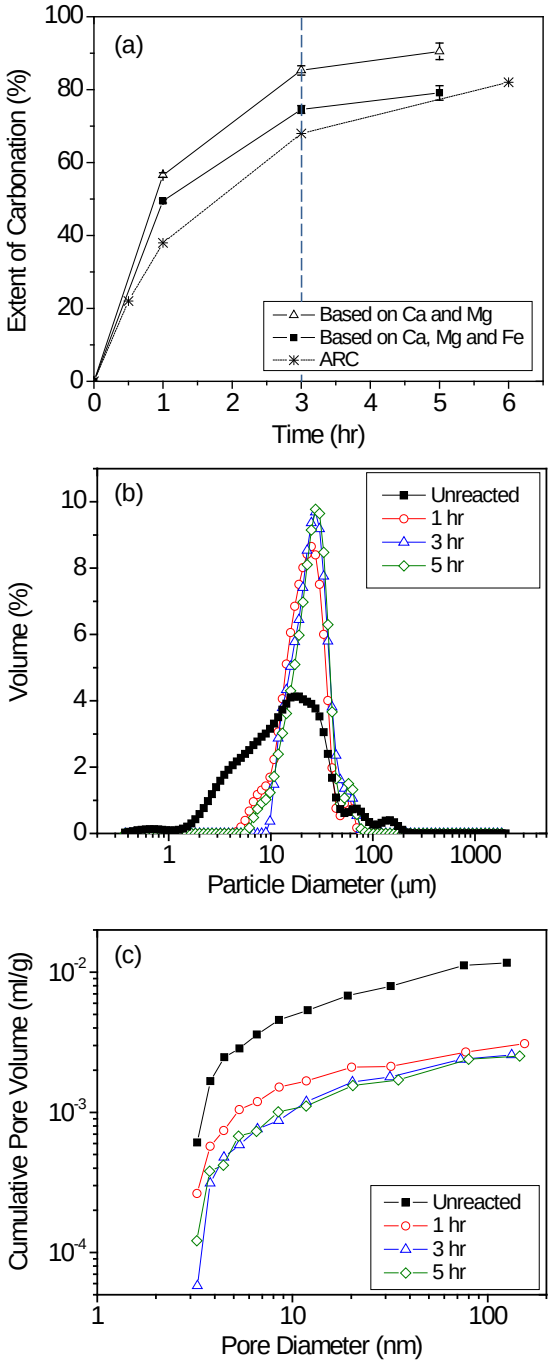


**Figure 6**. Effect of reaction time on (a) extent of olivine carbonation based on two $CO_2$ storage capacity calculations (Equations (2) and (3)), (b) particle size distribution, and (c) cumulative pore volume. Experiments were conducted at 185 $^{o}$C, $P_{CO2}$ = 139 atm in 1.0 M NaCl + 0.64 M $NaHCO_3$ with 15 wt% solid and a stirring speed of 800 rpm. ARC study was performed under same conditions but 1 hour, $P_{CO2}$ = 150 atm, 1000 rpm, and included Fe-carbonate formation (O'Connor et al., 2004)

As discussed earlier, estimating the extent of olivine carbonation proved to be a challenge due to the role of iron. The potential formation of Fe-carbonates (i.e., siderite) has been debated (Gerdemann et al., 2007; O'Connor et al., 2004; Saldi et al., 2013). As a result of their low solubility, iron oxide minerals may precipitate prior to the formation of siderite. In this study, siderite was not detected in any XRD analyses of carbonated olivine samples. Both Equations 7 and 8 were used to estimate the extent of olivine carbonation in order to compare our results with those of the ARC group. As summarized in Table 4, the extents of olivine carbonation via formation of Ca- and Mg-carbonates were 56.6, 85.3 and 90.5% for 1, 3 and 5 hour reactions, respectively. These values are 7 to 11 % higher than estimates made including the formation of siderite as well as Ca- and Mg-carbonates. The extent of olivine carbonation calculated for Fe-, Ca- and Mg carbonates resulted in values close to those of the ARC, since ARC included all of these in their calculations. In any case, the rate of olivine carbonation was reduced after 3 hours in our results and those of the ARC, as shown in Figure 6(a).

The analysis of fluid samples revealed that the total concentration of Mg-species was 39.8, 27.6 and 24.5 ppm at the end of 1, 3 and 5 hour reactions, respectively. These values are significantly lower than the equilibrium total Mg concentration of 218 ppm at the given reaction conditions based on PhreeqC calculations (Parkhurst & Appelo, 1999). The concentration of Mg in solution could increase over time due to olivine dissolution alone, and decrease due to precipitation of carbonate minerals. In our experiments, combined olivine dissolution and carbonate precipitation resulted in a net decrease in the concentration of Mg in solution over time. This implies that as olivine dissolved to release Mg into solution, the dissolved species were readily carbonated to precipitate magnesium carbonates. This indicates that olivine dissolution may have been the rate limiting step in the process. Also, because precipitation of Mg-carbonates held dissolved Mg concentrations below the equilibrium level, olivine dissolution rates may have remained relatively high throughout the experiments.

In order to provide further insights into the olivine carbonation mechanism, the changes in the morphological structure of olivine in terms of the surface area, particle size and pore volume distributions were investigated. As olivine was carbonated for 1, 3 and 5 hours, its mean particle size increased from 21.40 μm to 23.97, 27.34 and 27.70 μm, respectively (Table 4). A comparison of the particle size distributions before and after carbonation revealed that fine particles smaller than 10 μm dissolved much faster than coarser grains, resulting in a narrower particle size distribution shifted towards larger particle sizes (Figure 6(b)). Precipitation of carbonates on olivine surfaces also contributed to increasing particle size. The particle size distributions of 3 and 5-hour runs were not significantly different, as they had similar extents of carbonation. BET analyses also showed a significant reduction in surface area, from an initial value of 3.77 to 1.25, 0.96 and 0.15 $m^2/g$ when olivine was reacted for 1, 3, and 5 hours, respectively. A similar trend was observed for the cumulative pore volume of olivine during the experiments. A reduction in the cumulative pore volumes from 0.0120 to 0.0030, 0.0026, and 0.0025 ml/g was observed when olivine was reacted for 1, 3 and 5 hours, respectively (Figure

6(c)). The reduction of the surface area and the pore volume suggest the rapid disappearance of fine particles with high surface to volume ratios (< 10 μm) as well as the growth of carbonate precipitates in the pores and surfaces of olivine particles.

These morphological data are valuable since mineral weathering studies typically assume negligible changes in the surface area and the pore volume during reactions, which is not always the case. Therefore, throughout this study the discussion of the extent of olivine carbonation was accompanied with its morphological change results.

### 4.3.3. Effect of Partial Pressure of $CO_2$

Since pressures of 100-150 atm have been considered as the optimum pressure for $CO_2$ transportation in pipelines, most previous studies on mineral carbonation were performed within this $P_{CO2}$ range (Gerdemann et al., 2007; O'Connor et al., 2004). In order to more fully quantify the effect of $CO_2$ pressure on mineral carbonation rates, our experiments were performed at $P_{CO2}$ ranging from 64 to 164 atm, while holding other reaction parameters constant at 185 $^{o}$C in 1.0 M NaCl + 0.64 M $NaHCO_3$ (as in many previous experiments at ARC (Gerdemann et al., 2007; O'Connor et al., 2004) and Arizona State University (Chizmeshya et al., 2007) for 3 hours with 15 wt% solid and at a stirring rate of 800 rpm. The extent of olivine carbonation at 64, 89, 139, and 164 atm was 39.3, 59.9, 85.3, and 83.9%, respectively, based on the average value of TCA and TGA data assuming the formation of Ca and Mg-carbonates.

As shown in Figure 7(a), the difference between TCA and TGA data was not significant. The complete list of carbonation data is given in Table 4, where the extents of olivine carbonation are reported as an average of TGA and TCA estimates for both equations 9 and 10. The extents of carbonation were lower by about 5% and 10% for cases with low and high extents of carbonation, respectively, if the potential formation of siderite was included. In any case, a significant increase in the extent of carbonation from 64 atm to 139 atm was observed, while the extents of carbonation leveled off beyond 139 atm. ARC group's 1 hour experiments agreed with this observation (Gerdemann et al., 2007; O'Connor et al., 2004).

Ignoring the result for the experiment at 164 atm, because olivine was almost completely consumed at both 139 and 164 atm, the net rate of olivine carbonation (mass fraction per second) could be represented by the following equation where $P_{CO2}$ is in atm.

$$Rate\ of\ Olivine\ Carbonation = -5.13 \times 10^{-5} + 1.11 \times 10^{-5}\sqrt{P_{CO2}} \qquad \text{(Eq. 11)}$$

Strikingly, despite differences in grain size and experimental run duration, the dependence on $P_{CO2}$ in this study was almost identical to the slope of the expression fit to the results of O'Connor et al., (2004) by Kelemen & Matter (2008) as represented by the following equation.

$$Rate\ of\ Olivine\ Carbonation = 1.15 \times 10^{-5}\sqrt{P_{CO2}} \qquad \text{(Eq. 12)}$$

The rate of reaction in our study was systematically ~ 2x slower than the extent of reaction in the ARC study at similar temperature and $P_{CO2}$ (see Kelemen and Matter (2008), Supplementary Figures S5 and S4). A combined fit for the two data sets resulted in the following expression that is quite similar to the expression for each data set individually.

$$Rate\ of\ Olivine\ Carbonation = 1.031 \times 10^{-5}\sqrt{P_{CO2}} \quad \text{(Eq. 13)}$$

The $CO_2$ pressure influences a number of parameters during aqueous mineral carbonation including the pH of the solution, the dissolution of carbon into the aqueous phase, and speciation of dissolved carbon in bicarbonate and carbonate ions. In order to investigate the effect of $P_{CO2}$ on these parameters, PhreeqC modeling was performed for a closed system of forsterite-reaction fluid-$CO_2$. Forsterite, $Mg_2SiO_4$ (no Ca or Fe), is the Mg-end member of the olivine solid solution series, and is included in the PhreeqC database. As expected, the equilibrium pH of the solution, calculated using PhreeqC, decreased from 6.65 to 6.53, 6.36 and 6.29 as the partial pressure of $CO_2$ was increased from 64 atm to 89, 139 and 164 atm, respectively. While this change in the pH is relatively small, the mineral carbonation is a multistep process with a number of parallel and competing reactions. At low pH, olivine dissolution is rapid, but precipitation of $MgCO_3$ is limited. At high pH, $MgCO_3$ forms readily, but olivine dissolution is very slow. Our experiments and previous work revealed that high concentrations of $NaHCO_3$ in solution buffer pH at intermediate values where both olivine dissolution and carbonate precipitation are both favored. The high $CO_2$ pressure caused higher solubility of carbon species in the fluid, increasingly high compared to equilibrium values for $MgCO_3$ precipitation. A detailed discussion of the role of $CO_2$ hydration in olivine carbonation is given in the Section 4.3.5.

Particle size analyses of carbonated solids showed that the mean particle size did not change significantly when olivine was carbonated at 64 atm, whereas at 89, 139 and 164 atm, the particle size increased from 21.40 to 26.19, 27.34 and 27.96 μm, respectively (Table 4). The particle size distributions provide more insights into the olivine carbonation mechanism. In all cases, the number of fines decreased significantly and progressively, and the particle size distributions became narrower and shifted towards larger sizes with increasing $P_{CO2}$ (Figure 7(b)). The extents of olivine carbonation at 139 and 164 atm cases were quite similar at about 84-85%, and the particle size distribution results matched as well (Figure 7(a), 7(b) and Table 4).

The increase in particle size is also reflected in changing surface area and pore volume of carbonated olivine. The surface area of the olivine decreased from 3.77 $m^2/g$ for unreacted olivine to 3.20, 1.73, 0.96, and 0.80 $m^2/g$ at 64, 89, 139 and 164 atm, respectively (Table 4). Cumulative pore volume followed the same trend as surface area. The cumulative pore volume decreased from 0.012 ml/g for unreacted olivine to 0.0094, 0.0036, 0.0026, and 0.0029 ml/g for samples carbonated at 64, 89, 139 and 164 atm, respectively (Figure 7(c)). The observed simultaneous changes in composition and morphology suggest that conventional methods of

estimating mineral dissolution and carbonation rates assuming constant pore volume and surface area during mineral carbonation may have resulted in significant inaccuracy in rate estimation.

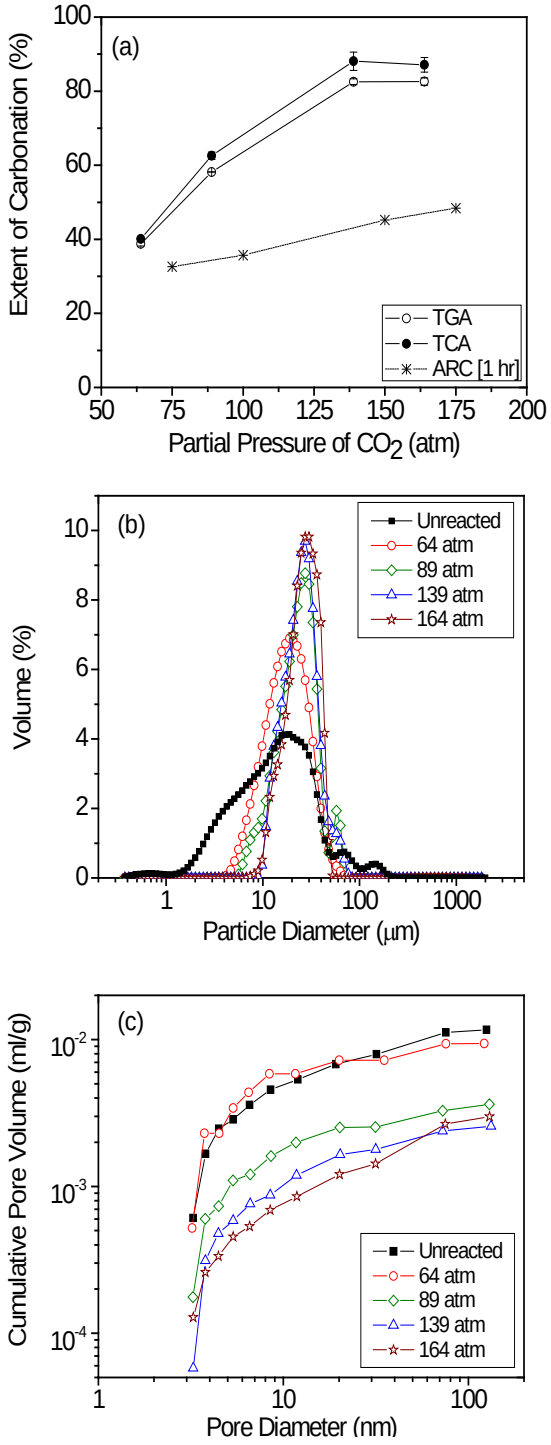


**Figure 7**. Effect of $CO_2$ partial pressure on (a) extent of olivine carbonation based on the formation of Mg and Ca carbonates, (b) particle size distribution, and (c) cumulative pore volume. Experiments were conducted at 185 $^{o}$C in 1.0 M NaCl + 0.64 M $NaHCO_3$ for 3 hours,

with 15 wt% solid and a stirring speed of 800 rpm. ARC study was performed under same conditions but 1 hour, $P_{CO2}$ = 150 atm, 1000 rpm, and included Fe-carbonate formation(O'Connor et al., 2004)

### 4.3.4. Effect of Reaction Temperature

A number of studies have investigated the effect of temperature on olivine dissolution (Awad et al., 2000; Chen & Brantley, 2000; Giammar et al., 2005; M. Hänchen et al., 2006; Oelkers, 2000) and carbonation (Chizmeshya et al., 2007; Gerdemann et al., 2007; O'Connor et al., 2004). Previous results indicate that dissolution is favored at high temperature, while olivine carbonation rate is maximized at ~ 185 °C over a range of $P_{CO2}$. Furthermore, it was also reported that magnesite, $MgCO_3$ – rather than hydrated magnesium carbonate minerals such as nesquehonite and hydromagnesite – forms at higher reaction temperatures, as we found in this study. In all of our experiments (90 – 185 $^{o}$C), the precipitated Mg-carbonate phase was magnesite. While the chemical compositions of the carbonated species have been well documented for various reaction conditions, the corresponding morphological features have not been well understood. Thus, a series of olivine carbonation experiments were performed, while monitoring the particle size, the surface area, and particle size and pore volume distributions. The temperature range of 90 to 185 $^{o}$C was selected since it is the temperature range commonly present at CO2 injection sites. The experiments were performed in a solution of 1.0 M NaCl + 0.64 M $NaHCO_3$ at $P_{CO2}$ = 139 atm for 3 hours with 15 wt% solid and at a stirring rate of 800 rpm.

The extents of olivine carbonation at 90, 125, 150 and 185 $^{o}$C were found to be 3.0, 28.2, 70.5 and 85.3%, respectively considering the formation of Mg and Ca-carbonates. These are the average values of the TGA and TCA data, which were quite consistent (Figure 8(a)). The ARC's results obtained for one-hour olivine carbonation study were compared to this study as shown in Figure 8(a) and the trend was very similar (Gerdemann et al., 2007; O'Connor et al., 2004).

These experimental results were well fit by the following expression (Equation 14) which was strikingly similar to the fit (Equation 15) obtained by Kelemen and Matter for the experimental data of O'Connor et al., (2004), despite differences in fluid/rock ratio, grain size and run duration. In the following equations, the unit of temperature is Celsius.

$$Rate\ of\ Olivine\ Carbonation = 9.3 \times 10^{-5} + e^{(-0.000383 \times (T-185)^2)} \quad \text{(Eq. 14)}$$

$$Rate\ of\ Olivine\ Carbonation = 1.38 \times 10^{-4} + e^{(-0.000334 \times (T-185)^2)} \quad \text{(Eq. 15)}$$

The expressions were similar despite the fact that time series results, both in our study and the ARC results, showed decreasing carbonation rates with reaction times varying from 1 to 3 hours. This temporal decrease in rates was relatively unimportant because the combined effects

of temperature and $P_{CO2}$, in the presence of $NaHCO_3$-rich aqueous solutions, yielded a four to five order of magnitude variation in experimental extents of olivine carbonation at temperatures from ~ 25 to 250 °C and $P_{CO2}$ from ~20 to 250 atm in the ARC results, and a one to two order of magnitude variation in our new results (90-185 °C, $P_{CO2}$ of 64 to 164 atm). A combined fit for our new data and those of O'Connor et al., (2004) yielded the following expression:

$$Rate\ of\ Olivine\ Carbonation = 1.13 \times 10^{-4} + e^{(-0.000330 \times (T-185)^2)} \quad \text{(Eq. 16)}$$

The consistency between these studies, and our other results described below, suggests that the rate expressions derived by Kelemen & Matter (2008) can be confidently used for order-of-magnitude estimation of olivine carbonation rates as a function of temperature and $P_{CO2}$ in aqueous fluids with > 0.5 M $NaHCO_3$ with olivine grain sizes of tens of microns.

A more comprehensive expression of the olivine carbonation rate incorporating temperature and partial pressure of $CO_2$ using ARC results O'Connor et al., (2004) in the presence of aqueous fluids with more than ~ 0.5 M $NaHCO_3$, with grain sizes of tens of microns was developed by Kelemen & Matter (2008) as represented by Equation 17.

$$Rate\ of\ Olivine\ Carbonation\ = 1.15\ \times 10^{-5} \sqrt{P_{CO2}} \times e^{-0.00033 \times (T-185)^2} \quad \text{(Eq. 17)}$$

A modified expression fit to our new results as well as the ARC results (O'Connor et al., 2004) which was very similar to Equation 4.12 is also represented below.

$$Rate\ of\ Olivine\ Carbonation\ = 1.03\ \times 10^{-5} \sqrt{P_{CO2}} \times e^{-0.00033 \times (T-185)^2} \quad \text{(Eq. 18)}$$

The small differences in the rate expressions are attributed to the uncertainty in olivine carbonation rates under the relevant experimental conditions.

Small deviations between our new data and the results of the ARC study were mainly due to the longer reaction times in our experiments, and the fact that we did not include carbonation of Fe for the $Y_{CO2}$ calculations in this study, as discussed in a previous section. The differences in the extents of carbonation when siderite formation was included vs. not considered were 0.4% at 90 $^oC$ and 10% at 185 $^oC$, as shown in Table 4. Solution analyses revealed the relative rates of mineral dissolution and carbonation at different temperatures. Mg concentrations in the fluid samples collected at the end of each run were 106.0, 87.3, 38.2 and 27.6 ppm at 90, 125, 150 and 185 $^oC$, respectively. These concentrations were measured after the reactor was cooled, depressurized, and the slurry was filtered at ambient temperature. However, comparing these concentrations with equilibrium concentrations was challenging because simulations suggested that the speciation may have changed significantly as the reaction was quenched and the reactor was depressurized. Quench effects on the solubility of various species vary with temperature, but were found to be negligible compared to the mass of magnesite precipitated in the higher temperature experiments.

The effect of the increase in reaction temperature on olivine carbonation could be complex. For instance, higher temperature would (i) lower $CO_2$ solubility, (ii) in turn, increase the solution pH, (iii) favor mineral dissolution, (iv) enhance mineral dissolution and carbonation kinetics, and (v) reduce the solubility of magnesite(Bénézeth et al., 2011). To probe the temperature effect, a series of PhreeqC(Parkhurst & Appelo, 1999) thermodynamic simulations were performed using the Lawrence Livermore National Laboratory (LLNL) thermodynamic database. These simulations revealed that the solubility of magnesite decreases significantly with increasing temperature. In addition, the simulations revealed that the pH of the solution equilibrated with $CO_2$ were 6.19, 6.24 and 6.51 at 90, 125 and 185 $^{o}$C, respectively. As temperature increased from 90 to 185 $^{o}$C, the pH was increased by only 0.32. While past studies indicated that small changes in pH have a minor effect on olivine dissolution (Palandri & Kharaka, 2004), it is important to note that pH changes can impact carbonate concentrations. An equivalent change in the pH of 0.32 increased the concentration of carbonate ions in the liquid phase by 52% from $4.91x10^{-4}$ to $7.58x10^{-4}$ mol/kg based on PhreeqC calculations, which contributed to the enhancement in the extent of olivine carbonation with increasing temperature. Our studies indicated that as olivine was dissolved, the presence of carbonates ions served as a sink for Mg by forming magnesium carbonate. As a result, there was a constant driving force facilitating the release of Mg into solution, which was also favored by the decrease in the solubility of magnesite with increasing temperature.

Considering that the extent of olivine carbonation drastically increased from 3.0% at 90 $^{o}$C to 85.3% at 185 $^{o}$C, a large variation in the particle size and particle size distribution of the mineral slurry system was expected for products of reaction at different reaction temperatures. There are two competing factors influencing the particle size of the mineral particulate system: size reduction via mineral dissolution and size increase due to carbonate precipitation on remaining olivine particles. Instead, it was found that the mean particle size before and after the carbonation reaction was not significantly changed. However, there was an interesting trend in particle size and size distribution as a function of reaction temperature.

As shown in Figures 9(a) and 9(b), at lower temperatures (90 – 125 $^{o}$C), the measured mean particle sizes after olivine carbonation were slightly smaller (15.36 - 18.51 μm) than that of unreacted olivine (21.40 μm) whereas the Mg concentration was highest and the overall extent of carbonation remained low as discussed earlier.This suggests that olivine dissolution dominated over magnesium carbonate precipitation at lower end of our experimental temperature range. On the other hand, at 150 and 185 $^{o}$C, an increase in the mean particle size from 21.40 (unreacted) to 25.40 and 27.34 μm was observed.The narrower particle size distribution at higher reactiontemperatures led to an increased mean particle size while the upper limit of the particle size was slightly reduced.

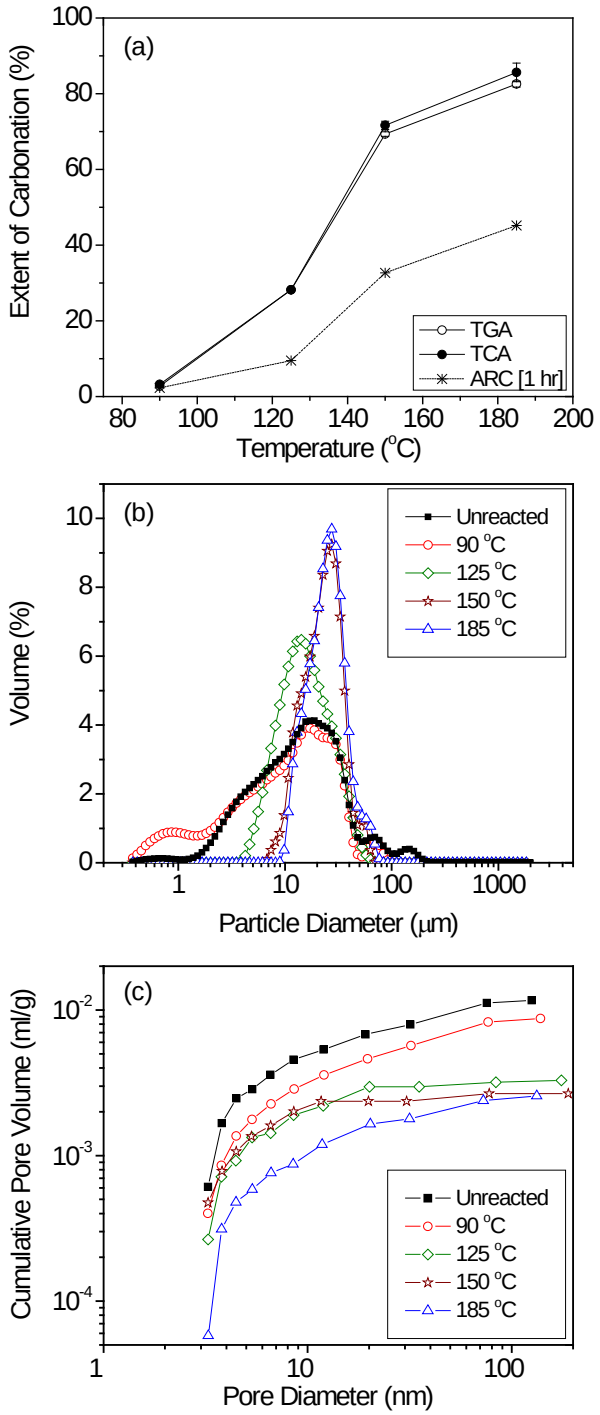


**Figure 8**. Effect of temperature on (a) extent of olivine carbonation based on the formation of Mg and Ca carbonates, (b) particle size distribution, and (c) cumulative pore volume. Experiments were conducted at $P_{CO2}$ = 139 atm in 1.0 M NaCl + 0.64 M $NaHCO_3$ for 3 hours, with 15 wt% solid and a stirring speed of 800 rpm. ARC study was performed under same conditions but 1 hour, $P_{CO2}$ = 150 atm, 1000 rpm, and included Fe-carbonate formation(O'Connor et al., 2004).

With an enhanced rate of mineral dissolution at high temperatures, a rapid disappearance of fines (< 10 μm) was expected. Figure 8(b) does show such a trend in all cases except there was an increased number of fines for the 90 °C case. A comparison of the SEM images in Figure 9 along with the previously discussed solid and liquid sample analyses suggests that fines were mostly likely small silica particles detached from the incongruently dissolved olivine surface, or small, newly nucleated magnesite crystals. For the higher temperature cases, such as at 185 $^{o}$C, significant magnesite growth to form larger crystals was evident.

BET analyses revealed that the surface area decreased from 3.77 (unreacted) to 2.01, 1.10, 1.07 and 0.96 $m^2$/g at 90, 125, 150 and 185 $^{o}$C, respectively, during olivine carbonation (Table 4). As shown in Figure 8(c), the changes in the cumulative pore volume followed the same trend as the surface area. The cumulative pore volume decreased from 0.012 (unreacted) to 0.0087, 0.0033, 0.0027, and 0.0026 $m^2$/g at 90, 125, 150 and 185 $^{o}$C, respectively. At higher temperatures where greater extents of olivine carbonation were achieved, the decrease in the cumulative pore volume was more notable due to the formation of carbonates in the pore spaces.

XRD analyses (as represented in Figure 10) were performed to identify the carbonated minerals, since the formation of different carbonate phases would influence the morphological characteristics of carbonated mineral. Prior studies have reported that reaction temperature is an important factor in controlling precipitation of nesquehonite ($MgCO_3.3H_2O$), hydromagnesite ($Mg_5(CO_3)_4(OH)_2 \cdot 4H_2O$) and magnesite ($MgCO_3$) in order of increasing temperature (Hänchen et al., 2008; Saldi et al., 2009, 2012). With increasing temperature, the coordination of water molecules is disrupted which results in the formation of magnesite(Hänchen et al., 2008).Thus, it was concluded that the morphological changes in carbonated olivine at different temperatures was not due to a change in the type of Mg-carbonate.

Meanwhile, as shown in Figures 9(b) and 9(c) the changes in the overall morphology of the carbonated olivine system, containing $MgCO_3$ as well as silica and unreacted olivine, were strongly affected by the extent of carbonation and the location of carbonation precipitation (i.e., on or away from the olivine substrate). The formation of magnesite and silica rich phases as discussed in Béarat et al., (2006), King et al., (2010), and Daval et al., (2011) was evident from Figures 10 (c), 10 (d), 10 (e), and 10 (f). The reduction in the pore spaces is attributed to the extensive growth of magnesite on the surface of olivine grains as evident from Figure 9 (e). Hövelmann et al., (2012) concluded that carbonation of only 10% reduced the porosity by half, and concluded that the carbonation reaction was self-limiting. In our studies however, despite almost an order of magnitude decrease in the pore volume of olivine reacted 185 $^{o}$C compared to unreacted olivine, about 85% carbonation was achieved. Since the highest carbonation of olivine was achieved at 185 $^{o}$C, in this and previous studies, all subsequent experiments were performed at this temperature.

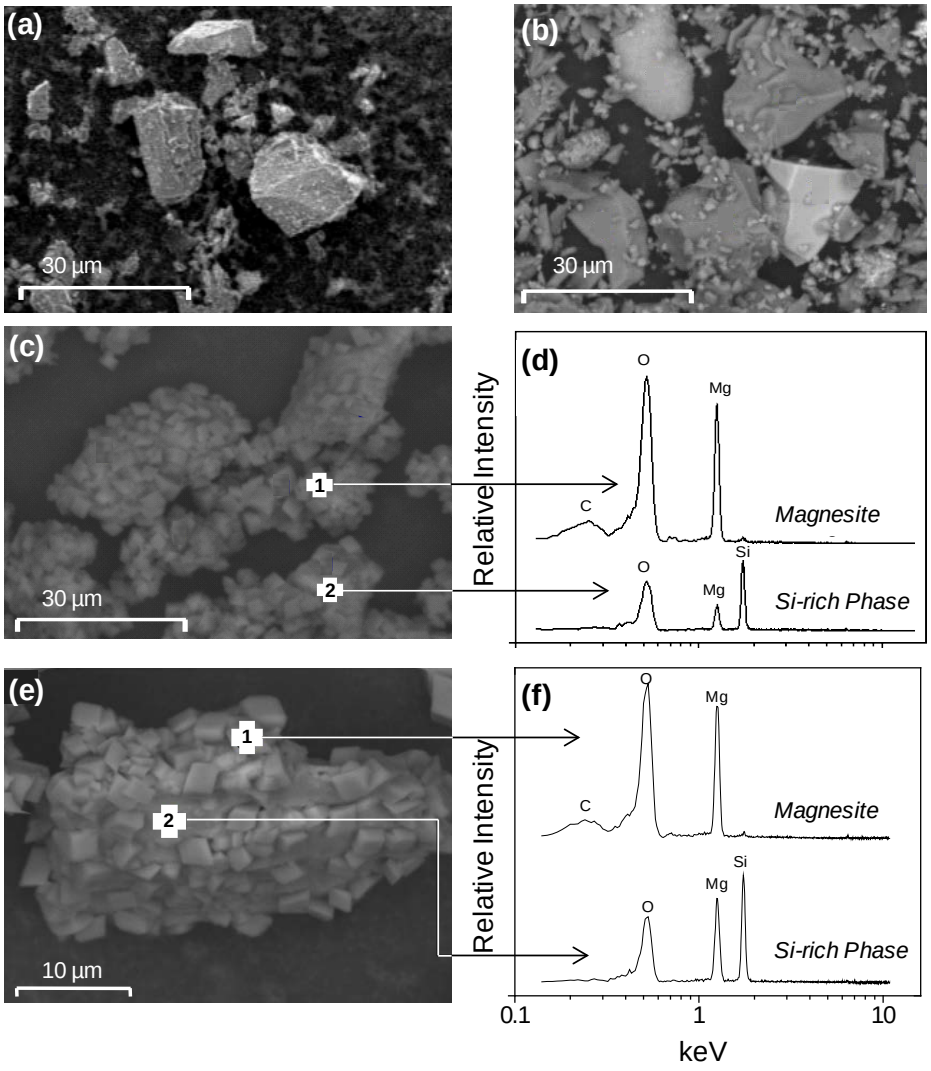


**Figure 9.** Comparison of morphological changes of (a) unreacted olivine, (b) olivine reacted at 90 $^{o}$C, (c), (e) olivine reacted at 185 $^{o}$C where (d), (f) represent the identification of magnesite and silica-rich phases via EDS, respectively. Experiments were performed at $P_{CO2}$ = 139 atm in 1.0 M NaCl + 0.64 M $NaHCO_3$ for 3 hours with 15 wt % solid and a stirring rate of 800 rpm.

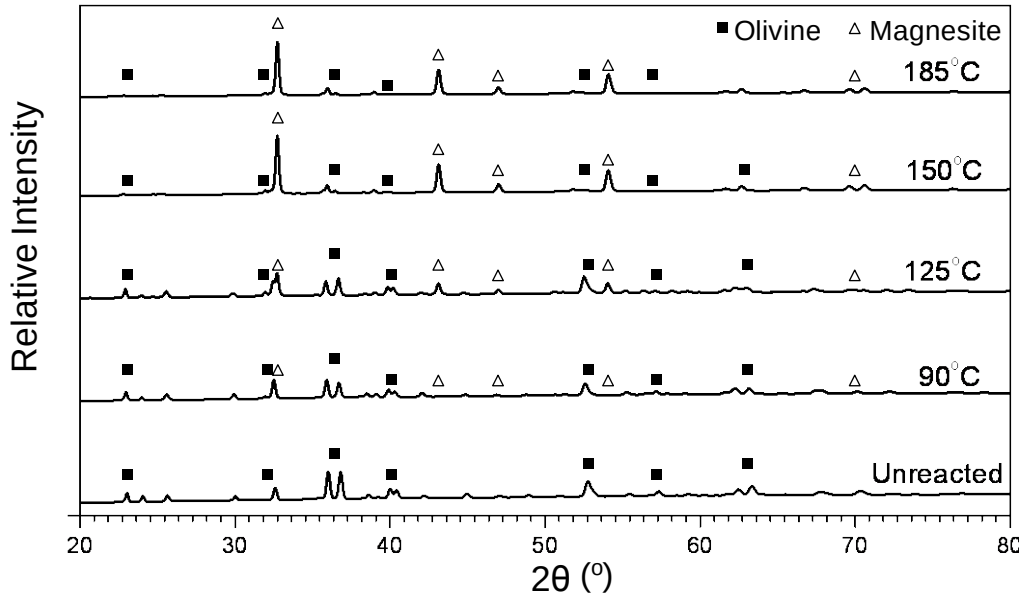


**Figure 10**. Phase transformation of olivine via carbonation at different temperatures. XRD patterns for samples carbonated at $P_{CO2}$ = 139 atm, in 1.0 M NaCl + 0.64 M $NaHCO_3$ for 3 hours with 15 wt% solid and a stirring speed of 800 rpm.

### 4.3.5. Role of $NaHCO_3$

Prior studies at ARC and Arizona State University revealed a significant enhancement in the rate of olivine carbonation in the presence of $NaHCO_3$. However, the prior experiments were all conducted in aqueous solutions including 1.0 M NaCl, so that the independent role of $NaHCO_3$ was not clearly quantified. Indeed, minor rate enhancements due to the presence of dissolved salts have been reported (Hänchen et al., 2006; Olsen, 2007; Prigiobbe et al., 2009). However, it is clear from studies of the olivine carbonation rate as a function of varying dissolved $NaHCO_3$, $KHCO_3$ and $RbHCO_3$ concentrations that most of the rate enhancement due to dissolves species in these studies derives from dissolved bicarbonate (Chizmeshya et al., 2007). The improved olivine carbonation rate was explained as a "catalytic effect" since the bicarbonate concentrations in the liquid phase did not significantly change before and after the carbonation experiments (Chizmeshya et al., 2007; Gerdemann et al., 2007; O'Connor et al., 2004). However, the actual bicarbonate concentration during the reaction at elevated temperature and $P_{CO2}$ was not reported, and thus, it has also been suggested that the role of $NaHCO_3$ may not be catalytic but rather buffering. Furthermore, by providing initial high concentration of bicarbonate ions, a potential rate-limiting $CO_2$ hydration step could be bypassed and the equilibrium can be shifted towards producing more carbonate ions to react with dissolved Mg ions. In order to isolate the effect of $NaHCO_3$ and investigate proposed mechanisms of rate enhancement, a series of experiments was performed at different $NaHCO_3$ concentrations while monitoring the extent of olivine carbonation as well as the corresponding chemical and

morphological changes. The findings from this study were compared to results of 1-hour experiments performed by Chizmeshya et al., (2007) at Arizona State University (ASU).

In this study, olivine carbonation experiments with varying concentrations of $NaHCO_3$ were performed at a reaction time of 3 hours, while keeping the reaction temperature of 185 $^oC$ and $P_{CO2}$ of 139 atm with 15 wt% solid and a stirring rate of 800 rpm. There was no dissolved NaCl in the fluid. Considering the formation of Mg and Ca-carbonates (i.e., no siderite formation), the extents of olivine carbonation were reported as an average of TGA and TCA estimates. For deionized water containing 0.32, 0.48, 0.64, 1.0 and 2.0 M $NaHCO_3$, the extents of olivine carbonation were found to be 5.8, 10.9, 56.0, 82.7, 85.0 and 91.2%, respectively (Table 4 and Figure 11(a)). Addition of $NaHCO_3$ substantially increased the extent of olivine carbonation, though this effect was smaller at $NaHCO_3$ concentrations higher than 0.64 M. This trend matched that of the experiments performed at ASU (Chizmeshya et al., 2007) for a reaction time of 1 hour. The extents of olivine carbonation in ASU's experiments, in the range of 1.5-2.5 M $NaHCO_3$, match the conversion results of this study performed for 1 hour in 1.0 M NaCl + 0.64 M $NaHCO_3$ shown in Figure 6, implying that the difference between this study and the ASU study was mainly due to the reaction time difference.

It was also interesting to notice that while most TGA and TCA estimates were in close agreement, the extents of olivine carbonation in 2.0 M $NaHCO_3$ solvent estimated via TGA and TCA methods differed by about 11%, which confirmed the importance of selecting the suitable carbon analysis method for mineral carbonation studies. This only occurred at the highest $NaHCO_3$ concentration because while 2.0 M $NaHCO_3$ is soluble at 185 $^oC$, the precipitation of $NaHCO_3$ may have occurred as the reactor was cooled before sampling. As a result, the TGA method, which can distinguish different carbon-containing phases, was probably more accurate than the TCA method. Decomposition of $NaHCO_3$ in the reacted sample was observed at 150 $^oC$ forming $Na_2CO_3$, $CO_2$ and $H_2O$, whereas the calcination of magnesite occurs at 560 – 680 $^oC$ (Heda et al., 1995). Therefore, only the second weight drop in the TGA analysis was used to estimate the extent of olivine carbonation. On the other hand, a significantly higher extent of carbonation would be estimated via the TCA method since all carbon in the solid sample – potentially including precipitated $NaHCO_3$ – would be used for the calculation.

The non-linear behavior shown in Figure 11(a) suggests that the role of $NaHCO_3$ on olivine carbonation is complex and multi-faceted. As discussed earlier, olivine dissolution and carbonate mineral precipitation are two key, sequential reactions determining the overall mineral carbonation rate. Depending on the reaction conditions (e.g., pH, temperature, fluid composition), the rate-limiting step may differ. Fluid samples collected at the end of each run were analyzed using the ICP-AES. The Mg concentrations were 219.7, 74.5, 63.5, 55.1, 25.8 and 22.3 ppm in the reacted liquid samples for deionized water containing 0, 0.32, 0.48, 0.64, 1.0 and 2.0 M $NaHCO_3$, respectively. As shown in Figure 11(b), these Mg concentrations are consistently lower than the equilibrium values obtained from PhreeqC simulations that were 781, 223, 187,

158, 120 and 73.2 ppm in deionized water containing 0, 0.32, 0.48, 0.64, 1.0 and 2.0 M $NaHCO_3$, respectively. A direct comparison of these equilibrium concentrations with measured Mg concentrations cannot be made. While the equilibrium concentrations can be calculated for the experimental conditions, the solution concentrations were measured at ambient conditions after the reactor was cooled, depressurized, and filtered to separate the reacted solid from the reaction fluid.

On the other hand, the trend of the extent of the olivine carbonation was affected by the relative concentrations of Mg and $CO_3^{2-}$ in the liquid phase, which is a strong function of pH.The pH of each carbonation case simulated by PhreeqC showed an increase from 5.42 in deionized water to 6.37, 6.49, 6.69, and 7.05 in the presence of 0.48, 0.64, 1.0 and 2.0 M $NaHCO_3$, respectively. As shown in Figure 11(b), over the pH range from 5.42 and 7.05, the equilibrium concentration of $CO_3^{2-}$ changed significantly compared to that of Mg. This explains the small extent of olivine carbonation in the low $NaHCO_3$ case and the increased olivine carbonation at higher concentrations of $NaHCO_3$. As the $CO_3^{2-}$ molar concentration approached and surpassed the Mg molar concentration at around 0.64~1 M $NaHCO_3$ (Figure 11(b)), the extent of carbonation leveled off as the overall olivine carbonation became limited by the amount of dissolved Mg in the system (Figure 11(a)). The comparison of the initial and final pHs of each $CO_2$-olivine-reaction fluid system suggest that $NaHCO_3$ acted as a buffer to maintain relatively constant pH throughout the olivine carbonation process. For instance, in pure, deionized water the pH was changed from 7.00 to 5.42 during olivine carbonation, whereas it only changed from 7.78 to 7.05 when the same reactions were performed in 2.0 M $NaHCO_3$ solution.

Additional insights into the role of $NaHCO_3$ were provided via analyses of particle and pore size distributions. The particle size decreased slightly from 21.4 μm (unreacted) to 16.43 and 17.64 μm after carbonation reaction in deionized water with 0 and 0.32 M $NaHCO_3$, which indicates that mineral dissolution controlled the morphological changes of the remaining olivine particles. It is also interesting to note that olivine reacted in deionized water had a reddish-brown color indicating the precipitation of iron oxide phase on the surface of olivine particles. (This was also observed in the case of NaCl only cases, described below). On the other hand, no iron oxide precipitation was detected in all the experimental runs with more concentrated NaHCO3 in solution, regardless of the presence or absence of NaCl. Olivine reacted with fluids containing $NaHCO_3$ concentrations of 0.48 M or higher had a mean particle size in the range of 26-30 μm, notably larger than that of unreacted olivine. As shown in Figure 11(c), a progressively narrower particle size distribution, shifted toward larger particles, was observed with increasing $NaHCO_3$ concentration. As in other experiments described in previous sections of this paper, both the dissolution of fine particles with a large surface area to volume ratio, and the precipitation of new phases (mainly magnesite), reduced the overall surface area of carbonated olivine particles from 3.77 $m^2/g$ for unreacted olivine to 2.79, 1.63, 1.51, 1.20, 1.15, and 1.15 $m^2/g$ for olivine reacted in deionized water, 0.32, 0.48, 0.64, 1.0 and 2.0 M $NaHCO_3$, respectively.

A comparison of the cumulative pore volume of reacted olivine samples revealed similar trends as the changes in their surface area. The cumulative pore volume decreased from 0.012 ml/g for unreacted olivine to 0.01, 0.0075, 0.0052, 0.0043, 0.004 and 0.0035 ml/g for olivine reacted in deionized water with 0, 0.32, 0.48, 0.64, 1.0 and 2.0 M $NaHCO_3$, respectively. As illustrated earlier, higher extents of olivine carbonation resulted in a significant reduction in the cumulative pore volumes as magnesium carbonates precipitated in the pores. In case of deionized water, the precipitation of iron oxide may have also contributed to a reduction in the pore volume.

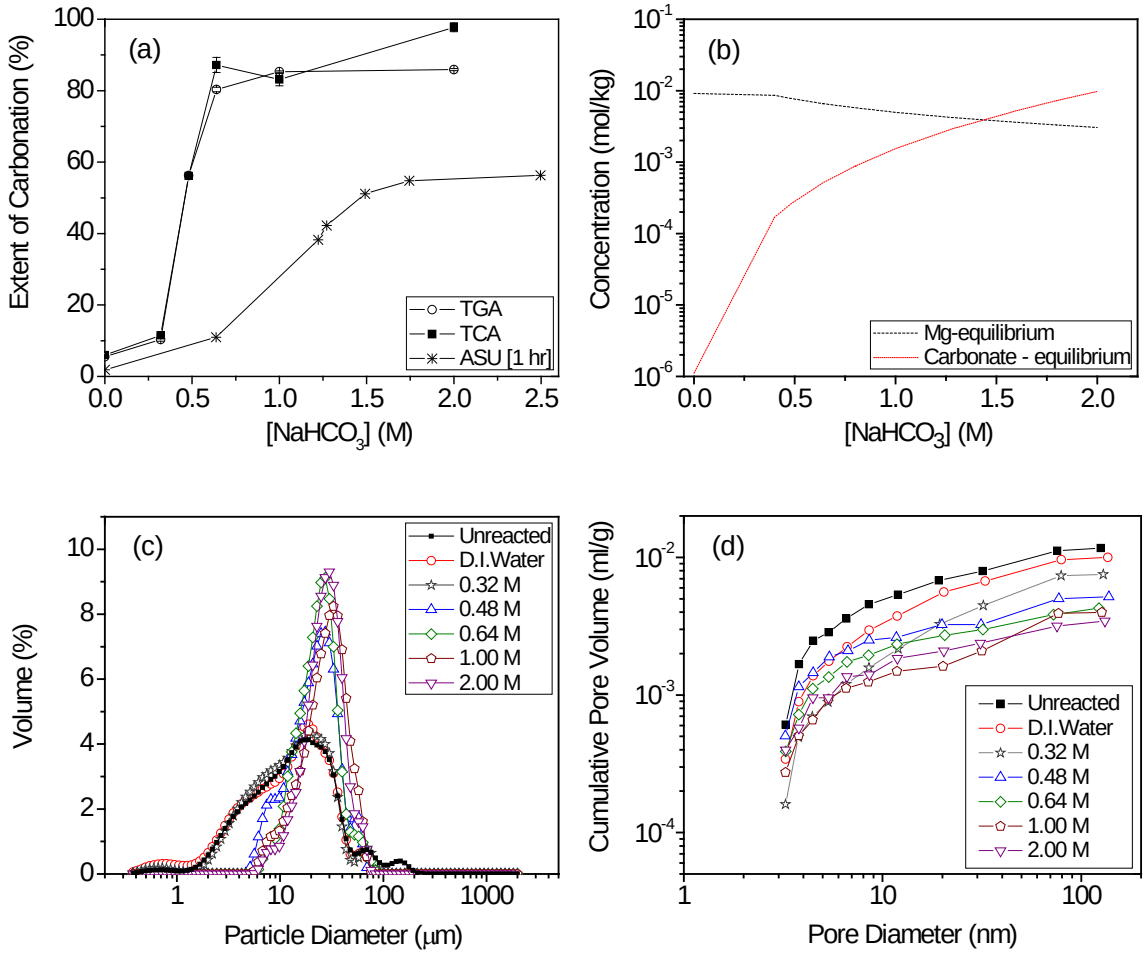


**Figure 11.** Effect of $NaHCO_3$ concentration on (a) extent of olivine carbonation based on the formation of Mg and Ca carbonates, (b) simulated Mg and $CO_3^{2-}$ concentrations, (c) particle size distribution, and (d) cumulative pore volume. Experiments were conducted at 185 $^oC$, at $P_{CO2}$ = 139 atm, for 3 hours, with 15 wt% solid and a stirring speed of 800 rpm. ASU study was performed under same conditions but 1 hour, $P_{CO2}$ = 150 atm, 1500 rpm, and included Fe-carbonate formation(Chizmeshya et al., 2007).

A comparison of the extents of olivine carbonation in 1.0 M NaCl + 0.64 M $NaHCO_3$ with 0.64 M $NaHCO_3$ and 1.0 M $NaHCO_3$ alone revealed that the extents of carbonation were

85.3%, 82.7%, and 85% respectively with a deviation of about ± 2-4%. Therefore, the effect of 1.0 M NaCl on enhancing carbonation did not appear to be significant. In order to delineate the role of NaCl further, olivine carbonation experiments with varying concentrations of NaCl were performed as discussed in the following section.

### 4.3.6. Role of NaCl

In order to further isolate the effects of NaHCO3 and NaCl on olivine carbonation, a series of experiments were performed at different NaCl concentrations ranging from 0.5 to 1 M in the absence of $NaHCO_3$, with other reaction parameters the same as for the experiments described in Section 4.3.5. A better understanding of the role of NaCl will provide insight into how saline water in deep, subsurface aquifers may impact olivine carbonation. Some have reported that compared to geologically slow natural weathering of olivine, $Cl^-$ slightly enhances the magnesium silicate dissolution rate by forming a weak bond with MgO, and thereby disrupting the crystal structure of the mineral and facilitating mineral dissolution (Gerdemann et al., 2007; O'Connor et al., 2004), while other studies revealed that varying the salt concentration changes the pH which in turn affects the dissolution behavior of olivine (Olsen, 2007). The role of cations such as $K^+$ or $Na^+$ is not as well understood, although it has been suggested that these cations may facilitate ion exchange across the solid/liquid interface by altering the surface charges (O'Connor et al., 2004).

As shown in Figure 12(a), the extents of olivine carbonation in fluids containing only NaCl were low compared to all other experimental cases. Even at the highest concentration of 1.0 M NaCl, olivine carbonation was limited to 14.1% in three hours, about twice the 6.0% extent of carbonation in deionized water. Thus, in the absence of a buffer such as $NaHCO_3$, olivine carbonation involving saline fluids would not be sufficiently fast to achieve a high degree of olivine carbonation within the a few hours. PhreeqC calculations suggest that in the presence of 139 atm $CO_2$ pressure, the pH of 1.0 M NaCl solution would be 5.51, whereas the calculated pH of 0.64 M $NaHCO_3$ and 1.0 M NaCl + 0.64 M $NaHCO_3$ solutions were 6.31 and 6.36, respectively. With lowered reaction pH, the concentrations of Mg in liquid samples were estimated to be greater than those in systems with higher, buffered pH (i.e., 219.7, 148.4, 123.2 and 95.7 ppm in deionized water, with 0, 0.5 M, 0.75 M and 1.0 M NaCl, respectively). The lower pH in 1.0 M NaCl solvent may have inhibited the formation of solid carbonate phases. Increasing the concentration of NaCl has also been reported to increase the ionic strength and in turn decrease the solubility of $CO_2$(Duan et al., 2006). Studies by King et al., (2010) revealed that increasing the ionic strength reduced the activity of water and aided the precipitation of magnesite.

In the presence of NaCl, without $NaHCO_3$, the particle size distribution remained almost unchanged (Figure 12(b)). As NaCl concentration increased from 0.5 to 1.0 M, the mean particle size, surface area and cumulative pore volume were slightly decreased (see Table 4 and Figure 12(c)).While the changes in morphological characteristics of olivine during its carbonation inthe

presence of NaCl were minimal, olivine samples carbonated in the presence of $NaHCO_3$all showed lighter and whiter colors,but olivine carbonated

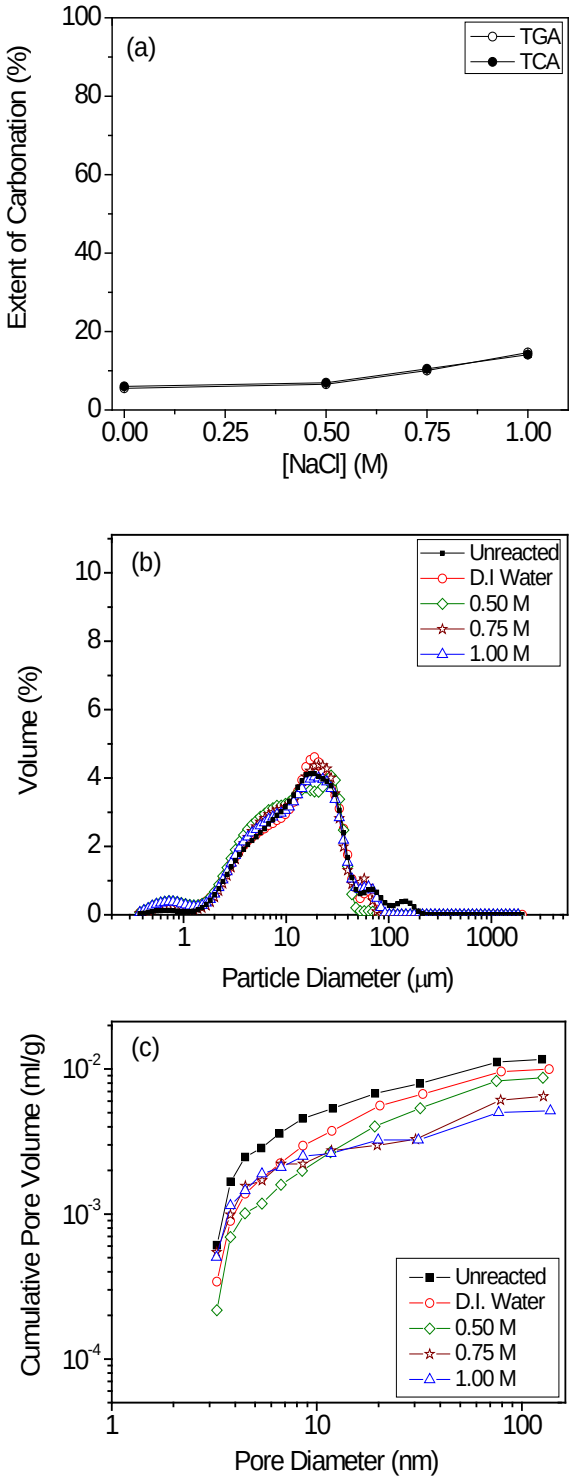


**Figure 12.** Effect of NaCl concentration on (a) extent of olivine carbonation based on the formation of Mg and Ca carbonates, (b) particle size distribution, and (c) cumulative pore

volume. Experiments were conducted at 185 $^{o}$C, at $P_{CO2}$ = 139 atm, for 3 hours, with 15 wt% solid and a stirring speed of 800 rpm.

without $NaHCO_3$ was distinctively reddish brown due to precipitation of iron oxides on olivine surfaces. The formation of this amorphous iron oxide layer, and its role in inhibiting mineral dissolution, have been previously reported (O'Connor et al., 2004; Park et al., 2003; Saldi et al., 2013). Other studies reported the precipitation of hematite at shorter reaction times but not at longer durations due to changes in the fluid composition, and carbonate concentrations over time (King et al., 2013). In the absence of a pH buffer (i.e., $NaHCO_3$), the olivine-NaCl solution-$CO_2$ system may experience an internal pH swing, which could have led to precipitation of iron oxides.

### 4.4. Conclusions

Olivine, an abundant, reactive silicate mineral suitable for mineral carbonation processes, was evaluated for its $CO_2$ storage capacity. Direct olivine carbonation is a complicated phenomenon due to simultaneous chemical and morphological changes in the olivine grains. For both *in situ* and *ex situ* carbon storage schemes via mineral carbonation, it is important to understand the reaction mechanisms and kinetics in order to estimate the $CO_2$ uptake rate, storage capacity, and long term stability of the geologically stored $CO_2$. This study showed that the reaction time, temperature, $CO_2$ pressure and fluid composition all have first-order effects on carbonation rates and reaction mechanisms. Olivine carbonation is considerably enhanced in solutions containing $NaHCO_3$, with or without dissolved NaCl. We infer that $NaHCO_3$ is not a catalyst, but rather serves as a pH buffer and a source of carbonate ions. At high $NaHCO_3$ concentrations, the calculated system pH was high (> 6.5) and thus, carbonate ions were more readily available for the formation of magnesium carbonate. In turn this lowers the Mg concentration in the fluid, which drives ongoing olivine dissolution. NaCl alone does not significantly enhance olivine carbonation. In some experiments using deionized water, with and without dissolved, NaCl, iron oxide precipitation was observed. Iron oxides did not precipitate in experiments with more than 0.32 M $NaHCO_3$. Overall, the results of this study are consistent with studies performed at Albany Research Center (Gerdemann et al., 2007; O'Connor et al., 2004) and Arizona State University (Chizmeshya et al., 2007).

In addition to changes in the chemical compositions of the solid and liquid phases, detailed analyses of the particle and pore size distributions revealed that as olivine dissolved, pores surrounded by Si-rich phases were opened, and magnesium carbonate phases precipitated in these pores, thereby limiting the pore space available for further reactivity. The changes in the pore volume may impact the long-term $CO_2$ storage capacity and need to be taken into account in future modeling studies to predict the long-term fate of $CO_2$. Order of magnitude estimates of the olivine carbonation rate – in mass fraction of olivine carbonated, per second – in the presence of aqueous fluids with more than ~ 0.5 M $NaHCO_3$, with grain sizes of tens of microns, can be confidently calculated using the expression developed by Kelemen & Matter, (2008) for the

ARC results (O'Connor et al., 2004), which is very similar to the expression derived based on the data presented in this study. While the expression derived in Kelemen & Matter, (2008), provided a somewhat better fit to the ARC (O'Connor et al., 2004) data alone, the second one (Eq. 16) may be more robust in some ways. Alternatively, different results from the twoexpressions can be interpreted as a partial indication of the current level of uncertainty in olivine carbonation rates under the relevant experimental conditions.

***Nomenclature***

| | |
|---|---|
| $M$ | alkaline metal |
| $W_{CO_2}$ | weight of $CO_2$ |
| $W_{mineral}$ | weight of mineral |
| $R_{CO_2}$ | mass of raw mineral needed to store a unit mass of $CO_2$ |
| $1/R_{CO_2}$ | mass of $CO_2$ stored in a unit mass of mineral |
| $y_m$ | weight fraction of alkaline metal in mineral that can react with $CO_2$ to form carbonates |
| $MW_m$ | molecular weight of alkaline metal, $M$ |
| $MW_{CO_2}$ | molecular weight of $CO_2$ (44 g/mol) |
| $Y_{CO_2,TGA}$ | yield or extent of carbonation: mass of $CO_2$ stored in the mineral as solid carbonate measured via TGA, relative to $CO_2$ storage capacity |
| $TGA$ | the percent weight change of the solid sample at its calcination temperature $\left(= \left[\frac{Weight of CO_2 released}{Weight of solid sample}\right] \times 100\% \right)$ |
| $Y_{CO_2,TCA}$ | yield or extent of carbonation: mass of $CO_2$ stored in the mineral as solid carbonate measured via TCA, relative to the $CO_2$ storage capacity |
| $TCA$ | the weight fraction of carbon in the solid sample $\left(= \left[\frac{Weight of carbon}{Weight of solid sample}\right]\right)$ |
| $P_{CO_2}$ | partial pressure of $CO_2$ (atm) |

## 5. Comparison of the Carbon Mineralization Behavior of Various Minerals

### 5.1 Introduction

Combustion of fossil fuels to meet rising energy demand is one of the primary causes for increasing concentrations of $CO_2$ in the atmosphere, which has detrimental environmental consequences. A safe and permanent method for long-term carbon storage is to react calcium and magnesium rich minerals with $CO_2$ to form insoluble, thermodynamically stable and environmentally benign calcium and magnesium carbonates (Lackner, 2002), which is also known as carbon mineralization. Besides the studies conducted at Albany Research Center (Gerdemann et al., 2007; O'Connor et al.,2004) to compare the carbonation behavior of olivine ($(Mg,Fe)_2SiO_4$), heat-treated serpentine ($Mg_3Si_2O_5(OH)_4$) and wollastonite ($CaSiO_3$) under the same conditions, there has been a lack of systematic studies devoted to understanding the effects of temperature, $CO_2$ partial pressures, and variable concentrations of NaCl and $NaHCO_3$ on rocks and minerals with different compositions. In particular, there have been very few studies of mineral carbonation rates in rocks containing substantial amounts of plagioclase, the most abundant rock forming mineral in the Earth's crust. Instead, it has been common to estimate full carbonation rates using the results of dissolution rate experiments at high fluid/rock ratios, with the assumption that dissolution is the rate-limiting step in mineral carbonation. While this assumption may often be warranted, it is not valid for olivine carbonation in the presence of $NaHCO_3$-rich fluids (Matter & Kelemen, 2009; Kelemen et al. 2011).

Studies of the rate of mineral carbonation are of interest for *ex situ* carbon mineralization, in which minerals are mined and reacted with $CO_2$ to form carbonates in above-ground, highly engineered reactors, and for *in situ* carbon storage, where $CO_2$ is injected into formations rich in calcium and magnesium silicates and alumino-silicates, and $CO_2$ reacts over time to form Ca and Mg carbonate minerals. The aim of this study is to compare the relative carbonation rates of olivine ($Mg_{1.74}Fe_{0.26}SiO_4$), labradorite ($(Ca_{0.51}Na_{0.49})(Al_{1.51}Si_{2.49})O_8$), anorthosite (a mixture of plagioclase ($Ca_{0.96}Na_{0.04}Al_{1.96}Si_{2.04}O_8$) olivine ($Mg_{1.32}Fe_{0.68}SiO_4$) and magnetite), and basalt (a mixture of plagioclase ($Ca_{0.44}Na_{0.56}Al_{1.44}Si_{2.56}O_8$), augite ($(\sim Mg_{0.49}Fe_{0.51}CaSi_2O_6$), low calcium pyroxene ($\sim Mg_{0.98}Fe_{1.02}Si_2O_6$) and Fe-Ti oxides), in fluids shown in previous studies to produce rapid olivine carbonation (Chizmeshya et al., 2007; Gadikota et al., 2013; Gerdemann et al., 2007; O'Connor et al., 2004).

Understanding the relative reactivities of these minerals should provide insight into the fate of $CO_2$ injected into geologic formations. Pilot-scale demonstrations of $CO_2$ injection into basalt formations in Iceland (Gislason et al., 2010) and Washington State, USA (McGrail et al., 2011) have been underway for a few years now. In addition, there are ~ 15,000 $km^3$ of peridotite (rocks with more than 40% olivine) in Oman, and similar amounts on each of the continents, that could be used for either *in situ* or *ex situ* carbon mineralization (Kelemen et al., 2011; Kelemen & Matter, 2008). As reviewed by Matter & Kelemen (2009) and Kelemen et al., (2011), numerous studies have focused on understanding the dissolution behavior of olivine (Awad et al.,

2000; Rosso & Rimstidt, 2000; Brady et al., 1999; Chen & Brantley, 2000; Giammar et al., 2005; Oelkers, 2000; Pokrovsky & Schott, 2000; Wogelius & Walther, 1992), labradorite (Carroll & Knauss, 2005; Cygan et al., 1989; Siegel & Pfannkuch, 1984; van Hees et al., 2002), plagioclase, a key mineral in anorthosite, gabbro and basalt (Amrhein & Suarez, 1992; Oelkers & Schott, 1995) and basalt (Gislason & Oelkers, 2003; Gudbrandsson et al., 2011; Guy & Schott, 1989; Oelkers & Gislason, 2001; Schaef & McGrail, 2009; Wolff-Boenisch et al., 2004, 2006, 2011). However, the process of carbon mineralization involves $CO_2$ hydration (Stirling & Pápai, 2010; Wang et al., 2009) and formation of carbonate minerals (Hänchen et al., 2008; Saldi et al., 2009, 2012) in addition to mineral dissolution. Depending on the pH, $CO_2$ partial pressure, temperature and the presence of chemical additives, $CO_2$ hydration, mineral dissolution or formation of mineral carbonates can be rate limiting.

While extensive studies have been carried out to understand the dissolution and carbonation of magnesium and calcium silicate minerals such as olivine, serpentine and wollastonite (Awad et al., 2000; Chen & Brantley, 2000; Chizmeshya et al., 2007; Gerdemann et al., 2007; Giammar et al., 2005; Gislason et al., 2010; Hänchen et al., 2006; Hövelmann et al., 2012; Kelemen & Hirth, 2012; Kelemen & Matter, 2008; Kelemen et al., 2011; Lackner, 2002; Matter & Kelemen, 2009; McGrail et al., 2006; O'Connor et al., 2004; Park et al., 2003; Park & Fan, 2004; Saldi et al., 2009, 2012; Yegulalp et al., 2001), the carbonation of plagioclase feldspars, such as labradorite, is less well understood. This is important because plagioclase is the most abundant mineral in the Earth's crust, and forms a primary constituent of basaltic lava and its plutonic equivalent, gabbro, which form the oceanic crust. Carbonation studies of basalt (McGrail et al., 2006; Schaef et al., 2013, 2009) and labradorite (Munz et al., 2012) have been performed in the past but not at the same experimental conditions as for magnesium and calcium silicates. A direct comparison of the carbonation rates for these different minerals is essential. In this study, the carbonation behavior of labradorite, and two rocks containing abundant plagioclase, anorthosite and basalt, were compared with previous results for olivine carbonation under the same experimental conditions (Gadikota et al., 2013).

Previous studies showed that increasing reaction temperature enhances the rate and extent of mineral carbonation (Chizmeshya et al., 2007; Gadikota et al., 2013; Gerdemann et al., 2007; Giammar et al., 2005; Hangx & Spiers, 2009; Munz et al., 2012; O'Connor et al., 2004). In the case of *in situ* carbon mineralization, higher temperatures at depth along the geothermal gradient can be utilized to achieve faster conversion to carbonates. High partial pressures of $CO_2$ also enhance the carbonation of silicate minerals such as olivine, serpentine and wollastonite (Gadikota et al., 2013; Gerdemann et al., 2007; O'Connor et al., 2004), but the effect of elevated $P_{CO2}$ on plagioclase has not been as well studied.

Another important consideration is the role of pH. While mineral dissolution is favored at low pH, formation of carbonates is favored at high pH. Therefore, a buffer that maintains pH in the range of 6-8 – such that as silicate minerals are dissolved, there are sufficient carbonate species in solution to facilitate Mg or Ca-carbonate mineral precipitation – enhances olivine

carbonation rates. Previous studies have showed that 0.5 to 5 M $NaHCO_3$, $KHCO_3$ and $RbHCO_3$in brines are effective in enhancing olivine and serpentine dissolution and carbonation (Chizmeshya et al., 2007; Gadikota et al., 2013; Gerdemann et al., 2007; O'Connor et al., 2004). In this study, the effectiveness of $NaHCO_3$ on the carbonation of labradorite, anorthosite and basalt was investigated.

Studies at Albany Research Center and Arizona State University showed that a solution of 1.0 M NaCl + 0.64 M $NaHCO_3$ was effective in enhancing the carbonation of olivine, heat-treated serpentine and wollastonite (Chizmeshya et al., 2007; Gerdemann et al., 2007; O'Connor et al., 2004). However, the individual roles of NaCl and $NaHCO_3$ alone are not as well understood. Recently, Gadikota et al., (2013) separated these variables, and showed that there is a substantial enhancement in olivine carbonation due to $NaHCO_3$, with and without NaCl, while there is a negligible effect due to NaCl alone. Similarly, in this study, we investigate the effect of varying concentrations of NaCl on the extents of carbonation of labradorite, anorthosite and basalt. In addition, changes in the morphological structure of the minerals such as the particle size, pore volume and surface area were analyzed.

## 5.2 Experimental Methods

### 5.2.1 Procurement and Characterization of Materials

Rough labradorite from the Norcross-Madagascar Mine in the south of Madagascar, was purchased from the Madagascar Mineral Company. The labradorite sample was then ground to a fine powder. An anorthosite sample procured from Albany Research Center was originally from Grass Valley, California. Columbia River Basalt was also procured from Albany Research Center. This light gray, fine grained basalt was from a vesicular core from a depth of 2263.3 feet. As reported in a previous study (Gadikota et al., 2013), Twin Sisters olivine was procured from Albany Research Center. Since our studies of olivine, and previous studies of diopside (Eggleston et al., 1989), showed that aging of ground mineral powders reduces their reactivity, freshly ground mineral and rock samples were used in this study.

Of the samples, the anorthosite has the highest content of CaO (14.10% by weight) followed by labradorite (10.2%), basalt (8.15%) and olivine (0.16%). Labradorite has the least amount of MgO (0.24%), compared to basalt (4.82%), anorthosite (8.74%) and olivine (47.3%). Labradorite also has the least amount of iron oxide (0.97%) compared to anorthosite (10.6%), olivine (13.9%) and basalt (14.6%). On the basis of a CIPW norm calculation, we estimate that the anorthosite sample contains about 63wt% plagioclase feldspar (96% anorthite, $CaAl_2Si_2O_8$ + 4% albite $NaAlSi_3O_8$, abbreviated An96), 24% olivine (66% forsterite $Mg_2SiO_4$ + 34% fayalite $Fe_2SiO_4$), and 3% of both calcic pyroxene and iron-titanium oxide minerals. The CIPW norm of the basalt sample contains about 45% plagioclase (An44) 8% of both calcic pyroxene and Ca-poor pyroxene, both with molar Mg/(Mg+Fe) of 0.49, and 6% iron-titanium oxides.

The mineral and rock samples were ground such that more than 90% of the material was smaller than 37 μm. Particle size analyses showed that the mean diameters of labradorite, anorthosite, basalt and olivine particles were 8.44, 11.94, 7.81 and 21.4 μm, respectively (Table 8). In addition, the surface areas of labradorite, anorthosite, basalt and olivine were 4.46, 2.92, 4.48 and 3.77 $m^2/g$, respectively (Table 8).

Unreacted antigorite used to perform a single experiment had a grain size in the range of 2-80 μm and the surface area was 10.3 $m^2/g$. The unreacted antigorite sample was composed of 40.5% MgO, 37.1% $SiO_2$, and 7.80% $Fe_2O_3$.

### 5.2.2 Carbonation of Olivine and Quantification of Mineralized $CO_2$

The carbonation experiments were performed in a high temperature, high pressure batch reactor (Autoclave Engineers, 100 ml EZE-Seal) as discussed in Section 4.2.1 and in Gadikota et al., (2013). A high pressure syringe pump (Teledyne Isco, 500D, NE) was connected to the reactor to deliver pressurized $CO_2$. About 15 wt% solids were suspended in the reaction fluid containing deionized water and/or aqueous fluids with varying concentrations of NaCl and $NaHCO_3$. Once the reactor was sealed and the set-point of the reaction temperature was reached after about 40 minutes, the reactor pressure was increased to the desired partial pressure of $CO_2$, which marked the start of the experiment. At the end of the experiment, the reactor was cooled to temperatures below 70 $^oC$, which took about 75 minutes. The reactor was then depressurized, the interior was cleaned to collect all the solid material, and the fluid contents were filtered. The filtered liquid samples were diluted in 2% $HNO_3$ and the concentrations were measured using Inductively Coupled Plasma - Atomic Emission Spectroscopy (ICP-AES, Activa S model, Horiba Jobin Yvon).

In addition to the liquid analyses, a host of tests were conducted on the solids. These included measuring the changes in the pore structure and the specific surface area using BET (Brunauer–Emmett–Teller, QuantachromeNovaWin BET Analyzer), determining particle size via laser diffraction (Beckman Coulter, Inc., LS 13 320 MW), changes in the surface morphological features using Scanning Electron Microscopy (SEM, Tescan Vega II) and corresponding elemental concentrations using an Energy Dispersive X-ray Spectrometer (EDS, Oxford Instruments, Inca Software). These tests provided insight into the morphological changes in the minerals before and after carbonation. In addition, the elemental compositions in minerals were determined using Wavelength Dispersion X-Ray Fluorescence (WD-XRF, Pananalytical Axios) and the nature of the phases in run products was obtained using X-Ray Diffraction (XRD 3000, Inel Inc.) in the range of $20^o$ and $80^o$ and CuKα radiation (λ = 1.5406 Å).

The determination of the carbon content in the reacted samples was complicated by the relatively low content of carbon in reacted labradorite, anorthosite and basalt. The carbon content was measured using Thermogravimetric Analysis (TGA, Setaram SETSYS) and Total Carbon Analysis (TCA, UIC CM150) with a heating rate of 5°C per minute. Total Inorganic Carbon

(TIC) analysis using acid digestion was not used to measure the carbon content in the samples because the samples contained only carbonate as the carbon species and did not contain any organic carbon, and TIC is much slower than TCA. While the TGA determines the presence of various phases (e.g., hydroxides, carbonates) based on their decomposition temperature, the presence of overlapping weight drop curves made it challenging to accurately determine phase proportions, especially for experiments in which the carbonate content was low. In the TCA where the samples were combusted to convert all organic and inorganic carbon to CO and $CO_2$, the detection of small amounts of carbon was probably more accurate. In cases where the $CO_2$ trapped as carbonate was lower than 2%, TCA runs were considered to be the most accurate method for determining the carbon content. In reacted olivine samples that contained 2 to 30 wt% $CO_2$, both TGA and TCA were used to estimate the extents of carbonation. For labradorite, anorthosite and basalt, the extents of carbonation were estimated using TCA alone.

**Table 5**. Composition of olivine, labradorite, anorthosite, and basalt

| Analyte | Olivine (wt%) | Labradorite (wt%) | Anorthosite (wt%) | Basalt (wt%) |
|---|---|---|---|---|
| CaO | 0.16 | 10.20 | 14.10 | 8.15 |
| MgO | 47.30 | 0.24 | 8.74 | 4.82 |
| $Fe_2O_3$ | 13.90 | 0.97 | 10.60 | 14.60 |
| $SiO_2$ | 39.70 | 54.30 | 41.80 | 51.90 |
| $Al_2O_3$ | 0.20 | 28.00 | 24.20 | 13.40 |
| $Na_2O$ | 0.01 | 5.05 | 0.59 | 2.91 |
| $K_2O$ | <0.01 | 0.59 | 0.03 | 1.09 |
| $TiO_2$ | <0.01 | 0.14 | 0.04 | 1.74 |
| $P_2O_5$ | <0.01 | 0.04 | <0.01 | 0.32 |
| MnO | 0.15 | 0.01 | 0.13 | 0.21 |
| $Cr_2O_3$ | 0.78 | 0.10 | 0.08 | 0.10 |
| $V_2O_5$ | <0.01 | <0.01 | <0.01 | 0.06 |
| LOI* | -0.70 | 0.32 | 0.12 | 0.27 |
| Carbonation Potential, $\frac{W_{CO_{2,max}}}{W_{mineral}}$ (assuming that Fe does not react to form $FeCO_3$) | 0.343 | 0.171 | 0.105 | 0.076 |
| Carbonation Potential, $\frac{W_{CO_{2,max}}}{W_{mineral}}$ (assuming that Fe reacts to form $FeCO_3$) | 0.374 | 0.206 | 0.157 | 0.081 |
| Mg#[1] | 87 | - | 66 | 48 |
| An#[2] | - | 51 | 96 | 44 |

*LOI: Loss of Ignition; Material is heated to 1000 $^oC$ until there is no change in the weight of the sample.
[1] $Mg\# = \frac{Mg}{Mg+Fe}$; [2] $An\# = \frac{Ca}{Ca+Na}$; Mg# and An# are molar ratios that represent relative abundances of one element.

The following equation was used to estimate the extent of carbonation using TCA:

$$Y_{CO_2,TCA} = R_{CO_2} \times \left(\frac{3.67 \times TCA}{(1 - 3.67 \times TCA)}\right) \times 100\% \quad \text{(Eq. 1)}$$

where $Y_{CO_2}$, the yield or the extent of carbonation is then defined as the measured amount of $CO_2$ stored in the mineral as solid carbonate relative to the $CO_2$ storage capacity, $\frac{1}{R_{CO_2}}$, the theoretical carbon storage capacity is the mass of $CO_2$ that can be trapped in a unit mass of the unreacted mineral, and *TCA* represents the weight fraction of carbon in the carbonated sample with a unit of $\left[\frac{Weight\ of\ carbon}{Weight\ of\ solid\ sample}\right]$. The coefficient 3.67 is the ratio of the molecular weights of $CO_2$ to carbon. The extents of olivine carbonation were also estimated using TGA and the values reported in Table 7 are an average of TGA and TCA estimates. The extents of carbonation were reported using two different theoretical carbon storage capacity estimates. The first estimation is based on the assumption that Fe reacts to form siderite ($FeCO_3$) as represented by Equation 2, and another assuming that the formation of siderite is inhibited by the low solubility of iron oxide which may precipitate from the solution before the formation of siderite (Equation 3).

$$\frac{W_{CO_2}}{W_{mineral}} = \frac{1}{R_{CO_2}} = \left(\frac{y_{Mg}}{MW_{Mg}} + \frac{y_{Ca}}{MW_{Ca}} + \frac{y_{Fe}}{MW_{Fe}}\right) \times MW_{CO_2} \quad \text{(Eq. 2)}$$

$$\frac{W_{CO_2}}{W_{mineral}} = \frac{1}{R_{CO_2}} = \left(\frac{y_{Mg}}{MW_{Mg}} + \frac{y_{Ca}}{MW_{Ca}}\right) \times MW_{CO_2} \quad \text{(Eq. 3)}$$

The possible formation of Na, K and Al carbonates was not considered in our estimates of carbon storage capacity since Na and K form soluble carbonates and the formation of aluminum carbonates was not evident in the carbonated samples, as expected for these highly soluble minerals in our experiments at high water/rock ratio. In natural systems with Na-rich plagioclase, the carbon storage capacity could be substantially increased if Na- and K-carbonate saturation was achieved.

## 5.3 Results and Discussion

### 5.3.1 Effect of Reaction Time

Figure 13 shows the relative reactivities of the labradorite, anorthosite and basalt compared to olivine (Gadikota et al., 2013) over time. These experiments were performed at reaction times of 1, 3 and 5 hours at 185 $^oC$, $P_{CO2}$ of 139 atm ($P_{total}$ = 150 atm) in 1.0 M NaCl + 0.64 M $NaHCO_3$ with 15 wt% solid and a stirring rate of 800 rpm. These conditions were the same as those reported for our previously reported olivine carbonation study (Gadikota et al., 2013) and similar to those of the ARC group (Gerdemann et al., 2007; O'Connor et al., 2004).

**Table 6.** Summary of the amount of $CO_2$ stored as carbonate (wt%) in olivine, labradorite, anorthosite and basalt reacted at varying reaction times, temperatures, $CO_2$ partial pressures and in the presence of various chemical additives. The proportion of solid reactants was 15 wt% and a stirring speed of 800 rpm was maintained. Extents of carbonation are reported as an average of TCA estimates for labradorite, anorthosite and basalt , and as an average of both TCA and TGA for olivine (Reported values are the average and standard deviation (1 sigma) for three runs of Total Carbon Analysis.) An experiment on antigorite at 185 $^oC$, $P_{CO2}$ =139 atm, 1.0 M NaCl+0.64 M $NaHCO_3$ for a reaction time of 1 hour resulted in a carbon content of 2.1%.

| | $CO_2$ in reacted minerals (wt%) | | | |
|---|---|---|---|---|
| | Olivine | Labradorite | Anorthosite | Basalt |
| ***Effect of Reaction Time*** *(185 $^oC$, $P_{CO2}$ =139 atm, 1.0 M NaCl+0.64 M $NaHCO_3$)* | | | | |
| 1 hour | 22.48 ± 0.08 | 0.89 ± 0.05 | 1.59 ± 0.10 | 0.97 ± 0.07 |
| 3 hours | 30.86 ± 0.62 | 2.84 ± 0.03 | 4.26 ± 0.10 | 1.00 ± 0.01 |
| 5 hours | 32.08 ± 1.19 | 3.66 ± 0.01 | 4.26 ± 0.09 | 1.14 ± 0.06 |
| ***Effect of Partial Pressure of $CO_2$*** *(185 $^oC$, 3 hours, 1.0 M NaCl+0.64 M $NaHCO_3$)* | | | | |
| 64 atm | 17.22 ± 0.09 | 2.76 ± 0.03 | 3.98 ± 0.05 | 0.95 ± 0.03 |
| 89 atm | 24.31 ± 0.29 | 2.82 ± 0.08 | 4.33 ± 0.12 | 0.94 ± 0.03 |
| 139 atm | 30.86 ± 0.62 | 2.84 ± 0.03 | 4.26 ± 0.10 | 1.00 ± 0.01 |
| 164 atm | 30.78 ± 0.49 | 3.16 ± 0.06 | 4.11 ± 0.05 | 1.15 ± 0.07 |
| ***Effect of Temperature*** *( $P_{CO2}$ = 139 atm, 3 hours, 1.0 M NaCl+0.64 M $NaHCO_3$)* | | | | |
| 90 $^oC$ | 1.71 ± 0.01 | 1.14 ± 0.03 | 1.33 ± 0.07 | 0.64 ± 0.02 |
| 125 $^oC$ | 12.88 ± 0.14 | 1.16 ± 0.01 | 1.57 ± 0.07 | 0.83 ± 0.04 |
| 150 $^oC$ | 27.33 ± 0.41 | 2.08 ± 0.01 | 2.32 ± 0.08 | 0.89 ± 0.04 |
| 185 $^oC$ | 30.86 ± 0.62 | 2.84 ± 0.03 | 4.26 ± 0.10 | 1.00 ± 0.01 |
| ***Effect of [$NaHCO_3$]*** *(185 $^oC$, $P_{CO2}$ = 139 atm, 3 hours)* | | | | |
| Deionized Water | 3.03 ± 0.01 | 0.40 ± 0.02 | 1.74 ± 0.03 | 0.41± 0.04 |
| 0.48 M $NaHCO_3$ | 22.55 ± 0.10 | 0.69 ± 0.01 | 1.86 ± 0.01 | 1.20 ± 0.02 |
| 0.64 M $NaHCO_3$ | 30.73 ± 0.54 | 0.95 ± 0.03 | 2.34 ± 0.08 | 1.21 ± 0.01 |
| 1.0 M $NaHCO_3$ | 30.63 ± 0.43 | 2.72 ± 0.06 | 5.61 ± 0.02 | 1.65 ± 0.08 |
| ***Effect of [NaCl]*** *(185 $^oC$, $P_{CO2}$ = 139 atm, 3 hours)* | | | | |
| Deionized Water | 3.03 ± 0.01 | 0.40 ± 0.02 | 1.74 ± 0.03 | 0.41 ± 0.04 |
| 0.5 M NaCl | 3.50 ± 0.05 | 0.26 ± 0.06 | 1.63 ± 0.04 | 0.49 ± 0.01 |
| 1.0 M NaCl | 6.84 ± 0.32 | 0.20 ± 0.04 | 1.92 ± 0.10 | 0.44 ± 0.22 |

**Table 7.** Summary of the extents of carbonation of olivine, labradorite, anorthosite and basalt reacted at varying reaction times, temperatures, $CO_2$ partial pressures and in the presence of various chemical additives. The proportion of solid reactants was 15 wt% and a stirring speed of 800 rpm was maintained. Extents of carbonation are reported as an average of TCA estimates for labradorite, anorthosite and basalt , and as an average of both TCA and TGA for olivine. (Reported values are the average and standard deviation (1 sigma) for three runs of Total Carbon Analysis.) One experiment on antigorite at 185 $^oC$, $P_{CO2}$ =139 atm, 1.0 M NaCl+0.64 M $NaHCO_3$ for a reaction time of 1 hour resulted in an extent of carbonation of 17.3%.

| | Extent of Carbonation (%) | | | | | | | |
|---|---|---|---|---|---|---|---|---|
| | Olivine | | Labradorite | | Anorthosite | | Basalt | |
| | (assuming formation of Ca, Mg & Fe carbonates) | (assuming formation of Ca & Mg carbonates) | (assuming formation of Ca, Mg & Fe carbonates) | (assuming formation of Ca & Mg carbonates) | (assuming formation of Ca, Mg & Fe carbonates) | (assuming formation of Ca & Mg carbonates) | (assuming formation of Ca, Mg & Fe carbonates) | (assuming formation of Ca & Mg carbonates) |
| ***Effect of Reaction Time*** *(185 $^oC$, $P_{CO2}$ =139 atm, 1.0 M NaCl+0.64 M $NaHCO_3$)* | | | | | | | | |
| 1 hour | 49.4 ± 1.3 | 56.6 ± 1.5 | 10.1 ± 0.6 | 10.8 ± 0.6 | 5.8 ± 0.5 | 6.6 ± 0.5 | 5.3 ± 0.4 | 8.4 ± 0.6 |
| 3 hours | 73.5 ± 2.8 | 85.3 ± 3.1 | 33.0 ± 0.3 | 35.3 ± 0.4 | 17.1 ± 0.4 | 19.4 ± 0.5 | 5.4 ± 0.0 | 8.6 ± 0.1 |
| 5 hours | 79.1 ± 4.9 | 90.5 ± 5.6 | 42.9 ± 0.1 | 46.0 ± 0.1 | 17.8 ± 0.4 | 20.1 ± 0.4 | 6.2 ± 0.4 | 9.9 ± 0.6 |
| ***Effect of Partial Pressure of $CO_2$*** *(185 $^oC$, 3 hours, 1.0 M NaCl+0.64 M $NaHCO_3$)* | | | | | | | | |
| 64 atm | 34.3 ± 0.8 | 39.3 ± 0.9 | 31.6 ± 0.4 | 33.8 ± 0.4 | 16.3 ± 0.2 | 18.4 ± 0.2 | 5.1 ± 0.2 | 8.2 ± 0.3 |
| 89 atm | 52.3 ± 1.9 | 59.9 ± 2.1 | 32.6 ± 1.0 | 34.9 ± 1.0 | 16.9 ± 0.5 | 19.1 ± 0.6 | 5.1 ± 0.2 | 8.1 ± 0.2 |
| 139 atm | 73.5 ± 2.8 | 85.3 ± 3.1 | 32.8 ± 0.3 | 35.3 ± 0.4 | 17.5 ± 0.4 | 19.8 ± 0.5 | 5.4 ± 0.0 | 8.6 ± 0.1 |
| 164 atm | 73.3 ± 2.5 | 83.9 ± 2.8 | 36.0 ± 0.8 | 38.6 ± 0.8 | 16.7 ± 0.2 | 18.9 ± 0.2 | 6.2 ± 0.5 | 9.6 ± 0.8 |
| ***Effect of Temperature*** *( $P_{CO2}$ = 139 atm, 3 hours, 1.0 M NaCl+0.64 M $NaHCO_3$)* | | | | | | | | |
| 90 $^oC$ | 2.6 ± 0.3 | 3.0 ± 0.3 | 13.0 ± 0.3 | 13.9 ± 0.3 | 5.2 ± 0.3 | 5.9 ± 0.3 | 3.5 ± 0.1 | 5.5 ± 0.2 |
| 125 $^oC$ | 24.6 ± 0.3 | 28.2 ± 0.4 | 13.2 ± 0.1 | 14.1 ± 0.1 | 6.1 ± 0.3 | 6.9 ± 0.3 | 4.5 ± 0.2 | 7.1 ± 0.3 |
| 150 $^oC$ | 61.6 ± 1.6 | 70.5 ± 1.8 | 23.9 ± 0.2 | 25.6 ± 0.2 | 9.1 ± 0.3 | 10.3 ± 0.4 | 4.8 ± 0.2 | 7.7 ± 0.3 |
| 185 $^oC$ | 73.5 ± 2.8 | 85.3 ± 3.1 | 33.0 ± 0.3 | 35.3 ± 0.4 | 17.1 ± 0.4 | 19.3 ± 0.5 | 5.4 ± 0.0 | 8.6 ± 0.1 |
| ***Effect of [$NaHCO_3$]*** *(185 $^oC$, $P_{CO2}$ = 139 atm, 3 hours)* | | | | | | | | |
| Deionized Water | 5.0 ± 0.3 | 5.8 ± 0.3 | 4.5 ± 0.2 | 4.8 ± 0.2 | 6.8 ± 0.1 | 7.7 ± 0.1 | 2.2 ± 0.2 | 3.5 ± 0.3 |
| 0.48 M $NaHCO_3$ | 49.0 ± 0.4 | 56.0 ± 0.5 | 7.5 ± 0.4 | 8.4 ± 0.1 | 7.3 ± 0.2 | 8.2 ± 0.3 | 4.9 ± 0.3 | 7.8 ± 0.4 |
| 0.64 M $NaHCO_3$ | 72.2 ± 3.1 | 82.7 ± 3.6 | 10.8 ± 0.3 | 11.6 ± 0.4 | 9.2 ± 0.3 | 10.4 ± 0.4 | 6.5 ± 0.0 | 10.4 ± 0.0 |
| 1.0 M $NaHCO_3$ | 74.3 ± 1.7 | 85.0 ± 1.9 | 31.6 ± 0.7 | 33.8 ± 0.7 | 22.9 ± 0.1 | 25.8 ± 0.1 | 9.0 ± 0.5 | 14.5 ± 0.6 |
| ***Effect of [NaCl]*** *(185 $^oC$, $P_{CO2}$ = 139 atm, 3 hours)* | | | | | | | | |
| Deionized Water | 5.0 ± 0.3 | 5.8 ± 0.3 | 4.5 ± 0.2 | 4.8 ± 0.2 | 6.8 ± 0.1 | 7.7 ± 0.1 | 2.2 ± 0.2 | 3.5 ± 0.3 |
| 0.5 M NaCl | 5.9 ± 0.3 | 6.8 ± 0.3 | 3.7 ± 0.7 | 3.9 ± 0.7 | 6.4 ± 0.2 | 7.2 ± 0.2 | 2.6 ± 0.1 | 4.2 ± 0.1 |
| 1.0 M NaCl | 12.8 ± 0.4 | 14.4 ± 0.9 | 3.1 ± 0.4 | 3.4 ± 0.4 | 7.6 ± 0.4 | 8.5 ± 0.5 | 3.6 ± 0.1 | 5.7 ± 0.1 |

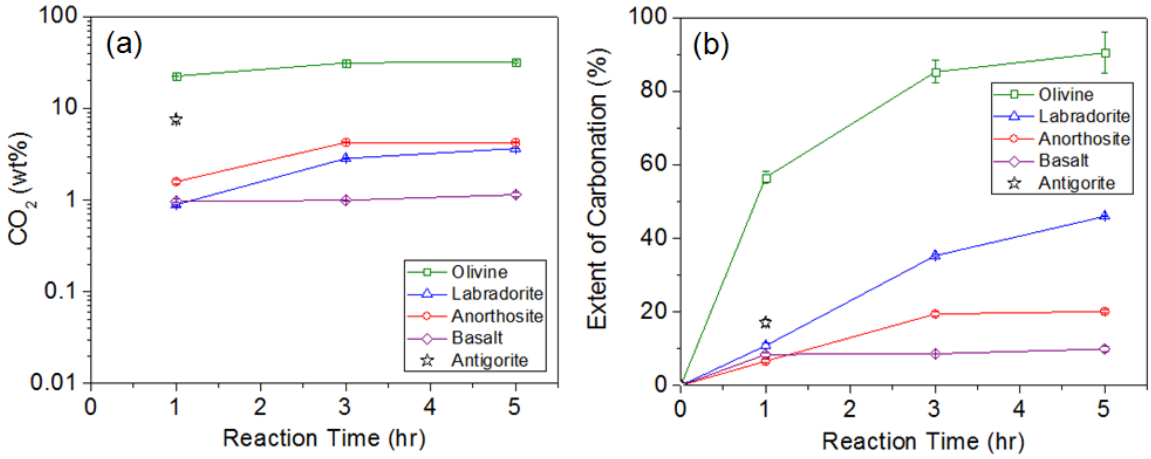


**Figure 13**. Effect of reaction time on (a) $CO_2$ stored as carbonates (Table 6) and (b) extent of carbonation (Table 7) of olivine, labradorite, anorthosite, and basalt. Experiments were conducted at 185 $^oC$, $P_{CO2}$ = 139 atm in 1.0 M NaCl + 0.64 M $NaHCO_3$ with 15 wt% solid and a stirring speed of 800 rpm. One test with antigorite at 185 $^oC$, $P_{CO2}$ =139 atm, 1.0 M NaCl+0.64 M $NaHCO_3$ for a reaction time of 1 hour resulted in a carbon content of 2.1%, which corresponded to an extent of carbonation of 17.3%. Extents of carbonation reported based on the formation of calcium and magnesium carbonates, and do not include possible formation of iron or sodium carbonates.

The raw data as represented by the wt% of $CO_2$ present in the reacted solid sample and the yield or extent of carbonation are reported in Tables 6 and 7, respectively. The extents of carbonation were calculated based on the formation of (i) calcium and magnesium carbonates alone, and (ii) calcium, magnesium and iron carbonates. Possible formation of sodium carbonates was not considered, which could be important in systems involving carbonation of Na-rich feldspars, such as labradorite, at low water/rock ratios.

Based on the amount of $CO_2$ trapped as carbonate, the reactivity of olivine was greater than that of anorthosite followed by labradorite and basalt (Table 6 and Figure 13 (a)). This trend followed that of the maximum carbonation potential, equivalent to the maximum amount of $CO_2$ that can be trapped by complete reaction of these minerals to form carbonates, which is 34, 17, 10 and 8 wt% in olivine, anorthosite, basalt and labradorite, respectively.

Of all the minerals, olivine was closest to achieving the maximum carbonation potential with 32 wt% $CO_2$ trapped, resulting in a conversion of 90% in a reaction time of 5 hours. Carbonation of antigorite was performed for a reaction time of 1 hour, which resulted in an extent of carbonation of 17.3%, about the same as that reported for antigorite by O'Connor et al. (2004, Figure 3), but much lower than the 49% carbonation they reported for heat-treated antigorite. This was followed by anorthosite which had a maximum carbonation potential of 17 wt%, but only contained 4.3 wt% $CO_2$ trapped as carbonates, resulting in an extent of carbonation of 20% at the end of 5 hours. While labradorite had the lowest carbonation potential

of 8 wt%, about 4 wt% $CO_2$ was present as carbonates, resulting in an extent of carbonation of 46%. Inclusion of possible $Na_2CO_3$ in our calculations would yield an even lower calculated extent of carbonation, ~ 30%. Though basalt had a carbonation potential of 10 wt%, slightly larger than labradorite, the reacted basalt contained only about 1 wt% $CO_2$ as carbonate, resulting the lowest extent of carbonation of 10%, at the end of 5 hours. Again, inclusion of possible formation of $Na_2CO_3$ and $K_2CO_3$ would reduce this value to ~ 7.5%. The wt% of $CO_2$ in anorthosite (4.3 wt%), labradorite (3.7 wt%), and basalt (1.14 wt%) is roughly proportional to the CaO concentration in anorthosite (14 wt%), labradorite (10wt%) and basalt (8 wt%), and to the carbonation potentials, which are 0.171 in anorthosite, 0.105 in labradorite, and 0.076 in basalt. The mineral carbonation trend olivine > labradorite > crystalline basalt (not including antigorite) follows the relative order of their predicted dissolution rates at high dilution in water at moderate to high pH and temperature greater than ~ 125°C (See Figure 5 of Kelemen et al., (Annual Review of Earth and Planetary Sciences, 2011)).

Reaction slowed after 3 hours for all minerals. In olivine, $CO_2$ stored (wt%) was 22, 31, and 32% and extents of carbonation were 57, 85 and 90% for reaction times of 1, 3 and 5 hours, respectively. These data correspond closely to the results of simple depletion models using a constant rate of 55 to 60% olivine carbonation per hour, acting on the remaining fresh olivine. In labradorite, $CO_2$ stored (wt%) was about 1, 3 and 4% and extents of carbonation were 11, 35 and 46% for reaction times of 1, 3, and 5 hours, respectively. In anorthosite, the $CO_2$ stored (wt%) was about 2, 4.3 and 4.3% and corresponding extents of carbonation were 7, 20, and 20% for reaction times of 1, 3 and 5 hours, respectively. The data for labradorite and anorthosite thus suggest an increase in the carbonation rate in the second hour of the experiments, followed by essentially no reaction in the third hour. In basalt, the $CO_2$ stored (wt%) did not change significantly beyond 1% after the first hour of reaction and the extent of reaction was 8-10%, for reaction times of 1, 3 and 5 hours, suggesting that the reaction rate dropped sharply during or soon after the first hour of the experiments.

Unlike in the case of olivine, where more than 85% conversion to carbonate was achieved, the rate of carbonation for plagioclase, and plagioclase-bearing rocks, appeared to slow down after three hours. This was most evident in solids with a significant amount of iron - basalt, and anorthosite.

All the experiments discussed in the following sections of this paper were performed for a reaction time of 3 hours, since significant enhancement in the reactivity of these minerals was not noted beyond a reaction time of 3 hours. Carbonation studies of plagioclase feldspars by Hangx & Spiers (2009) and Munz et al., (2011) showed that the precipitation of clay minerals such as smectite and kaolinite occurred during the reaction. Equilibrium simulations, using the PhreeqC software (Parkhurst & Appelo, 1999) with the LLNL database, also predict precipitation of magnesium-bearing clay minerals such as sepiolite during some mineral carbonation processes. The formation of clays may have limited carbonation of the plagioclase-bearing assemblages in our experiments.

The low reactivity of basalt is also attributed, in part, to the crystalline nature of the basalt sample we used. Glassy basalts are farther from equilibrium with water, and have much higher experimental dissolution rates than crystalline basalts (e.g., data of Gislason & Oelkers, 2003, plotted in Kelemen et al., 2011, Figure 5). Glassy basalts are thus expected to have higher carbonation rates compared to crystalline basalt.

### 5.3.2 Effect of Partial Pressure of $CO_2$

As indicated in Gadikota et al., (2013), high $CO_2$ partial pressures in the range of 100-150 atm are available for injection post $CO_2$ capture and compression. Therefore, many studies (Chizmeshya et al., 2007; Gerdemann et al., 2007; Giammar et al., 2005; Hangx & Spiers, 2009; Munz et al., 2012; O'Connor et al., 2004) have focused on understanding high pressure $CO_2$-mineral-reaction fluid interactions. In this study, the effects of $CO_2$ partial pressure on labradorite, anorthosite and basalt carbonation are compared with our previously published results for olivine at the same experimental conditions: $P_{CO2}$ of 64, 89, 139 and 164 atm, other reaction parameters of 185 $^{o}$C, 1.0 M NaCl + 0.64 M $NaHCO_3$, for 3 hours with 15 wt% solid and at a stirring rate of 800 rpm, (Gadikota et al., (2013).

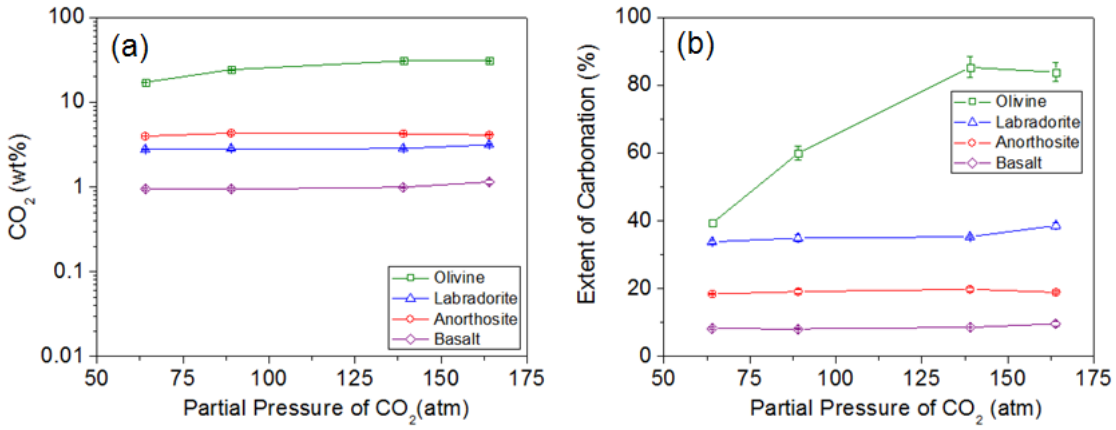


**Figure 14**. Effect of $CO_2$ partial pressure on (a) $CO_2$ stored as carbonates and (b) extent of carbonation of olivine, labradorite, anorthosite, and basalt. Experiments were conducted at 185 $^{o}$C in 1.0 M NaCl + 0.64 M $NaHCO_3$ for 3 hours, with 15 wt% solid and a stirring speed of 800 rpm. Extents of carbonation reported based on the formation of calcium and magnesium carbonates.

Figure 14 shows that increasing the partial pressure of $CO_2$ from 64 to 139 atm increases the extent of olivine carbonation from 39 to 85%, corresponding to an increase from 17wt% to 31wt% $CO_2$ in newly formed carbonate minerals (Table 6, Table 7 and Figure 14). In contrast, the extent of carbonation of labradorite, anorthosite, and basalt did not vary significantly with $P_{CO2}$. Carbonation extents of labradorite, anorthosite, and basalt were in the range of 33-39%, 18-20%, and 8-10% respectively, independent of $P_{CO2}$, calculated assuming that only calcium

and magnesium reacted to form carbonates. Assuming that iron can also react to form carbonates resulted in extents of carbonation of labradorite, anorthosite, and basalt of 31-36%, 16-18%, and 5-7%, respectively.

Note that these experiments were performed in the presence of 1.0 M NaCl + 0.64 M $NaHCO_3$. Carbonation experiments performed with plagioclase (An67-An73) with an average grain size of 10 μm in deionized water over the course of 24 hours at 200 $^oC$, showed 16% carbonation at a $P_{CO2}$ of 100 bar and 7% carbonation at a $P_{CO2}$ of 40 bar (Munz et al., 2012). These are about half and one quarter, respectively, of the extent of carbonation we observed under similar conditions. Also, the Munz et al. data show a substantial effect of varying $P_{CO2}$ whereas we observe almost no effect. In the absence of a buffer such as $NaHCO_3$, high $P_{CO2}$ in water could lead to a low pH which favors dissolution but destabilizes carbonates of calcium and magnesium, which are less soluble in aqueous fluids at high pH. In our experiments, the pH was buffered by dissolving $NaHCO_3$, and there was little change in pH with changing $P_{CO2}$.

### 5.3.3 Effect of Temperature

As reviewed by Palandri & Kharaka (2004), and confirmed by more recent work (Carroll & Knauss, 2005; Giammar et al., 2005; Wolff-Boenisch et al., 2006, 2004, 2011), studies have showed that increasing reaction temperature increases the dissolution rates of olivine and plagioclase. Another factor that aids the formation of magnesium and calcium carbonates at higher temperatures, is that carbonate solubility decreases with increasing temperature (Weyl, 1959).

As in the olivine carbonation studies conducted by Gadikota et al. (2013), our experiments with anorthosite, labradorite and basalt were performed in a solution of 1.0 M NaCl + 0.64 M $NaHCO_3$ at $P_{CO2}$ = 139 atm for 3 hours with 15 wt% solid and at a stirring rate of 800 rpm. Raising the temperature from 90 to 125, 150 and 185 $^oC$ in experiments on olivine increased the $CO_2$ content in solid products from 1.7 to 12.9, 27.3 and 30.9 wt%, respectively. In the case of anorthosite, the $CO_2$ contents were 1.3, 1.6, 2.3 and 4.3 wt% at 90, 125, 150 and 185 $^oC$, respectively. In labradorite, the $CO_2$ contents were 1.1, 1.2, 2.1 and 2.8 wt% at 90, 125, 150 and 185 $^oC$. Basalt trapped the lowest amounts of $CO_2$ as carbonate, with 0.6, 0.8, 0.9 and 1.0 wt% $CO_2$ at 90, 125, 150 and 185 $^oC$ (Table 6 and Figure 15). Thus, at 125 to 185°C, olivine carbonation trapped almost ten times more $CO_2$ compared to carbonation of any of the other solid reactants that we studied. The relative $CO_2$ contents in the carbonated compositions at higher temperatures were olivine > anorthosite > labradorite > basalt. As noted in Section 3.1, the relative order of reactivity follows that of the dissolution rates olivine > labradorite > crystalline basalt, whereas the full olivine carbonation rate in experiments such as ours, with dissolved $NaHCO_3$, is much higher than olivine dissolution rates at the same temperature and pH.

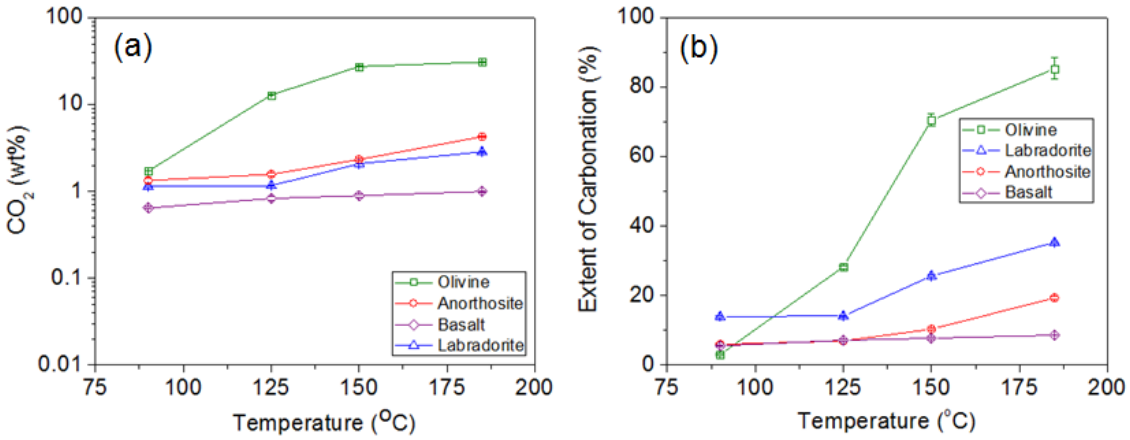


**Figure 15.** Effect of reaction temperature on (a) $CO_2$ stored as carbonates and (b) extent of carbonation of olivine, labradorite, anorthosite, and basalt. Experiments were conducted at $P_{CO2}$ = 139 atm in 1.0 M NaCl + 0.64 M $NaHCO_3$ for 3 hours, with 15 wt% solid and a stirring speed of 800 rpm. Extents of carbonation reported based on the formation of calcium and magnesium carbonates.

Increasing the temperature from 90 $^oC$ to 125, 150 and 185 $^oC$, increased the extent of labradorite carbonation from 13.9 to 14.1, 25.6 and 35.3%. Similarly, the extents of carbonation of anorthosite and basalt were 5.9, 6.9 10.3, 19.3% and 5.5, 7.1, 7.7, 8.6%, at 90, 125, 150 and 185 $^oC$ (Table 7 and Figure 15). Carbonation extents for all of these reactants over the range of experimental temperatures were much lower than olivine, whose extent of carbonation increased from 3.0% to 85.3% between 90 and 185°C. The extents of labradorite carbonation were higher than anorthosite but the carbon content is lower in labradorite because it has a lower weight fraction of CaO + MgO (~10 wt%) compared to anorthosite (~ 23 wt%) In other words, if the possible formation of $Na_2CO_3$ at low fluid/rock ratios is neglected (as in the calculations presented in this report), labradorite has a lower carbonation potential compared to anorthosite

In the preceding paragraph, carbonation extents are reported assuming that only calcium and magnesium reacted to form carbonates. Estimates assuming that iron may react to form carbonates are included in Table 7. Enhanced carbonation at higher temperatures is affected by enhanced dissolution and carbonation kinetics, reduced solubility of calcium and magnesite carbonates at higher temperatures, and lower $CO_2$ solubility with increasing temperature which in turn increases solution pH. PhreeqC calculations to determine the *in situ* conditions of anorthite reactions with $CO_2$, showed that the pH of the equilibrated system would have been 5.93, 6.22, 6.43 and 6.71 at 90, 125, 150 and 185 $^oC$. For olivine, the calculated pH values were 6.19, 6.24 and 6.51 at 90, 125 and 185 $^oC$. Maintaining the pH in the range of 6-7 with $NaHCO_3$ probably led to enhanced formation of carbonates in these experiments, compared to previous experiments without $NaHCO_3$, at lower pH.

Based on the rate data compiled by Kelemen et al., (2011), at temperatures in the range of 100-200 $^{o}$C, dissolution rates of olivine (Hänchen et al., 2006; Palandri & Kharaka, 2004) are greater than those of crystalline basalt (Schaef & McGrail, 2009) by almost an order of magnitude. Regardless, at higher pH in the range of 6-7 which are pertinent to the experimental conditions reported in this paper, the dissolution rate of Ca and Mg silicate minerals, such as olivine, are greater than those of plagioclase and plagioclase-rich rocks. One reason for the slower reaction rates of plagioclase compared to olivine may be nucleation of clay minerals such as smectite, kaolinite, and sepiolite, and/or amorphous aluminum hydroxides on the plagioclase surface (Munz et al., 2012; Hangx & Spiers, 2009).

### 5.3.4 Effect of $NaHCO_3$

Studies at Albany Research Center (Gerdemann et al., 2007; O'Connor et al., 2004) and Arizona State University (Chizmeshya et al., 2007) showed that adding $NaHCO_3$ enhances olivine carbonation. The independent effects of $NaHCO_3$ and NaCl on olivine carbonation were further investigated by Gadikota et al., (2013). The effect of $NaHCO_3$ on labradorite, anorthosite and basalt carbonation was investigated in experiments presented here. These experiments were performed at 185 $^{o}$C, $P_{CO2}$ of 139 atm for 3 hours, with 15 wt% solid and a stirring rate of 800 rpm, the same conditions as for olivine carbonation experiments conducted by Gadikota et al., (2013).

Increasing the concentration of $NaHCO_3$ from zero (deionized water) to 0.48, 0.64 and 1.0 M, enhanced the $CO_2$ content in reacted anorthosite from 1.7 wt% to 1.9, 2.3 and 5.6 wt%, respectively. Similarly, the $CO_2$ content in reacted labradorite and basalt were 0.4, 0.7, 1.0, and 2.7 wt% and 0.4, 1.2, 1.2, and 1.6 wt% from deionized water to 0.48, 0.64 and 1.0 M $NaHCO_3$, respectively. While all of the materials show increasing extents of carbonation with increasing concentration of $NaHCO_3$, up to 1.0M, olivine exhibits the most dramatic increase in $CO_2$ content with 3, 22, 31 and 31 wt% in 0, 0.48, 0.64 and 1.0 M $NaHCO_3$ (Figure 15). The enhancement achieved by using 1.0 M $NaHCO_3$ compared to the deionized water, in cases of olivine, labradorite, anorthosite and basalt were 15, 7, 3 and 4 - fold, respectively.

PhreeqC simulations showed that equilibrium pH for an anorthite-$CO_2$-reaction fluid system increased from 4.03 in deionized water to 6.36, 6.49 and 6.69, with dissolved carbonate concentrations from $5.7x\ 10^{-10}$ mol/kg to $2.5x10^{-4}$, $5x10^{-4}$ and $1.5x10^{-3}$ mol/kg, in 0.48, 0.64 and 1.0 M $NaHCO_3$, respectively at the experimental conditions. In the case of olivine, as noted in Gadikota et al., (2013), we determined similar equilibrium pH values and carbonate concentrations, except for deionized water for which a pH of 5.42 was calculated. In conclusion, we infer that $NaHCO_3$ was effective in enhancing the extents of carbonation of anorthosite, labradorite and basalt because it buffers the solution and serves as a carbon source.

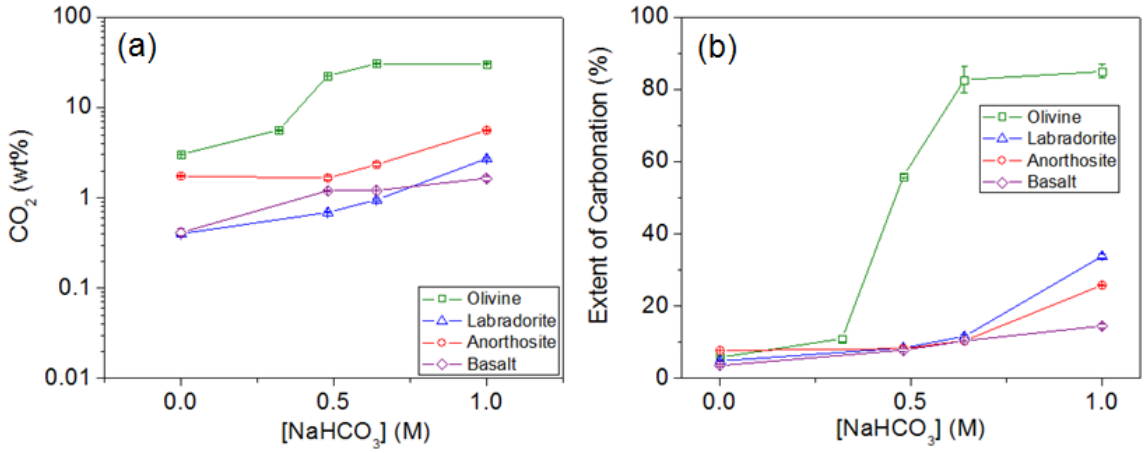


**Figure 16.** Effect of $NaHCO_3$ concentration on (a) $CO_2$ stored as carbonates and (b) extent of carbonation of olivine, labradorite, anorthosite, and basalt. Experiments were conducted at 185 $^oC$, at $P_{CO2}$ = 139 atm, for 3 hours, with 15 wt% solid and a stirring speed of 800 rpm. Extents of carbonation reported based on the formation of calcium and magnesium carbonates.

### 5.3.5 Effect of NaCl

Since proposed sites for geologic storage of $CO_2$ often contain saline aqueous fluids ("brine") in pore space, the effect of $CO_2$ interactions with minerals in the presence of NaCl-rich aqueous fluids was investigated. These experiments were performed at 185 $^oC$, $P_{CO2}$ of 139 atm for 3 hours, with 15 wt% solid and a stirring rate of 800 rpm, which were the same as those reported in our olivine carbonation study (Gadikota et al., 2013). Increasing the concentration of NaCl from 0 to 0.5 and 1.0 M NaCl had no significant on carbonation of labradorite, anorthosite and basalt; dissolved NaCl increased the carbonation rate of olivine from 6% in deionized water to 14% in 1.0 M NaCl (See Table 6, 7 and Figure 17).

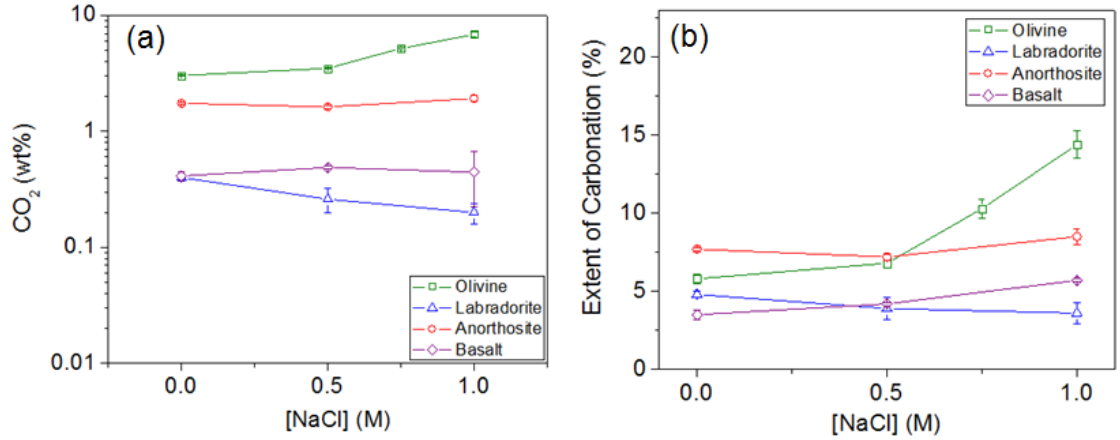


**Figure 17.** Effect of NaCl concentration on (a) $CO_2$ stored as carbonates and (b) extent of carbonation of olivine, labradorite, anorthosite, and basalt. Experiments were conducted at

185 $^{o}$C, at $P_{CO2}$ = 139 atm, for 3 hours, with 15 wt% solid and a stirring speed of 800 rpm. Extents of carbonation reported based on the formation of calcium and magnesium carbonates.

Many studies have reported on the role of NaCl on mineral carbonation. While Some studies suggest that $Cl^-$ enhances dissolution by binding to cations such as Mg (e.g. O'Connor et al., 2004), others suggest NaCl increases the ionic strength and reduces the solubility of $CO_2$ (Duan et al., 2006), which in turn limits the carbonate ions available to form $CaCO_3$ or $MgCO_3$. Olivine dissolution studies showed that adding salt changes the pH, which in turn may affect dissolution (Olsen, 2007). Olivine carbonation studies by King et al., (2010) showed that changing the ionic strength altered the crystal structure of magnesite. It is evident from the investigations of $CO_2$ interactions with plagioclase and plagioclase-rich rocks that NaCl does not have a significant effect on enhancing the carbonation of plagioclase and plagioclase-rich rocks.

As reported in Gadikota et al.(2013), the presence of NaCl alone, and in the absence of $NaHCO_3$ prompts the precipitation of iron oxide on reacting olivine surfaces. The formation of an iron oxide layer was evident in experiments on anorthosite and olivine. Previous studies (Béarat et al., 2006; King et al., 2010; Saldi et al., 2013) also showed the precipitation of iron oxide.

### 5.3.6 Morphological Changes due to Mineral Carbonation

As expected, SEM images revealed more extensive formation of carbonates in olivine compared to the other reacted minerals (Figure 18). Though the mean particle size of olivine was more than twice that of other minerals and rocks (Table 8), olivine carbonation proceeded at a much faster rate compared to the other minerals. If olivine had been ground to the same particle size as the other minerals and rocks, then much higher extents of carbonation could be expected.

In addition to determining the mineralogical changes in minerals, we measured changes in surface area and pore volume. The base case chosen for comparison was the experiment conducted at 185 $^{o}$C, $P_{CO2}$ = 139atm in 1.0 M NaCl + 0.64 M $NaHCO_3$ with 15 wt% solid and a stirring speed of 800 rpm, for a reaction time of 3 hours. Surface area decreased with increasing extent of carbonation (See Table 8). For example, the surface areas of reacted olivine, labradorite, anorthosite, and basalt decreased by 75%, 38%, 38%, and 19%, respectively for corresponding extents of carbonation of 85, 35, 19, and 9%, respectively. Changes in surface area were closely correlated with changes in the cumulative pore volume. For example, Figure 19 shows that in the case of olivine, which had the highest extent of carbonation, the cumulative pore volume decreased by an order of magnitude after carbonation. Pore volume profiles of anorthosite and labradorite were similar in that there was a significant reduction in the micro and mesopores but not in the larger pores. The cumulative pore volume of reacted basalt was virtually unchanged compared to the unreacted solid. This is presumably because of the low extent of carbonation of basalt compared to the other minerals and rocks.

**Table 8.** Changes in the mean particle diameter and specific surface area due to enhanced carbonation of olivine, labradorite, anorthosite and basalt. Experiments were conducted at 185 $^{o}$C, $P_{CO2}$ = 139 atm in 1.0 M NaCl + 0.64 M $NaHCO_3$ for 3 hours, with 15 wt% solid and a stirring speed of 800 rpm.

| Materials | Mean Particle Diameter ± Standard Deviation (μm) | Surface Area ± Standard Deviation ($m^2/g$) |
|---|---|---|
| Olivine | 21.41 ± 0.23 | 3.77 ± 0.17 |
| Carbonated Olivine | 27.34 ± 0.31 | 0.96 ± 0.29 |
| Labradorite | 8.20 ± 0.21 | 4.46 ± 0.01 |
| Carbonated Labradorite | 10.23 ± 0.33 | 2.74 ± 0.35 |
| Anorthosite | 9.68 ± 0.17 | 2.92 ± 0.05 |
| Carbonated Anorthosite | 10.05 ± 0.26 | 1.82 ± 0.16 |
| Basalt | 7.46 ± 0.08 | 4.48 ± 0.09 |
| Carbonated Basalt | 9.36 ± 0.07 | 4.32 ± 0.40 |

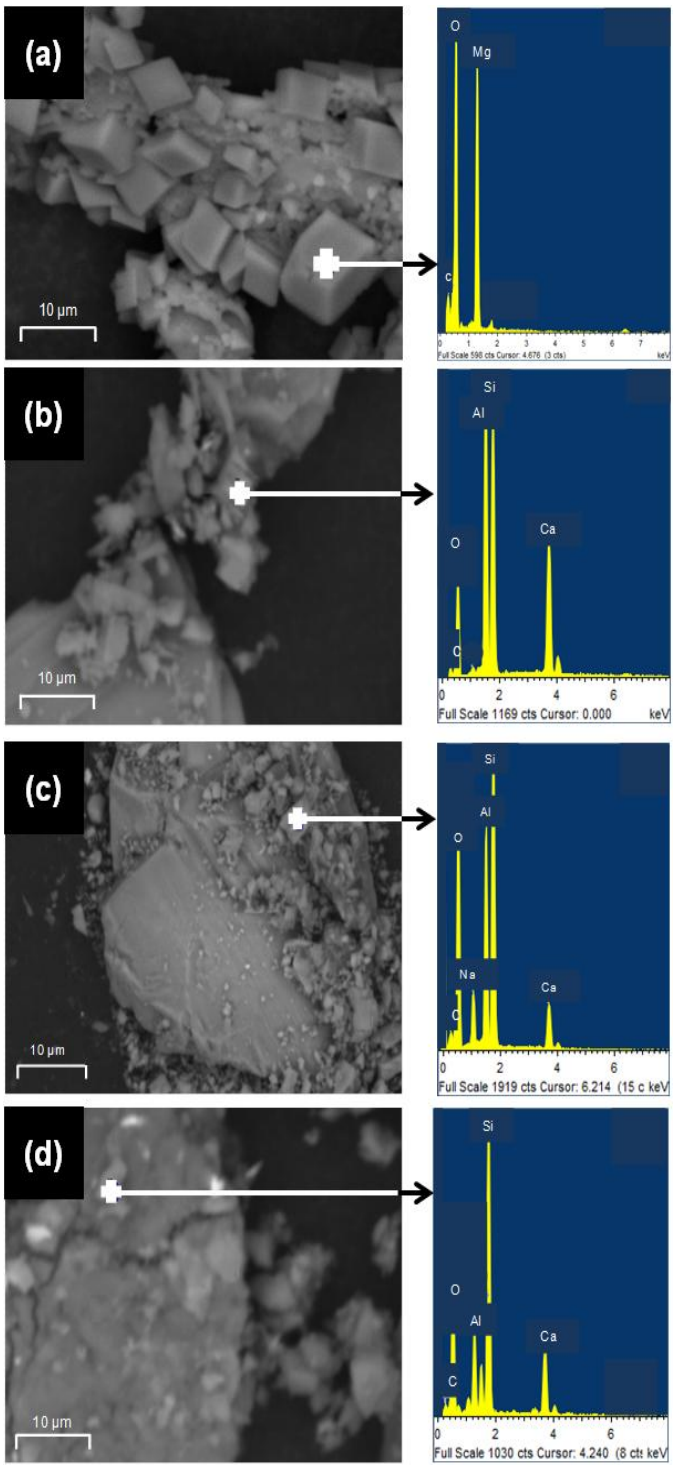


**Figure 18.** Formation of (i) magnesite in olivine, (ii) calcite in labradorite, (iii) magnesite and calcite in anorthosite, and (iv) magnesite and calcite in basalt. These SEM images represent samples that were reacted at 185 $^{o}$C, $P_{CO2}$ = 139 atm in 1.0 M NaCl + 0.64 M $NaHCO_3$ for 3 hours, with 15 wt% solid and a stirring speed of 800 rpm.

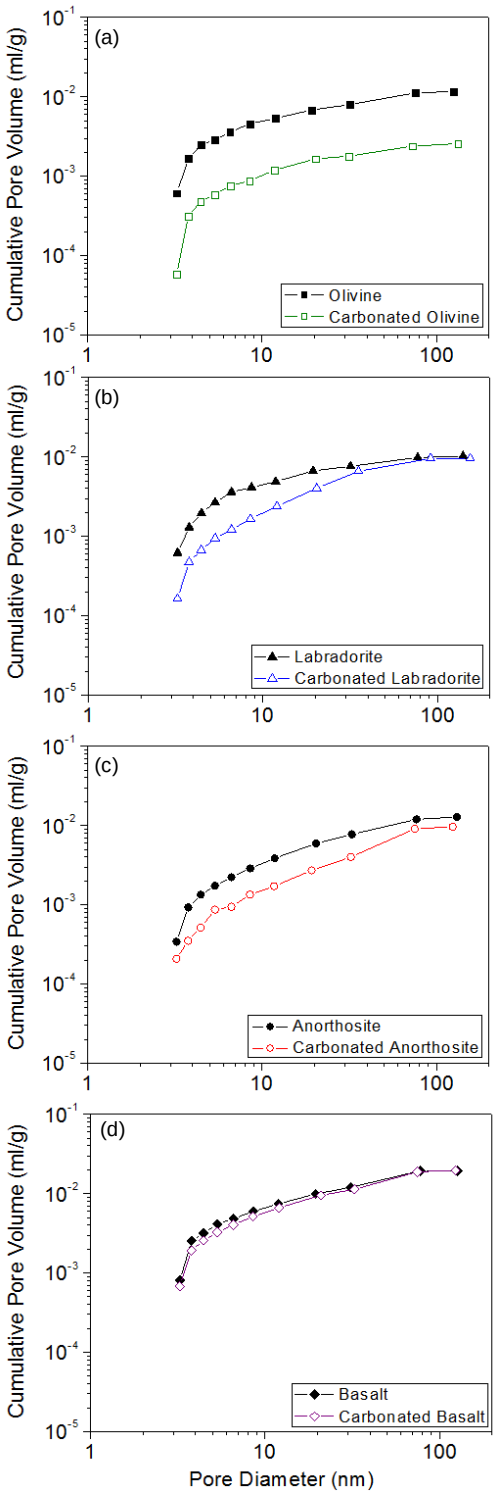


**Figure 19.** Changes in the cumulative pore volume of (a) olivine, (b) labradorite, (c) anorthosite, and (d) basalt when reacted at 185 $^{o}$C, $P_{CO2}$ = 139 atm in 1.0 M NaCl + 0.64 M $NaHCO_3$ for 3 hours, with 15 wt% solid and a stirring speed of 800 rpm.

## 6. Reactive Cracking

We prepared samples of Balsam Gap dunite (extensively studied by experimental petrologists and rock mechanics specialists) for these experiments by heating cylinders to 1200°C at controlled $fO_2$ corresponding to the quartz-magnetite-fayalite oxygen buffer in a gas mixing furnace, and then drop quenching them in water. This caused rapid thermal contraction, creating and opening microcracks along most olivine grain boundaries, as described by deMartin et al. (2006) who used the same technique. The permeability of these cylinders after heat treatment was approximately 0.1 to 1 mD, or $10^{-16}$ to $10^{-15}$ $m^2$. The average olivine grain size is approximately 1 mm, and the samples have a regular, polygonal texture (see deMartin et al., 2006 for more details). The heat treatment probably removed all minor alteration phases, such as serpentine and brucite. We now wonder if this affected mineral carbonation kinetics, perhaps by eliminating nuclei for initial magnesite crystallization and growth.

Experiments on this dunite saturated with reactive fluid and dunites saturated with distilled water were conducted. The reactive fluid consisted of distilled water with 1 M NaCl and 0.6 M $NaHCO_3$. It was then saturated with $CO_2$ at ~4MPa at 25°C, which corresponds to ~1.25 wt% $CO_2$ (using equation of state from Duan et al. 2006). Samples DUN-14 and DUN-15 showed an increased tendency toward compaction during a constant strain rate deformation as compared to sample DUN-11, a sample with behavior typical of dunites saturated with distilled water (Figure 20).

In DUN-11, DUN-14 and DUN-15, an initial volume reduction (compaction) was observed with the application of differential stress. With increasing differential stress, compaction lessened and a volume increase (dilation) became evident. Sample DUN-11 (saturated with distilled water) underwent a volume increase of ~0.4% during deformation (Figure 20). In comparison, dilation in DUN-14, which was saturated with a reactive fluid, was <0.1%. DUN-15, also saturated with reactive fluid, displayed a deformation history that could be described as intermediate between the other two samples, with more initial compaction than DUN-11, followed by more dilation than either DUN-11 or DUN-15.

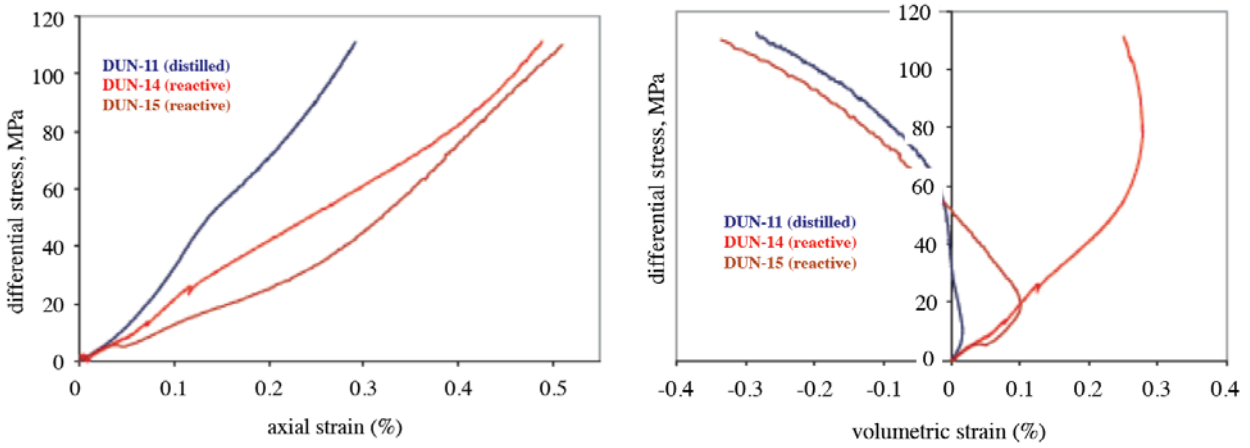


***Figure 20.*** *Differential stress versus axial and volumetric strain for constant strain rate deformation tests of dunite. Positive strain represents volume reduction and negative strain represents volume increase. Data from the dunite saturated with distilled water is in blue, while data from two dunites saturated with carbon dioxide saturated brine are in red.*

The difference in behavior can also be seen in the results of constant displacement, modified creep experiments. For these experiments, after loading the samples to a given stress level, 100 MPa differential stress in this case, the axial loading piston was held at a constant displacement and the deformation is allowed to progress for several days. Data for this type of experiment, at nearly constant stress, is presented in Figure 21. DUN-11, saturated with distilled water shows strongly dilatant behavior, progressing from an initial stage of accelerated deformation to roughly steady state dilatancy, with some perturbations due to permeability measurements (Figure 22). DUN-14, saturated with reactive fluid, shows an extremely brief episode of dilatancy at the very beginning of the deformation, then progresses to a roughly steady state compaction for the remainder of the deformation (plateaus at the end of the curve are due to changes in experimental temperature at the end of the run). Again, DUN-15 shows deformation intermediate between DUN-11 and DUN-14, with slight dilatency continuing throughout the run.

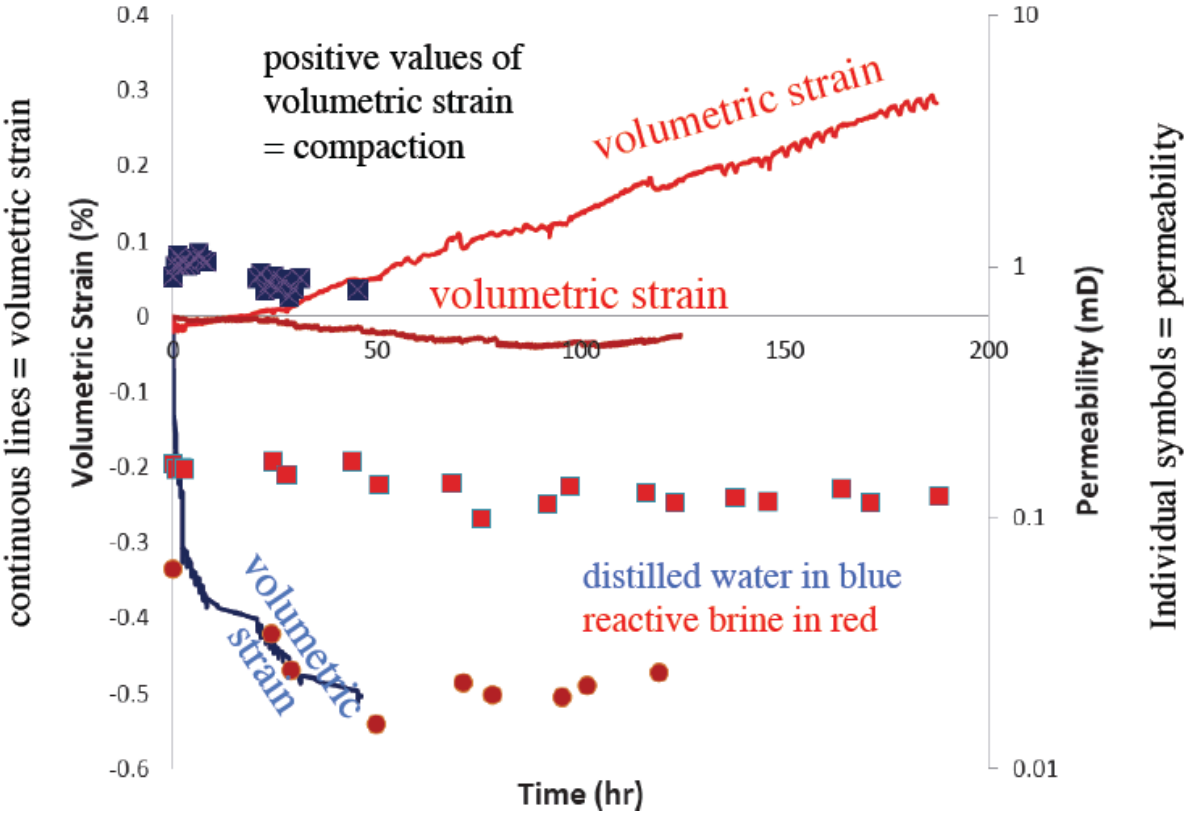


***Figure 21.*** *Volumetric strain (left hand axis, continuous lines) and permeability (right hand axis, individual symbols) versus time for a constant displacement, modified creep experiment at nearly constant stress. Positive strain represents volume reduction (compaction) and negative strain represents volume increase (dilation). Data from the dunite saturated with distilled water is in blue, while data from the two dunites saturated with carbon dioxide rich brine is in red.*

To further investigate the enhancement of compaction in the samples saturated with reactive fluid, we performed hydrostatic tests in which samples were serially saturated with distilled water followed by reactive fluid. Each sample was saturated with distilled water, placed in the deformation apparatus at 15

MPa confining pressure, 10 MPa pore pressure and 150°C and allowed to sit for a full day at these conditions. After this, brine saturated with carbon dioxide was introduced and flushed through the sample and all of the pore pressure plumbing. The sample was then allowed to sit for several additional days. The introduction of reactive pore fluid caused the hydrostatic compaction rate to increase by nearly an order of magnitude (Figure 3). The permeability in these two experiments showed an abrupt drop 20 to 30 hours after the introduction of reactive fluid. Note that this drop in permeability was significantly later than the increase in the compaction rate.

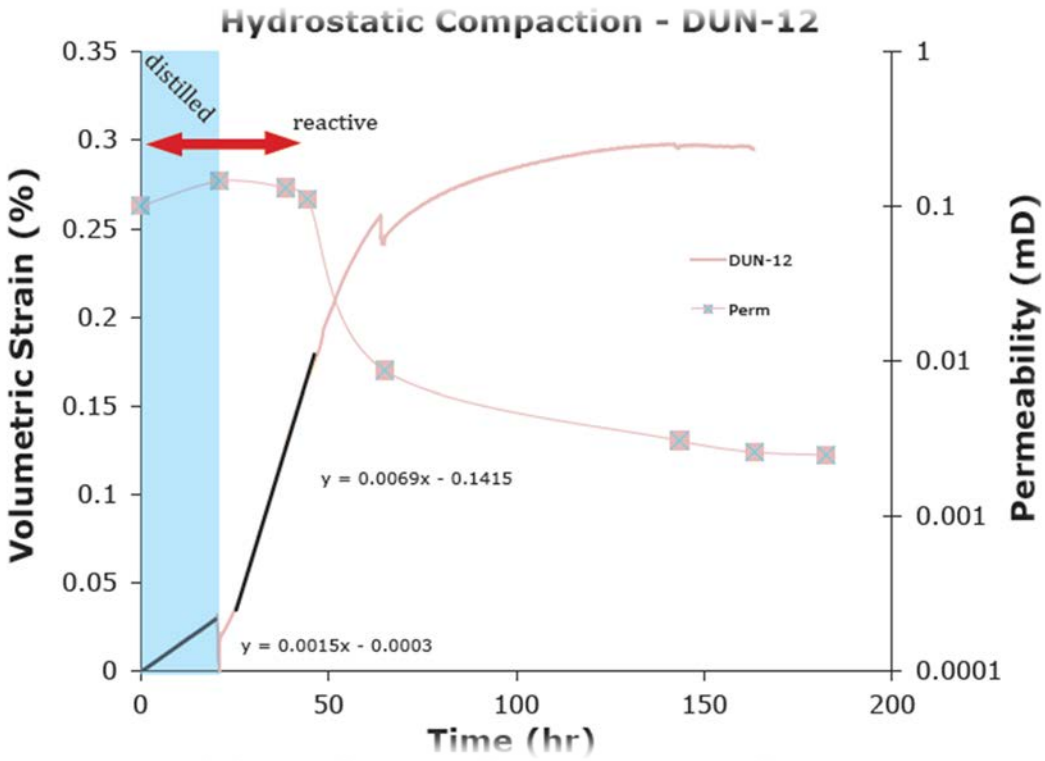

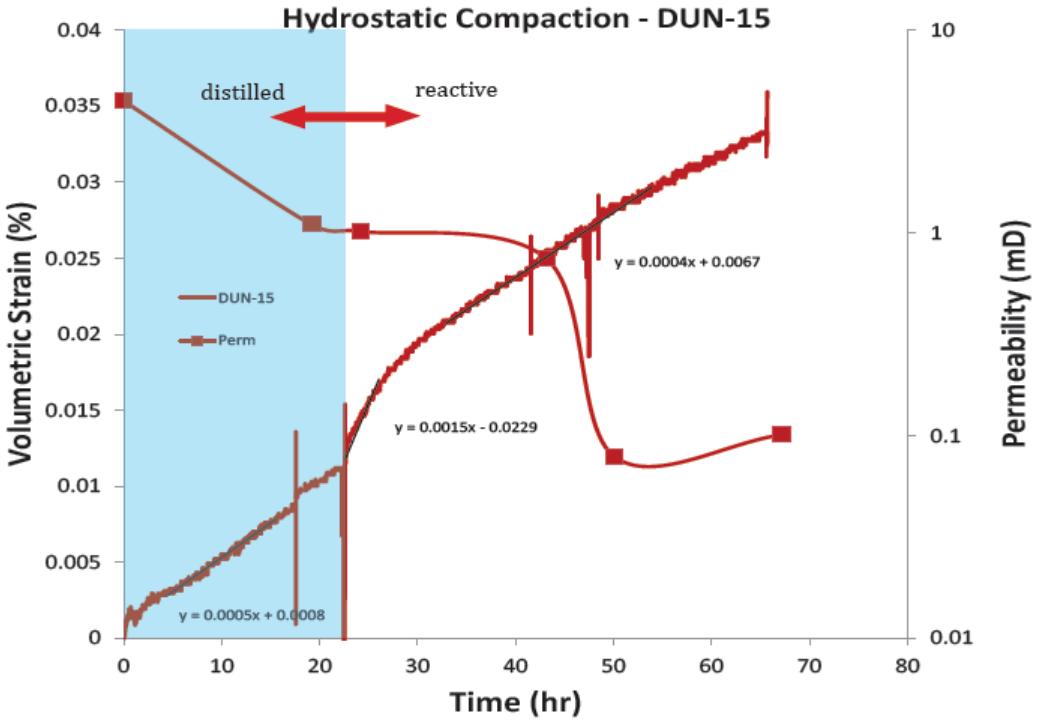


***Figure 22.*** *Volumetric strain versus time for hydrostatic deformation. From the beginning of the experiments to the end of the blue area, the sample was saturated with distilled water. Later, the sample was saturated with carbon dioxide rich brine. The labeled, linear fits approximate the hydrostatic compaction rate before and after the introduction of reactive fluid.*

DUN-11 and DUN-14 as well as samples of the fresh and heat-treated dunite material were analyzed by powder x-ray diffraction to see if any difference in sample chemistry was discernible after the experiments (Figure 23). The fresh dunite appears to have a larger amount of serpentine than the post-heat treated samples, as was expected (Figure 24). Apart from olivine and serpentine, no other phases were identifiable from the XRD data.

We infer that the increased compaction rate in the samples with reactive fluid is due to pitting of olivine surfaces due to dissolution of olivine (Figure 25). Such pitting has been widely reported in recent experiments on olivine hydration and carbonation (e.g., Figure 26). Formation of pits along crack surfaces decreases the solid-solid surface area, and thus the strength of the material in compression.

Initially, this enhanced compaction has a negligible effect on permeability, perhaps because it mainly affects only the smallest pore throats. However, under our experimental conditions, about 25 to 30 hours after the introduction of reactive fluid, we hypothesize that a threshold is crossed after which large, through-going fluid pathways collapse, leading to a permeability decrease of more than an order of magnitude in a few hours.

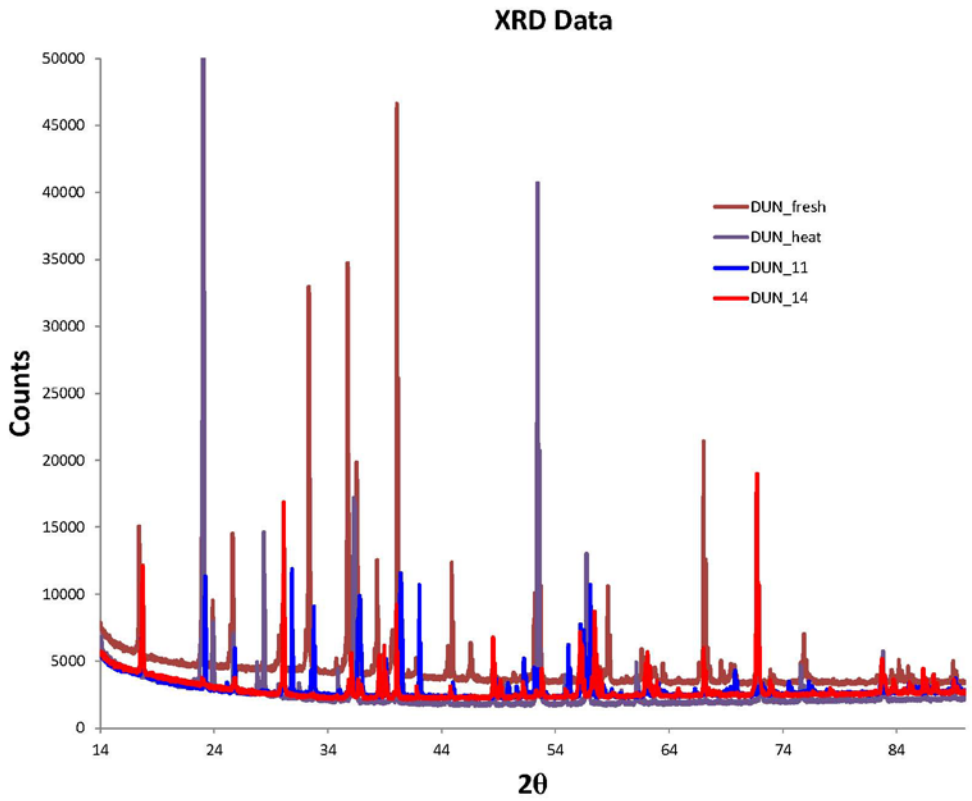


***Figure 23.*** *Counts versus 2θ for powder x-ray diffraction analyses. Data from the dunite saturated with distilled water are in blue, data from a dunite saturated with carbon dioxide rich brine are in red, data from fresh twin sisters dunite are in brown and data for thermally cracked dunite are in purple.*

Alternatively, the rapid decrease in permeability about 25 to 30 hours after addition of reactive fluid might not be related to the enhanced compaction rate in these experiments. Instead, it could represent onset of relatively rapid crystallization of reaction products (Mg-carbonates, serpentine) within pore space. However, we have only imaged small amounts of reaction products (Figure 8) and they are not yet apparent in the powder x-ray diffraction data (Figure 4). This, at this time we prefer the mechanical explanation for the permeability drop, described in the previous paragraph

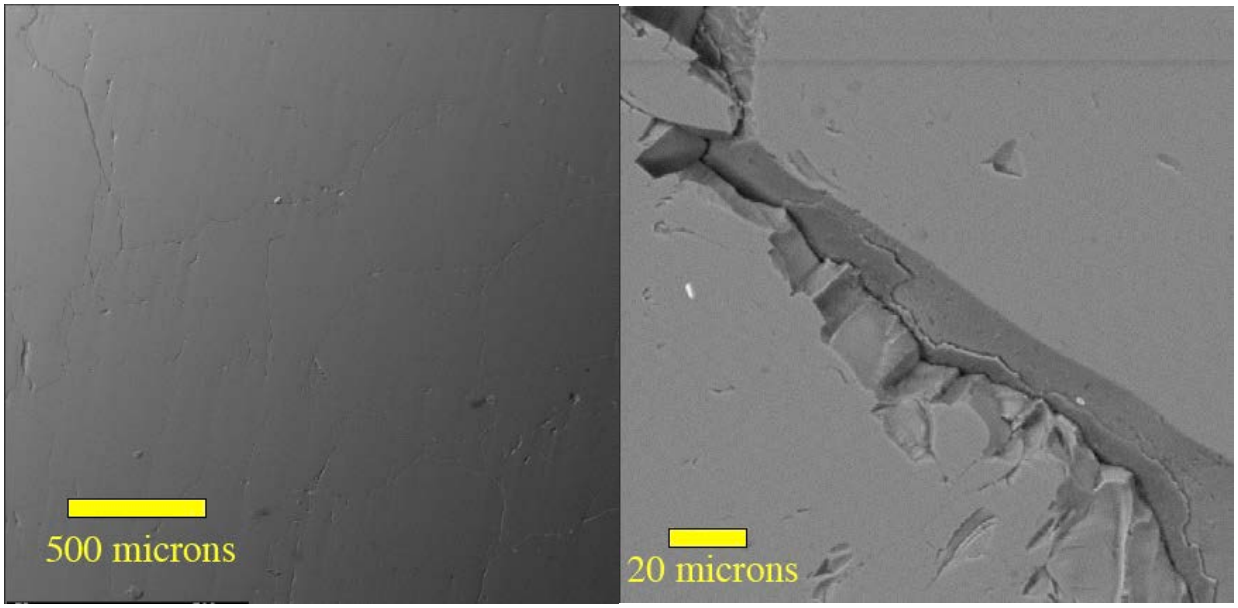


***Figure 24:*** *Starting material, thermally cracked dunite with ~ 1 mm grain size. Samples are heated to ~1200°C at controlled $fO_2$, and then rapidly quenched to room temperature to induce fractures along grain boundaries. The heating process completely removes minor amounts of serpentine present in the natural rock sample, accounting for the difference between the fresh dunite and the heat treated dunite in Figure 4. Small cracks are barely visible in the image on the left. The image on the right is a closeup of the smooth, uniform crack surfaces in this material.*

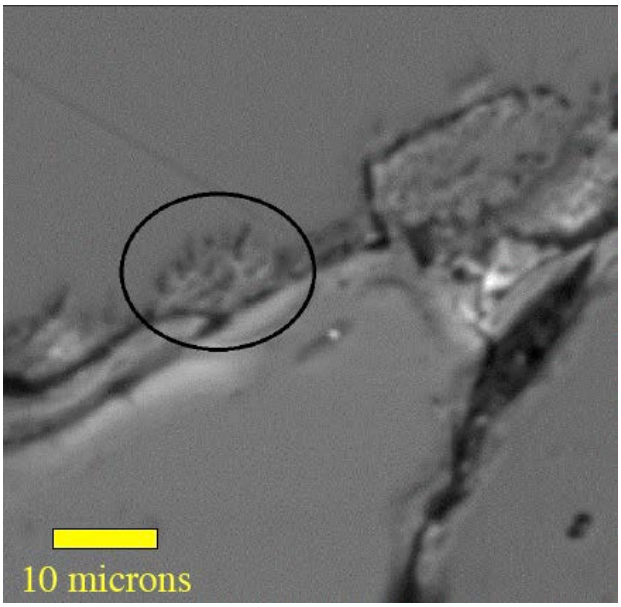


***Figure 25:*** *Pitted crack surfaces due to olivine dissolution along crack surfaces in a sample that was saturated with carbon dioxide rich brine in one of the University of Maryland experiments.*

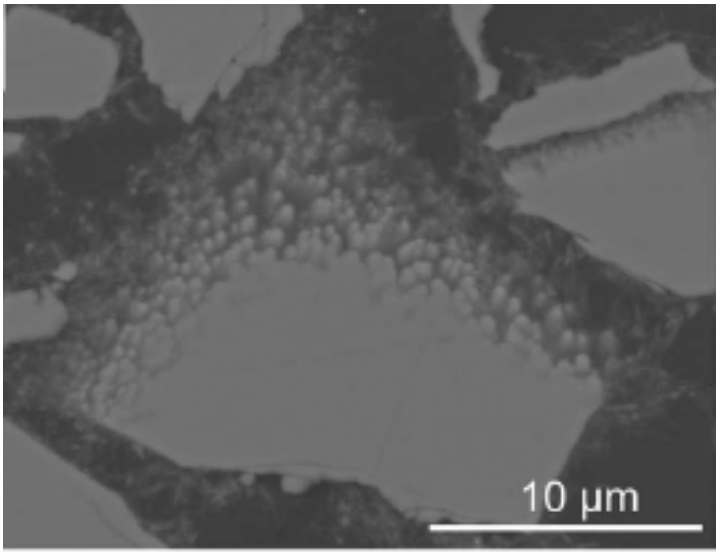


***Figure 26:*** *Higher resolution SEM image of etch pits along olivine crack surfaces in an experiment on olivine hydration (serpentinization). Malvoisin et al., J. Geophys. Res. 2012).*

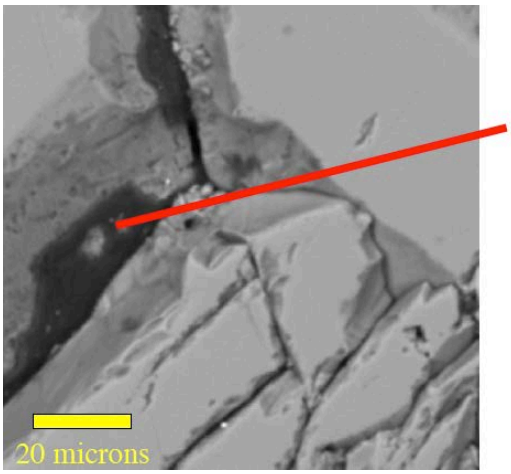


probable Mg-carbonate, magnesite ($MgCO_3$) or nesquehonite, hydromagnesite

***Figure 27:*** *SEM image of possible Mg-carbonate crystal within a crack in olivine in in a sample that was saturated with carbon dioxide rich brine in one of the University of Maryland experiments.*

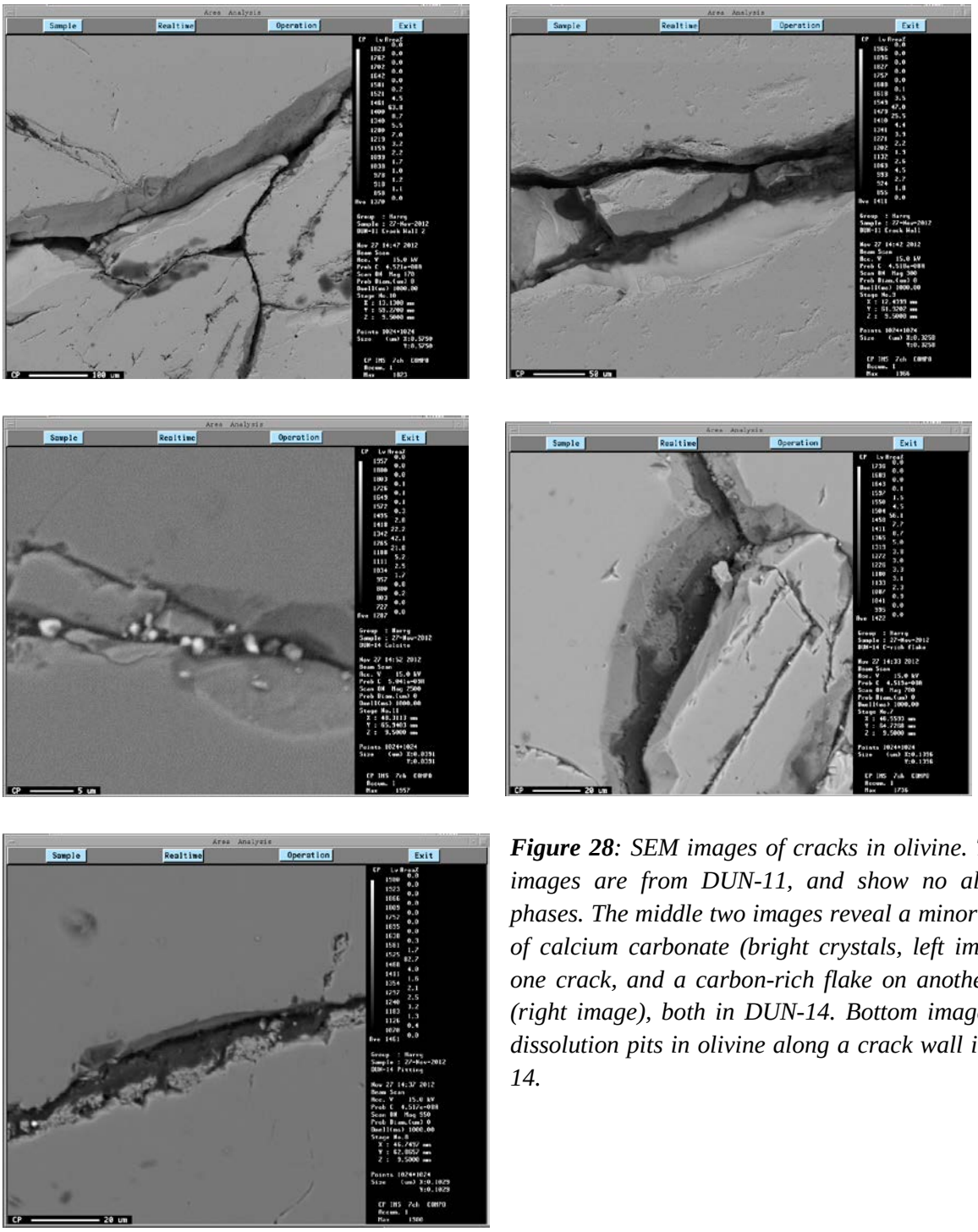


***Figure 28****: SEM images of cracks in olivine. Top two images are from DUN-11, and show no alteration phases. The middle two images reveal a minor amount of calcium carbonate (bright crystals, left image) on one crack, and a carbon-rich flake on another crack (right image), both in DUN-14. Bottom image shows dissolution pits in olivine along a crack wall in DUN-14.*

Additional images, which have somewhat better resolution than in Figures 25-27, are above (Figure 28). There is some Ca-carbonate (probably calcite; also see Figure 29) along one of the cracks in DUN-14, one of the samples deformed with reactive brine, but this is the only occurrence we could find, having allocated considerable time to the search. The crystals are quite small (<3 um), so we think we may have missed them in many cases. We suspect that there is some serpentine on cracks, but do not have clear mineral identification or analyses.

Powder XRD data illustrated in Figure 29 indicate that all the samples have the some phases (mostly forsterite-rich olivine and minor chromite).

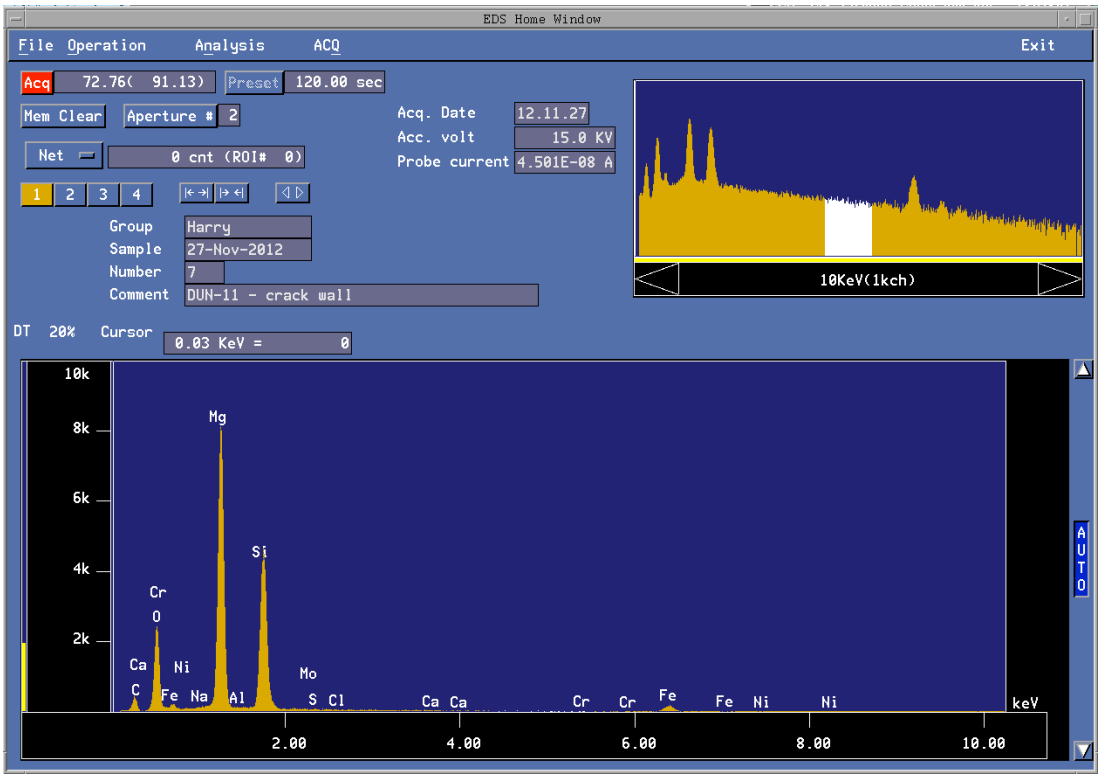


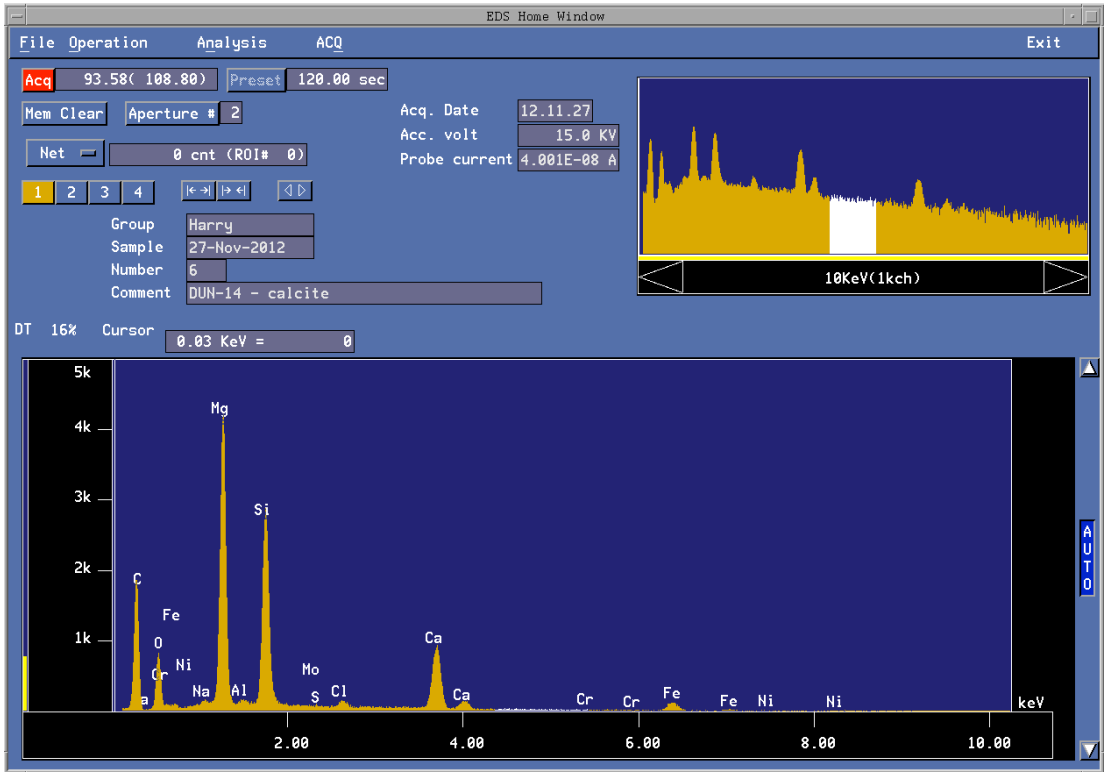

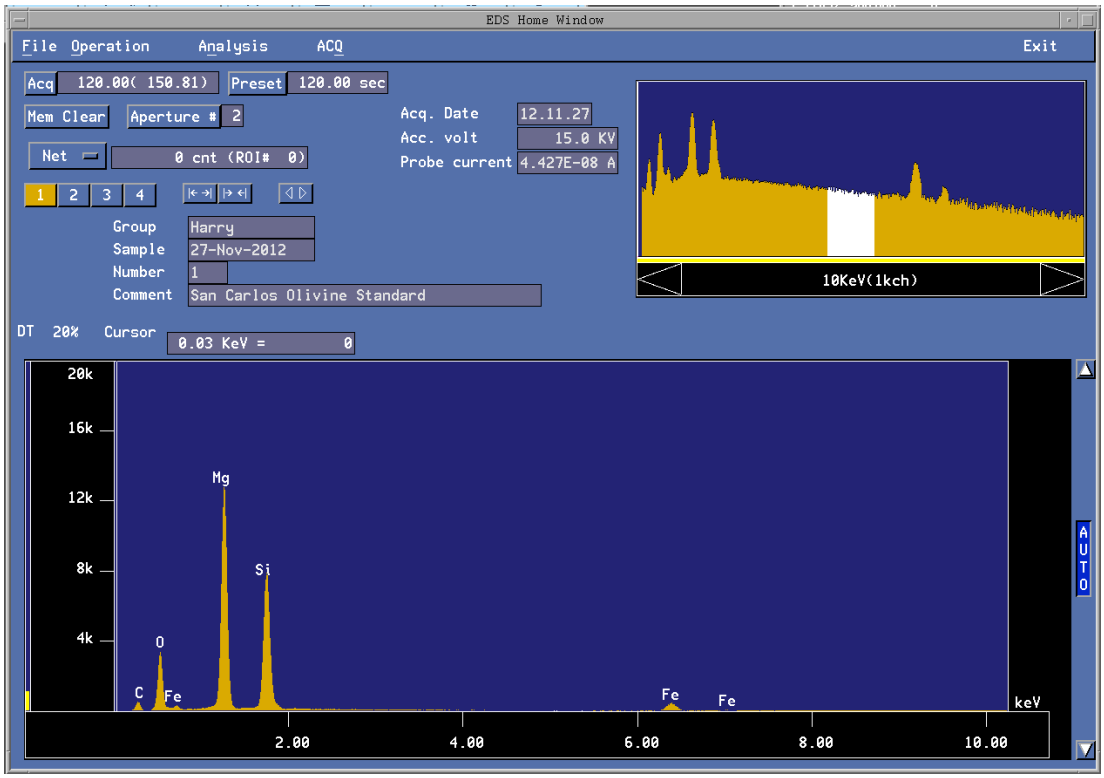


***Figure 29:*** *Energy dispersive spectra from SEM analyses of a crack wall in olivine (top), calcium carbonate mixed with olivine along a crack wall (middle), and a San Carlos olivine standard for comparison (bottom).*

## References


Amrhein, C., & Suarez, D. L. (1992). Some factors affecting the dissolution kinetics of anorthite at 25°C. *Geochimica et Cosmochimica Acta*, *56*(5), 1815–1826. doi:10.1016/0016-7037(92)90312-7

Awad, A., van Groos, A., & Guggenheim, S. (2000). Forsteritic olivine : Effect of crystallographic direction on dissolution kinetics. *Geochimica et Cosmochimica Acta*, *64*(10), 1765–1772.

Béarat, H., McKelvy, M. J., Chizmeshya, A. V. G., Gormley, D., Nunez, R., Carpenter, R. W., … Wolf, G. H. (2006). Carbon Sequestration via Aqueous Olivine Mineral Carbonation: Role of Passivating Layer Formation. *Environmental Science & Technology*, *40*(15), 4802–4808. doi:10.1021/es0523340

Bénézeth, P., Saldi, G. D., Dandurand, J.-L., & Schott, J. (2011). Experimental determination of the solubility product of magnesite at 50 to 200°C. *Chemical Geology*, *286*(1-2), 21–31. doi:10.1016/j.chemgeo.2011.04.016

Brady, P. V, Dorn, R. I., Brazel, A. J., Clark, J., Moore, R. B., & Glidewell, T. (1999). Direct measurement of the combined effects of lichen, rainfall, and temperature on silicate weathering. *Geochimica et Cosmochimica Acta*, *63*(19), 3293–3300.

Carroll, S. A., & Knauss, K. G. (2005). Dependence of labradorite dissolution kinetics on CO2(aq), Al(aq), and temperature. *Chemical Geology*, *217*(3-4), 213–225. doi:10.1016/j.chemgeo.2004.12.008

Chen, Y., & Brantley, S. L. (2000). Dissolution of forsteritic olivine at 65 8 C and 2 - pH - 5. *Chemical Geology*, *165*, 267–281.

Chizmeshya, A. V., McKelvy, M. J., Squires, K., Carpenter, R. W., & Béarat, H. (2007). *A novel approach to mineral carbonation: Enhancing carbonation while avoiding mineral pretreatment process cost: DOE Final Report 924162*.

Class, H., Ebigbo, A., Helmig, R., Dahle, H. K., Nordbotten, J. M., Celia, M., … Wei, L. (2009). A benchmark study on problems related to CO2 storage in geologic formations. *Computational Geosciences*, *13*(4), 409–434. doi:10.1007/s10596-009-9146-x

Cygan, R. T., Casey, W. H., Boslough, M. B., Westrich, H. R., Carr, M. J., & Holdren, G. R. (1989). Dissolution kinetics of experimentally shocked silicate minerals. *Chemical Geology*, *78*(3-4), 229–244. doi:10.1016/0009-2541(89)90060-0

deMartin, B., Hirth, G., and Evans, B. (2006) Experimental constraints on thermal cracking of peridotite at oceanic spreading centers: *AGU Monograph 148*, 167-185

Daval, D., Sissmann, O., Menguy, N., Saldi, G. D., Guyot, F., Martinez, I., … Hellmann, R. (2011). Influence of amorphous silica layer formation on the dissolution rate of olivine at 90°C and elevated pCO2. *Chemical Geology*, *284*(1-2), 193–209. doi:10.1016/j.chemgeo.2011.02.021

Demir, F., Donmez, B., Okur, H., & Sevim, F. (2003). Calcination kinetic of magnesite from thermogravimetric data. *Chem. Eng. Res. and Des*, *81*, 618–622.

Duan, Z., Sun, R., Zhu, C., & Chou, I.-M. (2006). An improved model for the calculation of CO2 solubility in aqueous solutions containing Na+, K+, Ca2+, Mg2+, Cl−, and SO42−. *Marine Chemistry*, *98*(2-4), 131–139. doi:10.1016/j.marchem.2005.09.001

Eggleston, C. M., Hochella Jr, M. F., & Parks, G. A. (1989). Sample preparation and aging effects on the dissolution rate and surface composition of diopside. *Geochimica et Cosmochimica Acta*, *53*, 797–804.

Frost, R. L., Adebajo, M., & Weier, M. L. (2004). A Raman spectroscopic study of thermally treated glushinskite—the natural magnesium oxalate dihydrate. *Spectrochimica Acta Part A: Molecular and Biomolecular Spectroscopy*, *60*(3), 643–651.

Gadikota, G., Matter, J., Kelemen, P. B., & Park, A.-H. A. (2014). Chemical and Morphological Changes during Olivine Carbonation for CO2 Storage in the presence of NaCl and NaHCO3. *Physical Chemistry and Chemical Physics*, *16*, 4679-4693.

Gadikota, G., Natali, C., Boschi, C., & Park, A.-H. A. (2014). Morphological changes during enhanced carbonation of asbestos containing material and its comparison to magnesium silicate minerals. *Journal of Hazardous Materials*, *264*, 42–52. doi:10.1016/j.jhazmat.2013.09.068

Gerdemann, S. J., O'Connor, W. K., Dahlin, D. C., Penner, L. R., & Rush, H. (2007). Ex situ aqueous mineral carbonation. *Environmental Science & Technology*, *41*(7), 2587–93. Retrieved from http://www.ncbi.nlm.nih.gov/pubmed/17438820

Giammar, D. E., Bruant, R. G., & Peters, C. a. (2005). Forsterite dissolution and magnesite precipitation at conditions relevant for deep saline aquifer storage and sequestration of carbon dioxide. *Chemical Geology*, *217*(3-4), 257–276. doi:10.1016/j.chemgeo.2004.12.013

Gislason, S. R., & Oelkers, E. H. (2003). Mechanism, rates, and consequences of basaltic glass dissolution: II. An experimental study of the dissolution rates of basaltic glass as a function of pH and temperature. *Geochimica et Cosmochimica Acta*, *67*(20), 3817–3832. doi:10.1016/S0016-7037(00)00176-5

Gislason, S. R., Wolff-Boenisch, D., Stefansson, A., Oelkers, E. H., Gunnlaugsson, E., Sigurdardottir, H., … Fridriksson, T. (2010). Mineral sequestration of carbon dioxide in basalt: A pre-injection overview of the CarbFix project. *International Journal of Greenhouse Gas Control*, *4*(3), 537–545. doi:10.1016/j.ijggc.2009.11.013

Gudbrandsson, S., Wolff-Boenisch, D., Gislason, S. R., & Oelkers, E. H. (2011). An experimental study of crystalline basalt dissolution from 2<=pH<=11 and temperatures from 5 to 75°C. *Geochimica et Cosmochimica Acta*, *75*(19), 5496–5509. doi:10.1016/j.gca.2011.06.035

Guy, C., & Schott, J. (1989). Multisite surface reaction versus transport control during the hydrolysis of a complex oxide. *Chemical Geology*, *78*(3-4), 181–204. doi:10.1016/0009-2541(89)90057-0

Hänchen, M., Prigiobbe, V., Baciocchi, R., & Mazzotti, M. (2008). Precipitation in the Mg-carbonate system—effects of temperature and CO2 pressure. *Chemical Engineering Science*, *63*(4), 1012–1028. doi:10.1016/j.ces.2007.09.052

Hänchen, M., Prigiobbe, V., Storti, G., Seward, T. M., & Mazzotti, M. (2006). Dissolution kinetics of fosteritic olivine at 90–150°C including effects of the presence of CO2. *Geochimica et Cosmochimica Acta*, *70*(17), 4403–4416. doi:10.1016/j.gca.2006.06.1560

Hangx, S. J. T., & Spiers, C. J. (2009). Reaction of plagioclase feldspars with CO2 under hydrothermal conditions. *Chemical Geology*, *265*(1-2), 88–98. doi:10.1016/j.chemgeo.2008.12.005

Heda, P. K., Dollimore, D., Alexander, K. S., Chen, D., Law, E., & Bicknell, P. (1995). A method of assessing solid state reactivity illustrated by thermal decomposition experiments on sodium bicarbonate. *Thermochimica Acta*, *255*, 255–272. doi:10.1016/0040-6031(94)02154-G

Hövelmann, J., Austrheim, H., & Jamtveit, B. (2012). Microstructure and porosity evolution during experimental carbonation of a natural peridotite. *Chemical Geology*, *334*, 254–265. doi:10.1016/j.chemgeo.2012.10.025

Kelemen, P. B., & Hirth, G. (2012). Reaction-driven cracking during retrograde metamorphism: Olivine hydration and carbonation. *Earth and Planetary Science Letters*, *345-348*, 81–89. doi:10.1016/j.epsl.2012.06.018

Kelemen, P. B., & Matter, J. M. (2008). In situ carbonation of peridotite for CO2 storage. *Proceedings of the National Academy of Sciences*, *105*(45), 17295–17300.

Kelemen, P. B., Matter, J., Streit, E. E., Rudge, J. F., Curry, W. B., & Blusztajn, J. (2011). Rates and Mechanisms of Mineral Carbonation in Peridotite: Natural Processes and Recipes for Enhanced, in situ CO 2 Capture and Storage. *Annual Review of Earth and Planetary Sciences*, *39*(1), 545–576. doi:10.1146/annurev-earth-092010-152509

Kelemen, P. B., Savage, H., & G. Hirth. (2013). Reaction-driven cracking during mineral hydration, carbonation and oxidation. In *Poromechanics V: Proceedings of the Fifth Biot Conference on Poromechanics, American Society of Civil Engineers* (pp. 823–826). Reston VA.

King, H. E., Plümper, O., & Putnis, A. (2010). Effect of secondary phase formation on the carbonation of olivine. *Environmental Science & Technology*, *44*(16), 6503–9. doi:10.1021/es9038193

Lackner, K. S. (2002). Carbonate Chemistry for Sequestering Fossil Carbon. *Annual Review of Energy and the Environment*, *27*(1), 193–232. doi:10.1146/annurev.energy.27.122001.083433

Matter, J. M., & Kelemen, P. B. (2009). Permanent storage of carbon dioxide in geological reservoirs by mineral carbonation. *Nature Geoscience*, *2*(12), 837–841. doi:10.1038/ngeo683

McGrail, B. P., Schaef, H. T., Ho, A. M., Chien, Y.-J., Dooley, J. J., & Davidson, C. L. (2006). Potential for carbon dioxide sequestration in flood basalts. *Journal of Geophysical Research*, *111*(B12), B12201. doi:10.1029/2005JB004169

McGrail, B. P., Spane, F. A., Sullivan, E. C., Bacon, D. H., & Hund, G. (2011). The Wallula basalt sequestration pilot project. *Energy Procedia*, *4*, 5653–5660. doi:10.1016/j.egypro.2011.02.557

Mervine, E.M., Humphris, S.E., Sims, K.W.W, Kelemen, P.B., Jenkins, W. J. (n.d.). Carbonation rates of peridotite in the Samail Ophiolite, Sultanate of Oman constrained through 14C dating and stable isotopes. *Geochimica et Cosmochimica Acta*.

Metz, B., Davidson;, O., Coninck;, H. de, Loos;, M., Meyer, L., & (eds.). (2005). *IPCC special report on carbon dioxide capture and storage*. Geneva, Switzerland: Cambridge University Press, UK.

Munz, I. A., Brandvoll, Ø., Haug, T. A., Iden, K., Smeets, R., Kihle, J., & Johansen, H. (2012). Mechanisms and rates of plagioclase carbonation reactions. *Geochimica et Cosmochimica Acta*, *77*, 27–51. doi:10.1016/j.gca.2011.10.036

Nicolas, A., Boudier, F., Ildefonse, B., & Ball, E. (2000). Accretion of Oman and United Arab Emirates ophiolite – Discussion of a new structural map. *Marine Geophysical Researches*, *21*, 147–179.

O'Connor, W. K., Dahlin, D. C., Rush, G. E., Gerdemann, S. J., & Nilsen, D. N. (2004). *Final report: Aqueous mineral carbonation: DOE/ARC-TR-04-002*.

Oelkers, E. H. (2000). An experimental study of forsterite dissolution rates as a function of temperature and aqueous Mg and Si concentrations. *Chemical Geology*, *175*, 485–494.

Oelkers, E. H., & Gislason, S. R. (2001). The mechanism, rates and consequences of basaltic glass dissolution: I. An experimental study of the dissolution rates of basaltic glass as a function of aqueous Al, Si and oxalic acid concentration at 25°C and pH = 3 and 11. *Geochimica et Cosmochimica Acta*, *65*(21), 3671–3681.

Oelkers, E. H., & Schott, J. (1995). Experimental study of anorthite dissolution and the relative mechanism of feldspar hydrolysis. *Geochimica et Cosmochimica Acta*, *59*(24), 5039–5053.

Olsen, A. . (2007). *Forsterite dissolution kinetics: Applications and implications for chemical weathering [PhD thesis]*. Blacksburg VA, USA.

Palandri, J. L., & Kharaka, Y. K. (2004). *A compilation of rate parameters of water-mineral interaction kinetics for application to geochemical modeling: Open File Report 2004-1068*.

Park, A. A., Jadhav, R., & Fan, L. (2003). CO2 mineral sequestration : chemically enhanced aqueous carbonation of serpentine. *The Canadian Journal of Chemical Engineering*, *81*, 885–890.

Park, A.-H. A., & Fan, L.-S. (2004). CO2 mineral sequestration: physically activated dissolution of serpentine and pH swing process. *Chemical Engineering Science*, *59*(22-23), 5241–5247. doi:10.1016/j.ces.2004.09.008

Parkhurst, D. L., & Appelo, C. A. . (1999). *User's guide to PHREEQC (Version 2). Water Resources Investigations Report: 99–4259*.

Paukert, A. P., Matter, J. M., Kelemen, P. B., Shock, E. L., & Havig, J. R. (2012). Reaction path modeling of enhanced in situ CO2 mineralization for carbon sequestration in the peridotite of the Samail Ophiolite, Sultanate of Oman. *Chemical Geology*, *330-331*, 86–100.

Pokrovsky, O., & Schott, J. (2000a). Forsterite surface composition in aqueous solutions : A combined potentiometric, electrokinetic, and spectroscopic approach. *Geochimica et Cosmochimica Acta*, *64*(19), 3299–3312.

Pokrovsky, O., & Schott, J. (2000b). Kinetics and mechanism of forsterite dissolution at 25 ° C and pH from 1 to 12. *Geochimica et Cosmochimica Acta*, *64*(19), 3313–3325.

Prigiobbe, V., Costa, G., Baciocchi, R., Hänchen, M., & Mazzotti, M. (2009). The effect of CO2 and salinity on olivine dissolution kinetics at. *Chemical Engineering Science*, *64*(15), 3510–3515. doi:10.1016/j.ces.2009.04.035

Rosso, J. ., & Rimstidt, D. J. (2000). A high resolution study of forsterite dissolution rates. *Geochimica et Cosmochimica Acta*, *64*(5), 797–811.

Rudge, J. F., Kelemen, P. B., & Spiegelman, M. (2010). A simple model of reaction-induced cracking applied to serpentinization and carbonation of peridotite. *Earth and Planetary Science Letters*, *291*(1-4), 215–227. doi:10.1016/j.epsl.2010.01.016

Saldi, G. D., Daval, D., Morvan, G., & Knauss, K. G. (2013). The role of Fe and redox conditions in olivine carbonation rates: An experimental study of the rate limiting reactions at 90 and 150°C in open and closed systems. *Geochimica et Cosmochimica Acta*, *118*, 157–183. doi:10.1016/j.gca.2013.04.029

Saldi, G. D., Jordan, G., Schott, J., & Oelkers, E. H. (2009). Magnesite growth rates as a function of temperature and saturation state. *Geochimica et Cosmochimica Acta*, *73*(19), 5646–5657. doi:10.1016/j.gca.2009.06.035

Saldi, G. D., Schott, J., Pokrovsky, O. S., Gautier, Q., & Oelkers, E. H. (2012). An experimental study of magnesite precipitation rates at neutral to alkaline conditions and 100–200°C as a function of pH, aqueous solution composition and chemical affinity. *Geochimica et Cosmochimica Acta*, *83*, 93–109. doi:10.1016/j.gca.2011.12.005

Schaef, H. T., & McGrail, B. P. (2009). Dissolution of Columbia River Basalt under mildly acidic conditions as a function of temperature: Experimental results relevant to the geological sequestration of carbon dioxide. *Applied Geochemistry*, *24*(5), 980–987. doi:10.1016/j.apgeochem.2009.02.025

Schaef, H. T., McGrail, B. P., & Owen, a. T. (2009). Basalt- CO2–H2O interactions and variability in carbonate mineralization rates. *Energy Procedia*, *1*(1), 4899–4906. doi:10.1016/j.egypro.2009.02.320

Schaef, H. T., Mcgrail, B. P., Owen, A. T., & Arey, B. W. (2013). Mineralization of basalts in the CO2 – H2O – H2S system. *International Journal of Greenhouse Gas Control*, *16*, 187–196. doi:10.1016/j.ijggc.2013.03.020

Seifritz, W. (1990). CO2 disposal by means of silicates. *Nature*, *345*, 486.

Siegel, D. I., & Pfannkuch, H. O. (1984). Silicate mineral dissolution at pH 4 and near standard temperature and pressure. *Geochimica et Cosmochimica Acta*, *48*(1), 197–201. doi:10.1016/0016-7037(84)90362-4

Stirling, A., & Pápai, I. (2010). H2CO3 Forms via HCO3− in Water. *The Journal of Physical Chemistry B*, *114*(50), 16854–16859. doi:10.1021/jp1099909

Streit, E., P.B. Kelemen, and J. E. (2012). Coexisting serpentine and quartz from carbonate-bearing serpentinized peridotite in the Samail Ophiolite, Oman. *Contributions to Mineralogy and Petrology*, *164*, 821–837.

Van Hees, P. A. ., Lundstro, U. S., & Morth, C.-M. (2002). Dissolution of microcline and labradorite in a forest O horizon extract : the effect of naturally occurring organic acids, *189*, 199–211.

Wang, X., Conway, W., Burns, R., McCann, N., & Maeder, M. (2009). Comprehensive Study of the Hydration and Dehydration Reactions of Carbon Dioxide in Aqueous Solution. *The Journal of Physical Chemistry A*, *114*(4), 1734–1740. doi:10.1021/jp909019u

Watson, J. G., Chow, J. C., & Chen, L.-W. A. (2005). Summary of organic and elemental carbon/black carbon methods and intercomparisons. *Aerosol and Air Quality Research*, *5*, 65–102.

Weyl, P. K. (1959). The change in solubility of calcium carbonate with temperature and carbon dioxide content. *Geochimica et Cosmochimica Acta*, *17*, 214–225.

Wogelius, R. A., & Walther, J. V. (1992). Olivine dissolution kinetics at near-surface conditions. *Chemical Geology*, *97*(1-2), 101–112. doi:10.1016/0009-2541(92)90138-U

Wolff-Boenisch, D., Gislason, S. R., & Oelkers, E. H. (2006). The effect of crystallinity on dissolution rates and CO2 consumption capacity of silicates. *Geochimica et Cosmochimica Acta*, *70*(4), 858–870. doi:10.1016/j.gca.2005.10.016

Wolff-Boenisch, D., Gislason, S. R., Oelkers, E. H., & Putnis, C. V. (2004). The dissolution rates of natural glasses as a function of their composition at pH 4 and 10.6, and temperatures from 25 to 74°C. *Geochimica et Cosmochimica Acta*, *68*(23), 4843–4858. doi:10.1016/j.gca.2004.05.027

Wolff-Boenisch, D., Wenau, S., Gislason, S. R., & Oelkers, E. H. (2011). Dissolution of basalts and peridotite in seawater, in the presence of ligands, and CO2: Implications for mineral sequestration of carbon dioxide. *Geochimica et Cosmochimica Acta*, *75*(19), 5510–5525. doi:10.1016/j.gca.2011.07.004

Xu, T., Apps, J. a, & Pruess, K. (2004). Numerical simulation of CO2 disposal by mineral trapping in deep aquifers. *Applied Geochemistry*, *19*(6), 917–936. doi:10.1016/j.apgeochem.2003.11.003

Yegulalp, T. M., Lackner, K. S., & Ziock, H. J. (2001). A Review of Emerging Technologies for Sustainable use of Coal for Power Generation. *International Journal of Surface Mining, Reclamation and Environment*, *15*(1), 52–68. doi:10.1076/ijsm.15.1.52.3423

## Technology Transfer Activities

***Publications***

- **Gadikota G**, Natali C, Boschi C and **Park A-H A**, "Morphological changes during enhanced carbonation of asbestos containing material and its comparison to magnesium silicate minerals", *Journal of Hazardous Materials*, 2013, http://dx.doi.org/10.1016/j.jhazmat.2013.09.068

- **Gadikota G, Kelemen P, Matter J and Park A-H A**, "Chemical and morphological changes during olivine carbonation and methods for estimating $CO_2$ stored in minerals", *Physical Chemistry Chemical Physics 16*, 4679-4693, 2014, **DOI:** 10.1039/C3CP54903H

***Presentations***

- **Gadikota G & Park A-H A**,"Thermodynamic and kinetic studies of mineral trapping of carbon in geologic formations", *AIChE Annual Meeting*, Salt Lake City, UT, November 7-12, 2010

- **Gadikota G**, Zhao H, **Park A-H A and Kelemen P**, "Carbon mineralization via carbonation of calcium and magnesium-bearing minerals as permanent storage of anthropogenic $CO_2$" *28th Annual International Pittsburgh Coal Conference*, Pittsburgh, PA, September 12-15, 2011

- **Gadikota G**, Zhao H, **Matter J, Kelemen P and Park A-H A**, "Natural and engineered carbon mineralization in geologic formations for permanent storage of $CO_2$", *Carbon Storage R&D Project Review Meeting: Developing the Technologies and Building the Infrastructure for $CO_2$ Storage*, Pittsburgh, PA, August 21-23, 2012 – *Poster Presentation*

- **Park A-H A, Kelemen P, Matter J** and **Gadikota G**, "Geo-chemo-mechanical studies for permanent storage of $CO_2$ in geologic formations", *Carbon Storage R&D Project Review Meeting: Developing the Technologies and Building the Infrastructure for $CO_2$ Storage*, Pittsburgh, PA, August 21-23, 2012

- **Gadikota G, Matter J, Kelemen P and Park A-H A**, "Geo-chemo-mechanical studies for permanent storage of $CO_2$ in geologic formations", *AIChE Annual Meeting*, Pittsburgh, PA, October 29- Nov 2, 2012

- **Gadikota G and Park A-H A**, "Morphological and chemical changes during mineral weathering for natural and engineered carbon storage", *US-Korea Conference 2013*, East Rutherford, New Jersey, August 7-11, 2013

- **Matter J, Kelemen P, Park A-H A,** and **Gadikota G**, "Geo-chemo-mechanical studies for permanent storage of $CO_2$ in geologic formations", *Carbon Storage R&D Project Review*

*Meeting: Developing the Technologies and Building the Infrastructure for $CO_2$ Storage*, Pittsburgh, PA, August 20-22, 2013

- **Lisabeth, HP**, W Zhu, **PB Kelemen**, The effect of CO2-saturated brines on the hydraulic and mechanical behavior of dunite, *Fall Meeting AGU Abstract*, MR33B-2328, 2013